

2007

Development of a New Spun Concrete Pole Reinforced With Carbon Fiber Reinforced Polymer Bars

Ashraf Mounir Mahmoud Shalaby
University of Alabama at Birmingham

Follow this and additional works at: <https://digitalcommons.library.uab.edu/etd-collection>

Recommended Citation

Shalaby, Ashraf Mounir Mahmoud, "Development of a New Spun Concrete Pole Reinforced With Carbon Fiber Reinforced Polymer Bars" (2007). *All ETDs from UAB*. 6685.
<https://digitalcommons.library.uab.edu/etd-collection/6685>

This content has been accepted for inclusion by an authorized administrator of the UAB Digital Commons, and is provided as a free open access item. All inquiries regarding this item or the UAB Digital Commons should be directed to the [UAB Libraries Office of Scholarly Communication](#).

DEVELOPMENT OF A NEW SPUN CONCRETE POLE REINFORCED WITH CAR-
BON FIBER REINFORCED POLYMER BARS

by

ASHRAF MOUNIR MAHMOUD SHALABY

FOUAD H. FOUAD, COMMITTEE CHAIR
ASHRAF AL HAMDAN
WILBUR A. HITCHCOCK
JASON T. KIRBY
TALAT SALAMA

A DISSERTATION

Submitted to the graduate faculty of The University of Alabama at Birmingham,
in partial fulfillment of the requirements for the degree of
Doctor of Philosophy

BIRMINGHAM, ALABAMA

2007

DEVELOPMENT OF A NEW SPUN CONCRETE POLE REINFORCED WITH CARBON FIBER REINFORCED POLYMER BARS

ASHRAF MOUNIR MAHMOUD SHALABY

CIVIL ENGINEERING

ABSTRACT

Prestressed spun concrete poles are used primarily for supporting electric power transmission lines and for area lighting. It is common to have them placed in aggressive environments, and in many applications they are placed directly in brackish or salt water, resulting in deterioration of the concrete pole due to steel corrosion. A new type of reinforcement that can provide the desired structural characteristics and at the same time address the issue of corrosion is needed. Such reinforcement could replace traditional steel reinforcement, reduce maintenance costs, and increase the service life of the structure. Carbon fiber-reinforced polymer (CFRP) composites are showing immense potential as a replacement to steel reinforcement due to their corrosion resistance, very high strength, and lighter weight compared to steel, which enables easier handling and reduces the self-weight of structures.

This research work presents an approach to studying the flexural behavior of spun concrete poles reinforced with CFRP bars. The flexural behavior of the CFRP pole was evaluated in terms of load deflection curves, cracking moment, ultimate moment capacities, and strains in the concrete and reinforcement. Primary design equations to estimate these terms were developed based on the equations available in the literature, and the design guidelines for concrete poles, and concrete structures reinforced with CFRP. Prototype specimens were manufactured and tested to verify the proposed equations. Finite element analysis was conducted to increase our understanding of the behavior of these

poles under loading. The prototype specimens were modeled using the ANSYS software package, and the results were compared with the test results. The results of this study provide a basis to develop recommendations and guidelines regarding the flexural design of spun concrete poles reinforced with CFRP.

DEDICATION

I would like to dedicate this work to my home country, Egypt, to my parents, wife, children, and brothers, and to my partners, with whose help and support I would not have been able to accomplish this work.

ACKNOWLEDGMENTS

The author wishes to express his sincere appreciation and gratitude to Dr. Fouad H. Fouad, Chair and Professor, Department of Civil, Construction, and Environmental Engineering, University of Alabama at Birmingham, for his supervision, planning, and continuous encouragement during the course of this research.

The author is indeed indebted to his committee, Dr. Ashraf Al Hamdan, Dr. Jason T. Kirby, Dr. Talat Salama, and Dr. Wilbur A. Hitchcock, for their guidance, valuable discussion, and real support during all of the stages of this dissertation.

The author also gratefully acknowledges the powerful support and tremendous help of Mohammed M. Shalaby, PhD candidate, University of Michigan, Ann Arbor, during the development of this research work.

The author would like to express his thankfulness and appreciation to Ron Albanese, Richard Hawkins, and Patrick Paolone for their help and support in executing the experimental part of this study.

Sincere thanks to the staff members of the Department of Civil, Construction, and Environmental Engineering for their support and cooperation.

Thanks to my family, my parents, and my wife for their help and encouragement.

Thanks to the faculty and staff members of the National Research Center in Egypt, the Cultural Affairs and Mission Sector in Egypt, and the Egyptian Cultural and Educational Bureau in the United States for their help and support.

TABLE OF CONTENTS

	<i>Page</i>
ABSTRACT.....	ii
DEDICATION.....	iv
ACKNOWLEDGMENTS	v
LIST OF TABLES	ix
LIST OF FIGURES	xi
LIST OF ABBREVIATIONS.....	xv
CHAPTER	
<u>1</u> INTRODUCTION	1
1.1 Background.....	1
1.2 Problem Statement.....	3
1.3 Objectives	5
1.4 Methodology and Approach	5
1.5 Organization of the Dissertation.....	7
<u>2</u> LITERATURE REVIEW	9
2.1 Introduction.....	9
2.2 Demonstrations and Field Applications.....	9
2.3 FRP Reinforcement Design Guidelines in the United States.....	11
2.4 FRP in Reinforced and Prestressed Concrete Applications.....	12
2.5 Flexural Behavior of Concrete Beams Reinforced with FRP.....	13
2.6 Characteristics of CFRP Reinforcement.....	20

2.7	Historical Development and Use of Spun Concrete Poles.....	21
2.8	CFRP in Spun Concrete Poles	22
2.9	Properties of Centrifugally Cast Concrete	24
2.10	Summary	25
3	EXPERIMENTAL PROGRAM	26
3.1	Introduction.....	26
3.2	Test Preparation	26
3.2.1	Material of Concrete Mixture	26
3.2.2	CFRP Bars	27
3.2.3	CFRP Grid (C-GRID).....	28
3.2.4	Specimens Dimensions and Reinforcement Details	29
3.2.5	Manufacturing Process.....	31
3.3	Test Setup and Instrumentation	40
3.4	Test Procedure	47
3.5	Test Results.....	51
3.5.1	Cracking Loads	52
3.5.2	Failure Loads	54
3.5.3	Deflection.....	57
3.5.4	Failure Modes	66
3.5.5	Compressive Strain Readings	76
3.5.6	Crack Width and Spacing	79
3.6	Summary	83
4	ANALYTICAL STUDY	86
4.1	General.....	86
4.2	Flexural Design Equations.....	86
4.2.1	Ultimate Moment Capacity Equation	87
4.2.2	Cracking Moment	89
4.2.3	Deflection.....	90
4.2.4	Crack Width.....	95
4.3	Spreadsheets Design and Verification	96
4.4	Summary	98
5	FINITE ELEMENT MODELING.....	99
5.1	Introduction.....	99
5.2	Finite Element Model	99
5.2.1	Element Types	100
5.2.2	Real Constants	100
5.2.3	Material Properties.....	101

5.2.4	Structure Modeling	105
5.2.5	Loads and Boundary Conditions.....	107
5.2.6	Analysis Type	110
5.3	RESULTS	115
5.4	Summary	118
6	DATA ANALYSIS AND DISCUSSION	119
6.1	Introduction.....	119
6.2	Experimental Versus Theoretical Data	120
6.2.1	Cracking and Ultimate Loads and Moments	120
6.2.2	Deflection.....	123
6.2.3	Crack width.....	128
6.3	Experimental Versus Finite Element Analysis Poles.....	131
6.3.1	Compressive Strains.....	131
6.3.2	Cracking and Ultimate Loads	133
6.3.3	Deflection.....	134
6.4	CFRP Versus Steel Reinforced Prestressed Poles	136
6.4.1	Cracking and Ultimate Loads	136
6.4.2	Deflection.....	138
7	SUMMARY AND CONCLUSION	140
7.1	Summary	140
7.2	Conclusion	143
7.3	Recommendations for Future Work.....	146
	REFERENCES	148
 <u>APPENDIX</u>		
<u>A</u>	FLOW CHART FOR THE SPREADSHEET DEVELOPED TO DESIGN SPUN CONCRETE POLES REINFORCED WITH CFRP BARS	154
<u>B</u>	FLOW CHART FOR THE CALCULATION OF THE CRACKING MOMENT OF INERTIA FOR SPUN CONCRETE POLES REINFORCED WITH CFRP BARS	164
<u>C</u>	FLOW CHART FOR THE LOAD-DEFLECTION CALCULATIONS OF SPUN CONCRETE POLES REINFORCED WITH CFRP BARS	172

LIST OF TABLES

<i>Table</i>	<i>Page</i>
1 Physical properties of CFRP Aslan 200.....	27
2 Typical properties of CFRP C-GRID	29
3 Strand physical properties of CFRP C-GRID.....	29
4 Experimental program and specimen details	31
5 Details of the C-GRID cutting list	39
6 Summary of test results.....	51
7 Compressive strength readings of concrete cylinders at 28 days	52
8 Average 28-day compressive strength of concrete including spinning factor .	52
9 Cracking load of the poles	54
10 Failure loads of the poles	56
11 Failure modes of the poles	67
12 Concrete and reinforcement details of six different sections of a CFRP pole (Terrasi et al. 2002).....	98
13 Real constants for Link8 element	101
14 Summary of Material Properties for Concrete.....	104
15 Load increment for the finite element model of the first pole	111
16 Load increment for the finite element model of the second pole	112
17 Displacement convergence criteria.....	115

18	Theoretical and experimental cracking and failure moments	121
19	Tip deflection at failure load.....	124
20	Modified tip deflection at failure load after reducing the I_{cr} by 10%	126
21	Tip deflection as a percentage from the free pole length.....	128
22	Experimental and theoretical maximum crack widths.....	129
23	Experimental and finite element model cracking loads	134
24	Experimental and finite element model failure loads	134
25	Experimental and finite element tip deflections at failure load	136

LIST OF FIGURES

<i>Figure</i>	<i>Page</i>
1 Aslan 200 CFRP Rebar Sample.....	27
2 C-GRID CFRP Grid Sample.....	28
3 Specimen concrete dimensions.....	30
4 Specimen cross-sectional details.....	30
5 Setting up the lower part of the mold and cleaning it.....	33
6 Adding the steel strands to hold the mold during spinning.....	33
7 Prestressing the strands to hold the mold during spinning.....	34
8 Adding the plastic pipes and the inside stirrups.....	34
9 The outer spiral stirrups with a pitch of 3.0 in.....	35
10 Plastic chairs to provide the required concrete cover.....	35
11 Concrete batch plant.....	36
12 Placing concrete into the open mold.....	36
13 Making the concrete cylinders for quality control testing.....	37
14 Placing the upper part of the mold and bolting it to the lower part.....	37
15 The steel mold on the spinner being spun.....	38
16 Cutting the C-GRID in to six parts.....	39
17 Tying the C-GRID to the bars using plastic ties.....	40
18 Schematic diagram showing the test setup.....	42

19 Test setup	43
20 Details of pole end supports.....	43
21 The clamp fixation of the supporting beams.....	44
22 The loading system at pole tip end	44
23 Strain gages location at 6” and 18” from the support	45
24 Deflection measurement scale at pole tip end.....	45
25 Concrete comparator for crack measurement	46
26 Data recording system.....	46
27 Dial gages locations for deflection measurements near the supports	47
28 Deflection measuring tape at the tip of the pole	49
29 LVDTs for deflection measurements and corrections	50
30 Strain gage rosette.....	50
31 Failure load of the two groups	57
32 Load deflection curves for the first group.....	59
33 Deflection of pole G01-01 prior to failure.....	60
34 Load deflection curves for the second group.....	61
35 Deflection of pole G02-02 prior to failure.....	65
36 Load deflection curve of the four specimens.....	66
37 Shear cracks between supports prior to G01-01 pole failure.....	67
38 Concrete crushing at failure from different views for G01-01	68
39 Slippage of prestressing strands during testing.....	68
40 Diagonal shear crack for pole G01-02	69
41 Concrete failure from different views for G01-02.....	70

42	Slippage of CFRP bars and prestressing strands at failure of pole G01-02.....	71
43	Shear cracks between supports prior to failure of pole G02-01.....	72
44	Concrete crushing at failure of pole G02-01.....	72
45	First shear crack for the pole G02-02	74
46	Failure of Pole G02-02 from different views.....	75
47	Failure of concrete and longitudinal CFRP bars.....	75
48	Failure of C-GRID reinforcement.....	76
49	Load versus compressive strain for G01 specimens	78
50	Load versus compressive strain for G02 specimens	78
51	Cracking pattern for pole G01-01	79
52	Crack width versus loading for the pole G01-02.....	80
53	Cracking pattern for pole G02-01	81
54	Crack width versus loading for G02 specimens	83
55	Concrete stress area and assumed stress distribution in pole section	87
56	Stress-strain curves of CFRP bars and steel strands	88
57	Crack width parameters for pole specimens	96
58	Ultimate moment capacities of CFRP prestressed spun concrete pole.....	97
59	Concrete stress-strain curve adopted in the FE model.....	103
60	Stress-strain curve for CFRP bars.....	105
61	Finite element meshing of the pole in the longitudinal direction	106
62	Finite element meshing of the pole in the cross-sectional direction.....	107
63	Finite element modeling of the CFRP bars.....	107
64	Sample of the out-of-plane joint restraints.....	108

65	Point loads applied to the pole	109
66	Load-compressive strain plot for the two poles	116
67	Load-deflection curve for the two poles	117
68	Cracking and failure loads of the G01 specimens	122
69	Cracking and failure load of the G02 specimens	122
70	Load-deflection curve for the G01 specimens	124
71	Load-deflection curve for the G02 specimens	125
72	Modified load-deflection curve for the G01 specimens	127
73	Modified load-deflection curve for the G02 specimens	127
74	Load-crack width curve for pole G01-02.....	130
75	Load-crack width curve for the G02 specimens	130
76	Load-compressive strain for the G01 specimens	132
77	Load-compressive strain for the G02 specimens	132
78	Load-deflection curve for the G01 specimens	135
79	Load-deflection curve for the G02 specimens	135
80	CFRP and prestressed cracking loads	137
81	CFRP and prestressed ultimate loads.....	138
82	Load-deflection curve for the G01 specimens	139
83	Load-deflection curve for the G02 specimens	139

LIST OF ABBREVIATIONS

α_b	Bond coefficient for the effective moment of inertia calculation
β_d	Reduction coefficient
Δ	Deflection of the pole
ε	Strain at any stress f
ε_0	Concrete peak strain in compression
ρ	Reinforcement ratio of the cross-section
ρ_b	Balanced reinforcement ratio of the cross-section
ν	Poisson's ratio of concrete
A	Effective tension area of concrete defined as the area of concrete having the same centroid as that of the farthest tensile reinforcement from the neutral axis
A_{f_i}	Area of the i^{th} reinforcement
c	Location of the neutral axis measured from the extreme compression fiber of the pole
d_c	The distance from the centroid of the effective tensions area of concrete to the extreme tensile fiber of the cross-section
d_i	Distance of the i^{th} reinforcement from the extreme compression fiber
E_c	Modulus of elasticity of concrete
E_f	Modulus of elasticity of FRP bars
E_s	Modulus of elasticity of steel
e_i	Distance of the i^{th} reinforcement to the neutral axis

f	Stress at any strain ε
f'_c	Cylinder compressive strength of concrete at 28 days
f_{fei}	Stress of the i^{th} reinforcement
f_{fu}	Ultimate strength of the CFRP bars
f_{pu}	Ultimate tensile strength of the prestressing strands
f_r	Modulus of rupture of concrete
I	Moment of inertia of the cross-section
I_{A_a}	Moment of inertia of annulus at the neutral axis
I_{cr}	Cracking moment of inertia
I_e	Effective moment of inertia of the cross-section
I_g	Gross moment of inertia of the section
k_b	Bond coefficient for calculation of the crack width
Kc	Position of the centroid of the stress block
L	Length of the pole
M	Applied moment
M_a	Maximum moment subjected to the pole
M_{cr}	Cracking moment of concrete
M_u	Ultimate moment capacity of the section
n_f	Modular ratio between CFRP and concrete
P_i	Effective prestressing force applied to the strands

w	Crack width in mils
w	Unit weight of concrete in lb/in ³
y_t	Distance from the centroidal axis to the extreme tensile fiber of the section
x	Distance from the support

CHAPTER 1

INTRODUCTION

1.1 Background

Poles are used for a variety of applications, such as area lighting and supporting electric power transmission lines. There are different types of transmission line supporting structures: wood poles, steel lattice towers, steel poles, and concrete poles. Wood poles have been the mainstay for utilities since the 1900s. Wood has been Mother Nature's gift to the utilities. For many years it was the natural choice for supporting wire. It was abundant and inexpensive. Lattice towers entered the market in the 1920s when the line design loads exceeded the reasonable capacity of wood structures. Tubular steel poles were introduced as an aesthetically pleasing structure in the 1960s, but they proved to be an economical choice for cross-country transmission lines. Concrete poles were first introduced in the United States in the 1930s in two major types, depending on the manufacturing method: the static cast poles and the centrifugally cast concrete poles. The latter are commonly referred to as spun poles and typically possess round, hollow cross-sections. Statically cast poles typically have a square cross-section. Prestressed spun concrete poles, however, were not used until the mid 1950s (Fouad et al 1992). Prestressed spun concrete poles offer many advantages in comparison to poles made from other materials, including non-prestressed reinforced concrete poles or static cast concrete poles. In September 2000, the world's first carbon fiber reinforced polymer (CFRP) prestressed

high strength concrete electricity pylon was installed in Switzerland (Terrasi et al 2001). The 90 ft high pole was manufactured using centrifugally cast, high strength concrete containing blended silica-fume cement.

Fiber reinforced polymer (FRP) composites have been proposed for use as reinforcing bars and prestressing tendons in concrete structures (ACI-440.4R-04). FRP materials are gaining acceptance because of their unique characteristics. FRP materials have high strength, lightweight, non-corrosive, non-conducting, and non-magnetic properties. Although the cost of using FRP materials are higher than conventional steel materials at the present time, the higher cost of FRP materials suggests that FRP use will be confined to applications where the unique characteristics of the material are most appropriate. Efficiencies in construction and reductions in fabrication costs will expand their potential market (ACI-440.4R-04).

FRP reinforcement is available in the form of bars, grids, plates, and tendons. Unlike conventional steel reinforcement, there are no standardized shapes, surface configurations, fiber orientations, constituent materials, and proportions for the final products. Similarly, there is no standardization of the methods of production, such as pultrusion, braiding, filament winding, or FRP preparation for specific application. FRP materials thus require considerable engineering effort to use properly (ACI-440.4R-04).

FRP are a combination of two materials; the fiber reinforcement material, such as carbon, glass, or aramid fibers, is impregnated in the polymeric matrices, which as the resins. Polyester, vinyl ester, and epoxy are examples of the commercially available polymeric matrices. The impregnation of the fibers in the matrices results in a heteroge-

neous and anisotropic material. The final characteristics of FRP reinforcement are dependent on fiber and resin properties, as well as the manufacturing process.

1.2 Problem Statement

Prestressed spun concrete poles are commonly used in aggressive environments, such as brackish or salt water. The presence of the poles in a highly corrosive environment, such as the marine environment, may present a durability problem, as they become vulnerable to corrosion. Prestressed concrete poles typically employ a small concrete cover to protect the underlying steel reinforcement. The small cover, which seldom exceeds one in, is used to ensure lighter weight poles that can be easily transported and erected in the field. On the other hand, high-strength prestressing steel, which is commonly being used in the form of 7-wire strands, is highly susceptible to corrosion, as compared to mild steel reinforcement. The corrosion issue in prestressed concrete poles in aggressive environments is a problem that must be contended with to ensure their long-term life and durability.

Prestressed spun concrete poles are generally designed using ultimate strength principles. While deflections are controlled and checked as part of the design, utility companies usually do not impose limits on the cracking of the concrete, and service loads are usually not well defined. As a result, it is conceivable that concrete poles will have cracks during under normal service loads. While this should not pose a problem under normal service conditions, it could be harmful in aggressive environments. Cracks in concrete will exacerbate the corrosion of the steel reinforcement if poles are present in aggressive environments. While cracking of the concrete can be controlled, it usually re-

sults in larger diameter poles that are heavy and difficult to handle. Corrosion of the steel reinforcement could reduce the structural capacity of the concrete pole, rendering it unable to perform its design function in extreme cases.

Proposed solutions to corrosion have included galvanized reinforced steel, polymer concrete, and epoxy coated bars. Unfortunately, galvanized reinforced steel loses its corrosion protections due to an electrolytic reaction between the steel and the zinc-based coating. Polymer concrete is not compatible with steel reinforcement because of the large difference in their thermal properties. Epoxy coating bars are used widely today in spite of serious concerns about damage from nicks and scratches, leading to corrosion concentrations and questionable bond properties. These facts demonstrate a genuine need for new forms of reinforcement (Toutanji and Saafi 1999).

It is obvious that corrosion will eventually force the replacement of the pole, which is very costly. Studies have shown that the replacement cost of a deteriorated pole is considerably higher than the initial cost of the pole. For example, the service life of the electric line is dependent upon the service life of the poles supporting it. Even if repair and protective measures are employed to extend the life of the structure, they could be costly and time consuming.

A new type of reinforcement that can provide the desired structural characteristics and at the same time address the issue of corrosion is needed. Such a technique could replace traditional steel reinforcement, reduce maintenance costs, and increase the service life of the structures.

Most CFRP reinforcing bars are stronger than prestressing steel, allowing them to replace prestressing steel without compromising the structural capacity of the pole. A

CFRP pole will be at least as strong as a steel reinforced pole but also immune to corrosion.

1.3 Objectives

The main objectives of this study are:

1. Perform an extensive literature review to assess the state-of-the-art use and design of concrete structures reinforced with CFRP.
2. Manufacture spun concrete poles using CFRP reinforcement as a substitute for conventional prestressing steel reinforcement.
3. Investigate analytically and experimentally the flexural behavior of spun concrete poles reinforced with CFRP bars.
4. Develop a finite element model that can accurately predict the structural response of spun concrete poles reinforced with CFRP bars.
5. Provide recommendations to the American Concrete Institute (ACI) and the Precast Prestressed Concrete Institute (PCI), who are concerned with the design of concrete structures, by studying the design and analysis of concrete non-rectangular sections reinforced with FRP bars.

1.4 Methodology and Approach

A detailed plan was developed, through which the following tasks were accomplished:

1. Experimental Program: The program was designed to address the flexural behavior of spun concrete poles reinforced with CFRP. The flexural behavior of

the CFRP poles was evaluated in terms of load deflection curves, cracking moment, ultimate moment capacities, and strains in the concrete and reinforcement. These terms were determined from the cantilever loading tests performed on CFRP prototype specimens. Two sets of four prototype specimens were tested. Each set of specimens was reinforced with a different reinforcement scheme using CFRP bars, while all other variables were kept constant.

2. Analytical Program: The main objective of the analytical program was to predict the behavior of the spun concrete poles reinforced with CFRP prior to testing, and to compare the results obtained from this study with the experimental one. Primary design equations to estimate the flexural capacity of the poles were developed based on equations available in the literature, as well as the design guidelines for concrete poles and for concrete structures reinforced with CFRP.
3. Finite Element Modeling: Finite element modeling was performed using the ANSYS software. The SOLID 65 element of the ANSYS specifically designed to model the 3D-reinforced concrete elements with its special cracking and crushing capabilities was used to model the tested poles. The objective of this work was to develop a finite element model that improves our understanding of the behavior of poles reinforced with CFRP bars under loading conditions.
4. Analysis of Results: A comparison of the results from the experimental, analytical, and finite element results was performed, focusing on the flexural behavior of spun concrete poles reinforced with CFRP. In addition, a compar-

tive study was performed between the experimental results of the CFRP poles and the theoretical results of conventional spun concrete poles having the same cross-section area, reinforcement ratio, and prestressed with steel strands.

1.5 Organization of the Dissertation

This dissertation consists of seven chapters. Chapter 1 is an introduction that discusses the background of the problem and presents the objectives of this research work and the methodology used to approach these objectives. Chapter 1 ends with the organization of the dissertation and a very brief introduction to each following chapter.

Chapter 2 reviews the properties of centrifugally cast concrete, provides a historical background on concrete poles and FRP reinforcement, and reviews the properties of CFRP reinforcement.

Chapter 3 presents the experimental program conducted through this study. The chapter describes the test setup, instrumentation, and procedure, and provides a summary of the results.

The analytical study is presented in chapter 4, which focuses on two main topics: the development of the flexural design equations based on an analytical model, and a spread sheet designed to incorporate the flexural design equations and provide quick solutions.

Chapter 5 presents the finite element analysis of the tested specimens. The types of elements used to model the concrete and CFRP bars, as well as the modeling of the

material properties of concrete and CFRP bars, are explained. The results of the finite element analysis are graphically summarized.

A comparison of the experimental, analytical, and finite element studies is given in chapter 6. The results of the various studies are compared and discussed.

Finally, Chapter 7 presents a summary of the work performed and the conclusions. Recommendations for future work are also provided.

CHAPTER 2

LITERATURE REVIEW

2.1 Introduction

FRP are formed of strong, stiff reinforcing fibers relatively abundant in nature, such as carbon, glass, or aramid, in tough and resilient polymer matrices, commonly referred to as resins, such as polyesters, vinyl esters, epoxies, or phenolics. The matrix resin generally accounts for 30% to 40%, by volume, of a composite material. In addition to maintaining the shape of the composite structure, aligning the reinforcement, and acting as a stress transfer medium, the matrix protects the fibers from abrasion and corrosion. FRP shows immense potential as a construction material due to its high strength-to-weight and stiffness-to-weight ratios, adaptable performance through anisotropy, light weight, corrosion resistance, and potentially high environmental durability.

This chapter reports on the application, use, and design of structures with FRP reinforcement. The limited literature on CFRP in spun concrete poles is identified and discussed.

2.2 Demonstrations and Field Applications

The successful implementation of advanced composite materials in civil infrastructure depends on the development of new structural concepts and systems that combine these new materials with conventional construction materials, such as concrete and

steel. Under this premise, Seible et al (1999) developed two design and construction systems for bridges using FRP reinforcement, the carbon shell system for short spans and the hybrid tube system for medium span modular bridges. The carbon shell system for short spans was used in the design of one of the two parallel structures of the Kings Stormwater Channel Bridge that was built along a California state highway near the Salton Sea. The design of the carbon tubes provides carbon fibers in the longitudinal tube direction for member bending stiffness and in the transverse direction for shear and concrete confinement reinforcement. The hybrid tube system for medium-span modular bridges was used in the Gilman Advanced Technology Bridge of the Interstate 5 in La Jolla, California. The bridge is a 450-ft-long dual-plane fan-type cable-stayed bridge supported by a 190-ft-high A-frame pylon. This system uses hollow E-glass, carbon, vinylester beams connected to a polypropylene fiber reinforced concrete deck system.

Six bridge superstructures in Canada have FRP reinforcements (Erki 1999). Two of these were new construction with concrete girders pretensioned with FRP tendons, three were composite bridges from concrete and steel whose decks were replaced by decks partially reinforced with FRP bars and grids, and one was designed as a stressed log bridge using FRP tendons.

The City of Calgary's Beddington Trail Bridge was completed in November 1993. The two-span, continuous skew bridge consists of precast, prestressed concrete girders in each span. Of the 26 girders, six were prestressed using two types of carbon fiber reinforced polymer tendons, and the continuity of the two spans was achieved using post-tensioned steel tendons over the entire length of the bridge. The bridge design ensured that the girders with FRP tendons would have identical behavior to those

prestressed with steel tendons under service loading conditions. Provisions for safety and continued performance of the bridge were made in the design. These included placing the FRP tendons in three layers to give a progressive warning of distress and providing detailing in the girders for an optional external prestressing system. Optical sensors on the FRP tendons monitor the bridge behavior. Measurements were made in November 1999, and no structural problems were detected (Tennyson et al. 2001).

The Taylor Bridge, Headingley, Manitoba, opened in October 1997, is a two-lane, 550-ft bridge having five equal spans. Straight and draped carbon fiber reinforced polymer tendons were used for prestressing of four 70-ft span girders. Carbon fiber reinforced polymer stirrups were used for shear reinforcement of two main girders, carbon fiber reinforced bars were used to reinforce a portion of the deck slab, and glass fiber reinforced polymer bars were used to reinforce a portion of the barrier wall. Experimental multiplexed fiber-optic sensors were installed to monitor bridge traffic and loads. No data have been published yet regarding the structural performance of the bridge (Tennyson et al. 2001).

2.3 FRP Reinforcement Design Guidelines in the United States

Several national programs define the design guidelines and testing protocols for FRP reinforcement in concrete structures. In the United States, the ACI has presented several technical reports for the design, construction, and repair of concrete structures using FRP reinforcement. One of these reports is the ACI 440.1R-03 committee report (ACI 440.1R-03), which provides recommendations for the design and construction of FRP reinforcement based on the knowledge gained from worldwide experimental re-

search. The report also presents the material characteristics of the commercially available FRP reinforcing bars. Flexural and shear design procedures and detailing for concrete structures reinforced with FRP reinforcement are presented in this report. This report includes very useful information on the design of concrete structures reinforced with FRP bars. A major limitation of the report is that it addresses structures with rectangular sections with a single layer of one type of FRP reinforcement, but no information is given on circular cross-sections.

2.4 FRP in Reinforced and Prestressed Concrete Applications

Lees (2001) reviewed the recent developments in the use of FRP in reinforced and prestressed concrete applications. The influence of FRP material properties on the design of concrete structures is considered, and applications are discussed in conjunction with the structural function of the FRP reinforcement. Examples of the practical implementation of the technology were included in the review, and a number of future considerations needs were identified.

Applications discussed ranged from the use of the CFRP tendons as bridge cables in Switzerland to CFRP shear stirrups in bridge decks in Canada, from carbon fiber prestressed piles in the USA to glass fiber reinforced polymer (GFRP) shotcrete reinforcement for underground petroleum storage facilities in Japan, and from GFRP reinforced barrier walls in Canada to bridge beams with internal CFRP prestressed tendons in the USA.

Lees concluded that, with a greater use of FRPs, economies of scale would contribute to reducing the cost of the materials. The establishment of optional supply chains

would also play a role. Lees raised an additional question regarding whether it is more important to establish the market share for FRPs or to have individual manufactures focus on their particular products. This is connected to a growing awareness of the need for standardization within the FRP market. At the moment, each company produces and markets its particular product. However, there can be great variation in such parameters as constituent materials and manufacturing methods, which hinders the extrapolation of one set of test results to another product.

2.5 Flexural Behavior of Concrete Beams Reinforced with FRP

Shahawy et al (1996) presented the results from an experimental investigation of the feasibility of using aramid fiber tendons, sold under the commercial name of ARAPEE, as prestressing strands in concrete bridge girders. The result of this study showed that the girders were able to exhibit excessively larger deformations in the post-cracking stage with an excellent deformation recovery of about 95% upon removal of applied load, which corresponds to about 80% of theoretical ultimate load. The author reported that the average measured prestress losses immediately after prestress release were approximately 11%, and the transfer length for rectangular ARAPEE tendons was determined to be in the range of 12 – 18 in. The author recommended that the development of a suitable anchorage system is essential to effectively using the ARAPREE tendons.

Pisani (1998) performed a numerical investigation of the behavior of beams prestressed with FRP cables and concluded that the non-linear behavior of concrete and an elastic modulus of the prestressing tendons much smaller than that of steel could prevent brittle behavior of a beam prestressed with GFRP or aramid fiber reinforced poly-

mers (AFRP) cables. The beam behavior and its load carrying capacity do not markedly change when substituting GFRP or AFRP cables with steel. Based on this conclusion and the mechanical and chemical properties of these materials, Pisani confirmed that GFRP or AFRP tendons could satisfactorily replace steel strands for the prestressing of beams placed in unfavorable environments. Pisani also concluded that GFRP cables are reliable for external prestressing, while AFRP cables are more suitable for bonded prestressing construction. Finally, Pisani recommended a significant research work to investigate both the mechanical and chemical properties of FRP reinforcement in more depth and to design reliable, durable anchorages. Pisani also recommended setting rules that determine and certify all of the properties of FRP commercial products already available on market to avoid incomplete and sometimes incorrect information about these products. Pisani's recommendation for designing reliable, durable anchorages conform with the recommendation of Shahawy et al (1996) that a suitable anchorage system be developed to effectively use ARAPRE tendons in prestressed applications. Pisani's recommendation for determining and certifying all of the properties of FRP commercial products conforms with the recommendation by Lees (2001) to establish the market share for FRPs material in order to standardize the FRP product.

Saafi and Toutanji (1998) carried out a series of flexural tests on beams with bonded or unbonded rectangular bars, or with additional regular reinforced bars, in order to improve the ductility of fiber reinforced prestressed beams. This study showed that the flexural capacity of the unbonded, prestressed concrete beams was lower than that of bonded beams; it also showed that the use of unbonded, prestressed AFRP significantly improved the ductility of the prestressed beams and decreased the number of cracks. The

study concluded that aramid fiber reinforced polymer composite rectangular bars have potential as reinforcement for concrete structures and recommended more tests to help confirm these results.

Furthermore, Toutanji and Saafi (1999) presented a new reinforcement method to avoid the brittle failure of concrete beams prestressed with AFRP tendons. The reinforcement consisted of a combination of non-tensioned and prestressed rectangular tendons. The results in this paper confirmed those of Saafi and Toutanji (1998).

Toutanji and Saafi studied the transfer length of the AFRP rectangular tendons in this paper, and it was found to be about 18 in, but since it was based on a limited number of tests, the author recommended more experimental data to develop a guideline design. Since this study used the same AFRP tendons used in the study of Shahawy et al (1996), the results of these studies could be compared, and it could be seen that the value of the transfer length obtained from Toutanji and Saafi (1999) was in the range proposed by Shahawy et al (1996). Although the transfer length was in the upper range proposed by Shahawy et al (1996), the consistency in the results was apparent and strengthens both studies.

Stoll et al (2000) performed a program in which full-scale FRP prestressed and reinforced high strength concrete bridge beams were designed, fabricated, and tested. This program provided a single-point assessment of the applicability of current design methods to FRP prestressed and reinforced concrete beams. Stoll et al observed the inconsistencies in the way characteristic strength values are established by commercial producers of CFRP tendons. In addition, the computed ultimate strength of the CFRP tendons used in this program was 33% greater than the value the manufacturer quoted. This result con-

forms to the results reported by Pisani (1998) and Lees (2001). The extensive cracking and large deflections before failure of the tendons exhibited by the tested beams were observed. These cracking and deflections occurred at load levels that correlate well with analytical predictions based on the calculated effective tendon strength. Stoll et al related the lower loading values where tension cracking occurred to either the under-estimation of the prestressing losses or the modulus of rupture of the high strength concrete being lower than the value predicted by AASHTO equations. It was concluded that the practice of linking CFRP tendons to steel cables during pretensioning can induce large twisting deformations in the CFRP tendon, as the steel cable untwists during tensioning, causing strength reduction stress concentrations where the CFRP tendon exits the grip. The authors recommended that fabrication handling and safety procedures must be scrutinized as CFRP prestressing tendons are adopted, because casual handling practices that are inconsequential with steel cables can damage CFRP tendons. It was also suggested that design relationships used for steel shear reinforcement may need revision for application to glass fiber reinforced polymer products.

Dolan and Swanson (2002) examine the overall development of a comprehensive theory for the strength of FRP tendons at various structural depths. Following the theoretical development, a comparison was made of the actual and predicted strength of three beams. Detailed equations were used to determine the flexural capacity of carbon fiber reinforced polymer prestressed beams with vertically distributed tendons. A premature failure in the straight reinforcement compromised the possibility for a direct comparison of the predicted strength and deflections with the experimental. When corrected for the apparent loss of tendon section, the predicted results correlated well with the experimen-

tal data. Theoretical flexural capacities were calculated with a simplified equation for tendons in a single layer and an equation for vertically distributed tendons. A comparison between the two theoretical capacities is within 1%. The primary difference between the two is how the location of the reinforcement tensile force is evaluated. The simplified method uses the centroid of the reinforcement, while the vertical distribution method accounts for the individual reinforcement locations.

Grace et al (2003) presented a study on the fabrication, instrumentation, and flexural testing of a full-scale double-tee (DT) beam, prestressed using bond prestensioned CFRP tendons and unbonded carbon fiber composite cable (CFCC) post-tensioning strands. The beam was designed to simulate the performance of the DT beams used for the construction of the three span Bridge Street Bridge. In addition, the response of the tested beam was theoretically evaluated. Grace et al (2003) noticed that the tested beam had significant reserve strength beyond the service load, and the combined internal and external prestressing forces induced the designed compressive strain in the cross-section. They also observed significant cracking prior to the failure of the tested beam; however, neither the external unbonded CFCC post-tensioning strands nor their anchors ruptured. Finally, the experimental results were very close to the theoretical values, especially under service load conditions.

Jeong (1994) dealt with the ductility of concrete members prestressed with FRP tendons. The work included experimental and analytical programs that led to a new method for defining, predicting, and improving the ductility of prestressed concrete members. Four under-reinforced T-beams and four over-reinforced rectangular beams, fully and partially prestressed with carbon fiber tendons, were subjected to four-point

loading tests. The fully prestressed T-beams showed a very brittle behavior. The partially prestressed T-beams showed more ductile behavior. This ductile behavior is due to the addition of non-prestress reinforcement bars, which help to increase the inelastic energy. Tests on the rectangular beams showed that an over-reinforced beam could achieve substantial ductility, provided that the ductility of the matrix is improved. A computerized parametric study was performed to investigate several methods to improve structural ductility. The parametric study conformed to the experimental work, and both showed that improving the ductility of concrete members reinforced with prestressed FRP tendons could be achieved by changing the reinforcement ratio, confinement of the members by means of stirrups, adding fibers to the concrete mix, and partially prestressing the concrete members by means of adding non-prestressing reinforcement. This later conclusion was later approved by Saafi and Toutanji (1998), as discussed in the previous section. Jeong proposed a new ductility index and design guide lines to estimate the nominal moment and the resistance factor for the design of concrete beams prestressed with FRP tendons.

Abdelrahman and Rizkalla (1999) introduced two simplified methods to calculate the deflection of concrete beams partially prestressed with CFRP under short-term and repeated loading. They also examined the applicability of current approaches to calculate the deflection, and a mathematical formula to calculate the location of the effective centroid of cracked sections prestressed with CFRP was presented. The author concluded that the prediction of the deflection, using either the integration of the curvature along the beam span or the proposed simplified method, was found to be in good agreement with the measured deflection. The behavior of concrete beams prestressed with CFRP under

repeated load is similar to that for beams prestressed with steel, provided that the steel is in the elastic stage before unloading. The method proposed to calculate the deflection of beams prestressed with CFRP bars under repeated loads was found to be in close agreement with the measured values.

Zou (2003a) reviewed the methods for evaluating the ductility indices and proposed a new method to evaluate the ductility or deformability of beams prestressed with FRP or steel. This method was verified by numerous test results, either from the author or in the literature. Of these methods evaluated was the method proposed by Jeong (1994). Zou indicated that the development of deflection from a cracking stage to an ultimate stage is a necessary measurement of deformability. Zou concluded that there is a need to consider not only the ratio of deflection at the ultimate limit state to that at the cracking state, but also the ratio of the moment at ultimate to moment at first cracking, in the estimation of deformability of prestressed concrete beams. Zou proposed a deformability factor that depends not only on the equivalent deformation of the uncracked section and the deformation at the ultimate state, but also on the ratio of ultimate load carrying capacity to cracking load. Zou concluded from that the conventional ductility index for concrete beams with steel reinforcement is not suitable for beams with FRP reinforcement. Zou stated that the use of the ratio of total energy to elastic energy, proposed by Jeong (1994), as the ductility index for beams prestressed with AFRP or CFRP is almost a constant and does not distinguish between beams of different deflection and deformability. On the other hand, using the deformability factor as the ratio of the deflection at the ultimate limit state to the deflection of the equivalent uncracked section gives a reasonable indication of deformability for beams prestressed with FRP. From the experimental analysis

and results, and from the data available in the literature, Zou verified the proposed equation for calculating the deformability of prestressed concrete beams using an overall deformability factor for both FRP and steel tendons.

Zou (2003b) tested six full-scale beams with rectangular cross-sections to verify the methods presented for predicting the short-term and long-term time-dependant deflections of fully or partially prestressed concrete beams with fiber reinforced polymer tendons under sustained bending moment and axial force. From the experimental results, Zou concluded that beams prestressed with FRP tendons, including CFRP and AFRP, performed in a manner similar to those with steel tendons, and the long-term deflections generally give satisfactory performance under the serviceability limits. He also concluded that it is important to include concrete tension stiffening in deflection calculations, since calculations without concrete tension stiffening overestimate the deflection.

2.6 Characteristics of CFRP Reinforcement

CFRP materials have many characteristics that make them different from other structural materials. These characteristics have helped CFRP to become a widespread replacement for steel reinforcement. Specific properties of CFRP can vary from one manufacturer to another; however, there are some properties that are common to all CFRP materials.

From the extensive literature review performed by Lyons (2003), the characteristics of CFRP can be summarized as follows:

- CFRP experienced loss of strength and material properties when exposed to severe environments, but considerably less than the loss of properties experienced by traditional steel strands under similar conditions.
- CFRP has a higher potential than both carbon steel and stainless steel, and the difference in potential between CFRP and carbon steel is ten times greater than the difference in potential between CFRP and stainless steel, which will result in higher corrosion rates of carbon steel than corrosion rates of stainless steel when getting in contact with CFRP.
- The difference in thermal expansion between CFRP and concrete did not result in significant detrimental effects.
- Although CFRP has a linear behavior up to failure, concrete members reinforced with CFRP showed a sufficient amount of deflection and cracking, making up for the lack of plasticity of the brittle CFRP reinforcement.

2.7 Historical Development and Use of Spun Concrete Poles

Fouad et al (1992) studied the historical development of spun concrete poles and reported that the first concrete poles were used in Germany in 1856, that concrete poles of round and square solid cross-sections were made in 1867, and that, the first spun concrete pole reinforced with mild steel was produced in Germany in 1907. In the mid 1930s, prestressed concrete poles were designed and constructed in Algeria by Freyssinet, who is regarded as the father of prestressed concrete.

After World War II, the usage of prestressed concrete poles flourished throughout Europe, and in the mid 1950s, the first spun concrete pole was produced in Europe.

Concrete poles were first introduced in the United States in the 1930s; however, prestressed spun concrete poles were not used until the mid 1950s. In 1967 Virginia Electric Power Company (VEPCO) initiated a research program that culminated in the development and production of the first spun tapered prestressed concrete pole for use by electric utilities in the United States. Since that time, the use of these structures by VEPCO and other utilities has grown steadily, and today the spun prestressed concrete pole has become a very popular alternative for electric utility companies across the United States (Fouad et al 1992).

2.8 CFRP in Spun Concrete Poles

CFRP has been used widely in reinforcing and prestressing concrete bridges, and it is gaining acceptance from governmental organizations because of its high corrosion resistance and low maintenance costs. However, few applications of CFRP to spun concrete poles have been demonstrated. In September 2000, the world's first CFRP prestressed high strength concrete electricity pylon was installed in Switzerland (Terrasi et al 2001). The 90-ft-high pole was manufactured using a centrifugally cast high strength concrete containing blended silica-fume cement. In March 2003, a 27-ft-high prototype lighting column was erected in the car park of a spun concrete production plant in Lenzburg, Switzerland (Terrasi and Lees 2003). The pole was reported to weigh 770 lbs, representing a weight loss of about 30% when compared to the conventional steel reinforced concrete lighting pole. In addition, the total material, production and installation costs were equal to that of an equivalent steel-prestressed concrete pole (Terrasi and Lees 2003).

Terrasi and Lees (2003) studied the bending, torsion, and shear behavior of CFRP prestressed concrete lighting columns. Five CFRP prestressed concrete lighting columns with a nominal height of 27.0 ft were designed according to European standards and subjected to full-scale testing. The poles were prestressed with six CFRP tendons 0.16 in in diameter. Three poles were reinforced with three different types of shear reinforcement.

The poles were designed to be fully prestressed at the maximum service load to limit the deflections. The tip deflection under wind load was limited to a calculated value of 0.8 in, and the ultimate moments of resistance were predicted. The poles were fixed at the butt and subjected to horizontal-point-load testing. The results of this study showed that the bending, torsion, and bending/torsion behavior of the tested poles were satisfactory and complied with European standards. The poles also showed sufficient bending rotation capacity to make up for the lack of plasticity of the brittle CFRP prestressing tendons. This study showed that the different types of CFRP shear reinforcement had no significant effect on the shear behavior of the poles.

Lyons (2003) performed a theoretical study to determine the structural feasibility of designing CFRP prestressed spun cast concrete poles for transmission line support and to examine the potential benefits of such designs over traditional steel prestressed poles. Lyons developed design procedures for CFRP and steel prestressed spun concrete poles for transmission line support. Lyons found that the bursting stresses have a significant effect on the allowable pole wall thickness, which greatly affects pole weight. If the prestress level in the strands is adjusted below the maximum of 75%, the reduced bursting stresses may result in thinner pole walls. This study concluded that CFRP prestressed spun cast concrete poles are structurally feasible, and the use of CFRP prestressing rein-

forcement will allow the code requirement of minimum wall thickness to be removed, resulting in thinner, lighter poles. Finally, this study observed a pole weight reduction of up to 37% through the use of CFRP as a replacement to the traditional prestressing steel reinforcement. Although these results are valuable, the study lacks the experimental work necessary to strengthen the results and the design procedure proposed. Moreover, the interaction diagrams developed in this study for designing prestressed spun concrete poles raise questions, because most of the design of spun prestressed concrete poles indicates that flexural capacity is the major concern and that the effect of the compression force is minor.

2.9 Properties of Centrifugally Cast Concrete

The concrete in centrifugally cast products, such as poles or pipes, is subjected to very high centrifugal force by the spinning operation. These forces provide centrifugal compaction to the concrete and expel excess water in the mix. As a result, the hardened concrete is exceptionally dense and of higher strength. The high strength is attributed mainly to the lower water/cement ratio present in the concrete after spinning. The spun concrete also exhibits improved permeability characteristics, since the overall porosity of the material is significantly reduced.

Fouad H. Fouad (1988) performed experiments to study certain physical and mechanical properties of centrifugally cast concrete and compare them to the corresponding properties of conventionally cast material by investigating compressive strength, modulus of elasticity, permeability, and absorption. About 600 concrete specimens, representing over 120 batches of concrete, were tested. Based on this research, the properties of centri-

fugally cast concrete compared to conventional casting concrete could be summarized as follows:

- Higher compressive strength.
- Higher modulus of elasticity.
- Higher density.
- Lower water/cement ratio.
- Lower permeability.
- Lower absorbability.

2.10 Summary

The literature review shows that concrete structures reinforced with CFRP have satisfactory flexural behavior and were able to produce sufficient deflection and cracking before failure to account for the lack of plasticity of the brittle FRP material. The literature review also shows that the existing equations for the design of concrete structures reinforced with the traditional steel may be modified to build new equations for the design of concrete structures reinforced with FRP. The literature pointed to the importance of the anchorage system for FRP prestressed applications. Prestressing FRP is impracticable if a well-designed anchorage system is not available.

CHAPTER 3

EXPERIMENTAL PROGRAM

3.1 Introduction

The main objective of the experiments was to study the flexural behavior of spun concrete poles reinforced with CFRP bars. In order to achieve our objectives, the experimental program consisted of producing and testing four prototype pole specimens. The specimens were divided into two groups, with each group composed of two identical specimens. Both groups of specimens were identical except for the reinforcement scheme. One group had 6 CFRP longitudinal bars, and the second group had 12 CFRP longitudinal bars. A CFRP grid for the spiral reinforcement was used on the second pole in each group.

3.2 Test Preparation

3.2.1 Material of Concrete Mixture

A specially formulated high strength concrete mix for spun concrete poles was produced by the batch plant of Valmont Newmark Company. The 28-day compressive strength of this mixture is about 11,000 psi. Ordinary Portland cement (ASTM type I) was used for all of the specimens, with a specific gravity of 3.15. Crushed limestone aggregate was used, with a maximum aggregate size of 5/8 in and a specific gravity of 2.79 and two types of fine aggregates were used. The first type of fine aggregate was natural

sand, with a specific gravity of 2.68, and the second type was manufactured sand, with a specific gravity of 2.59. The liquid admixture used was Master Builder R1000 superplasticizer with a dosage rate as recommended by the manufacture.

3.2.2 CFRP Bars

The CFRP bars used in this study were provided by Hughes Brothers Inc. under the commercial name of Aslan 200 (Figure 1). Aslan 200 is a solid rod specially treated to enhance the bond to Portland cement for new construction. The physical properties of the Aslan 200 used are listed in Table 1.



Figure 1. Aslan 200 CFRP rebar sample

Table 1

Physical properties of CFRP Aslan 200

Bar Dia. (in)	Cross-Sectional Area (in ²)	Nominal Diameter (in)	Tensile Strength (ksi)	Tensile Modulus of Elasticity (psi 10 ⁶)	Ultimate Strain (%)
#3	0.1010	0.362	300	18	1.7

3.2.3 CFRP Grid (C-GRID)

The CFRP grid used in this study was provided by TechFab Company under the commercial name of C-GRID (Figure 2). C-GRID is a high performance reinforcement made by bonding ultra-high strength carbon tows with epoxy resin in a controlled factory environment. The manufacture nomenclature for the C-GRID used is C50-2.9 x 2.9. The first letter “C” represents the type of fiber used in the grid, which is carbon in this study; the second two digits, 50, represent the grid series number. The grid series number indicates the relative size of the carbon strands in both the longitudinal and transverse directions. The last two numbers, 2.9 x 2.9, indicate the mesh size of the grid, so in our study we have a square mesh of 2.9 in each way. Table 2 shows typical C-GRID properties, and Table 3 shows the physical properties of the CFRP strand in the C-GRID.



Figure 2. C-GRID CFRP grid sample

Table 2

Typical properties of CFRP C-GRID

Grid Designation	Longitudinal Properties		Transverse Properties	
	Strand Spacing (in)	Grid Strength (kips/ft)	Strand Spacing (in)	Grid Strength (kips/ft)
C50-2.9x2.9	2.9	4.9	2.9	3.9

Table 3

Strand physical properties of CFRP C-GRID

Grid Designation	Tensile Strength (ksi)	Tensile Modulus of Elasticity (psi 10 ⁶)	Ultimate strain (%)	Longitudinal Cross-sectional Area (in ²)	Transverse Cross-sectional Area (in ²)
C50-2.9x2.9	340	34	1.0	0.0036	0.00312

3.2.4 Specimens Dimensions and Reinforcement Details

Four specimens 20-ft-long were tested to study the flexural behavior of the spun concrete poles reinforced with CFRP. All of the specimens were identical in geometry. Specimens had an outer diameter of 8.91 in and 13.23 in for the tip and butt, respectively, with an outside slope of 1.8% (0.216 in/ft). The inner diameters were 3.91 in and 7.75 in for the tip and butt, respectively, with an inside slope of 1.6% (0.192 in/ft). The wall thickness was 2.5 in and 2.74 in at the tip and butt, respectively. The dimensions of the specimens were chosen to fit the capabilities of the testing laboratory as well as the steel molds available for production. Additionally, the specimen dimensions were chosen to maintain easy transportation of the specimens from the production plant to the University of Alabama laboratory. The test was conducted in two groups, and each group consisted of two specimens. The only variable in these groups was the number of reinforcing bars.

The first group was designed to have 6 CFRP bars with a bar diameter of 3/8 in distributed almost uniformly around the poles' cross-sections. The second group was designed to have 12 CFRP bars with a bar diameter of 3/8 in distributed uniformly around the poles' cross-sections. Both groups were confined with steel spirals of bar diameter 3/16 in, a pitch of 3.0 in center to center, and a concrete cover of 0.75 in. The specimen's concrete dimensions are shown in Figure 3. Figure 4 shows the cross-sectional and reinforcement details of the two groups. Table 4 shows a summary for the experimental program and specimen details. In Table 4, the first two digits of the specimen ID represent the group number, and the second two numbers represent the specimen number.

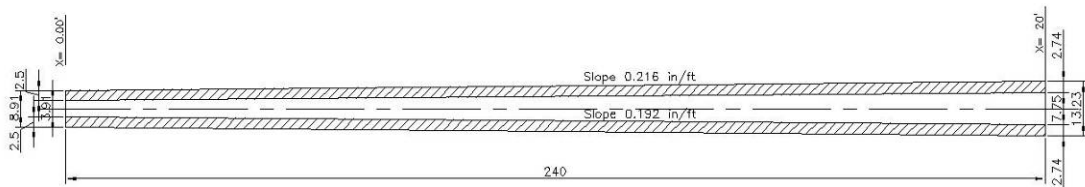


Figure 3. Specimen concrete dimensions

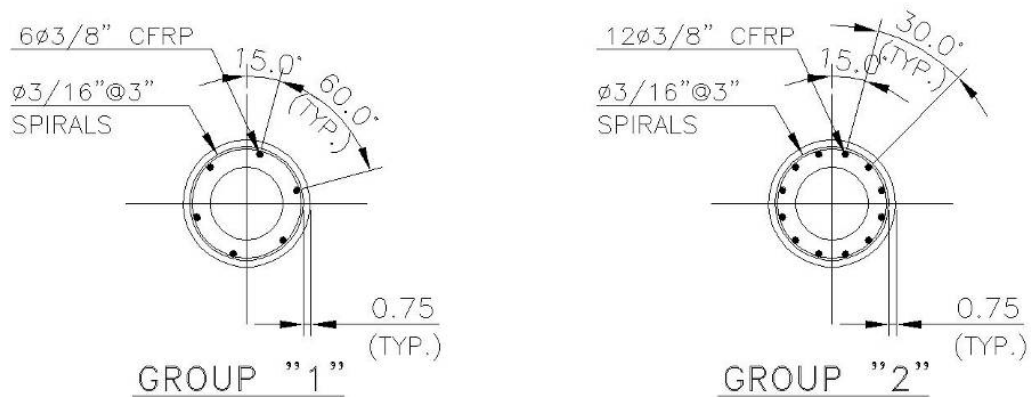


Figure 4. Specimen cross-sectional details

Table 4

Experimental program and specimen details

Group No.	Specimen ID	No. of Bars	Bar Dia. (in)	Bar Type	Stirrups RFT	Conc. Cover (in)	Pole Outer Dia. (in) At Tip At Butt	Pole Inner Dia. (in) At Tip At Butt	Pole Length (ft)	Conc. Strength (psi)
Group 1	G01-01	6	3/8	CFRP	#2 @ 3"	0.75	8.91 13.23	3.91 7.75	20	11,000
	G01-02									
Group 2	G02-01	12	3/8	CFRP	#2 @ 3"	0.75	8.91 13.23	3.91 7.75	20	11,000
	G02-02									

3.2.5 Manufacturing Process

The poles were manufactured on two different days at the Valmont Newmark production plant located in Tuscaloosa, Alabama. Two specimens, one from each group, were built on one day, and the two remaining specimens were built on another day.

The manufacture process starts by setting up the lower part of the concrete mold and cleaning and greasing it (Figure 5). As shown from Figure 6, four steel strands were added at 0°, 90°, 180°, and 360°, respectively, to hold the mold. These strands were prestressed to be kept in the exact location (Figure 7). In order to insure that these strands would not affect the behavior of the specimens, plastic pipes were added to these strands. The plastic pipes will prevent the bond between the concrete and the strands. Steel stirrups were added every 30 in to the inside of the existing steel strands to hold the strands and reinforcements in place during the spinning process, as shown in Figure 8. The main reinforcement of the specimens, consisting of 6 CFRP bars for the first specimen and 12 CFRP for the second specimen, was cleaned of any dust or impurities that might affect its bond with the concrete and then placed in its exact location and tied to the inside steel

stirrups. The spiral steel stirrups were then distributed all over the pole length with a pitch of 3.0 in, and tied to the pole reinforcement, as shown in Figure 9. Plastic chairs were placed between the concrete molds inner side and the stirrups' outer side to ensure a concrete cover of 0.75 in all over the pole length (Figure 10). After that, the mold was blown out with a blower to clean any dust and make it ready for concrete casting. The concrete was mixed in the batch plant of Valmont Newmark production plant, shown in Figure 11, and moved and cast to the concrete mold through a loader, as shown in Figure 12. During the casting process, the amount sufficient to build 10 concrete cylinders of 4.0 in diameter and 8 in length was taken, and the concrete cylinders were prepared and cured at the laboratory of the Valmont Newmark production plant (Figure 13). These cylinders were taken to determine the actual concrete strength used for casting the poles. After the concrete casting was finished, the upper part of the concrete mold was placed and bolted (Figure 14), and then the poles were moved to the spinning machine and spun, as shown in Figure 15. The specimens remained on the spinning machine for 10 minutes, with a revolution in the range of 250-300 rpm, where the concrete is subjected to a centrifugal acceleration about 20 times as great as the gravity acceleration. After the spinning process was finished, the specimens were moved from the spinning machine and kept for two days, until the concrete hardened, then the molds were removed and the concrete specimens cured for at least 28 days before testing.



Figure 5. Setting up the lower part of the mold and cleaning it

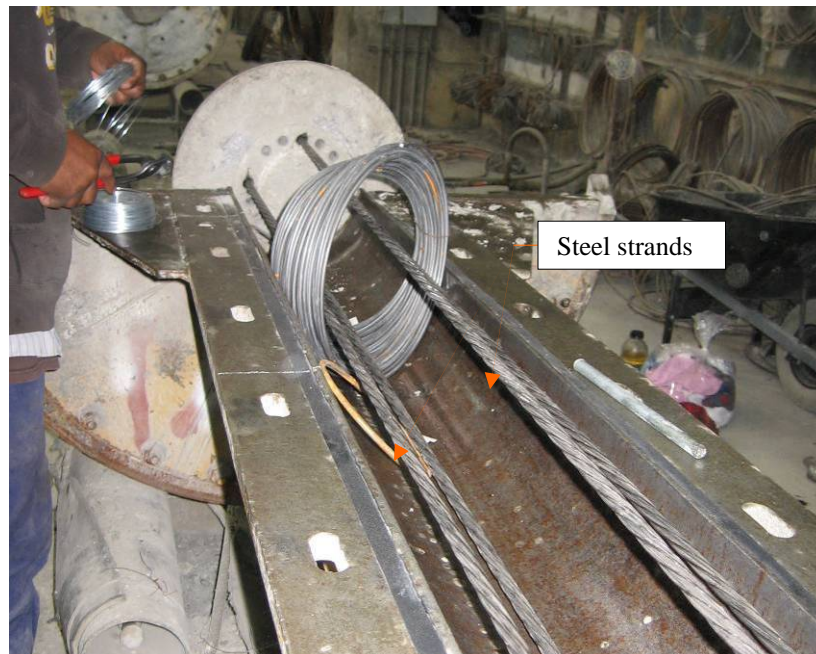


Figure 6. Adding the steel strands to hold the mold during spinning



Figure 7. Prestressing the strands to hold the mold during spinning

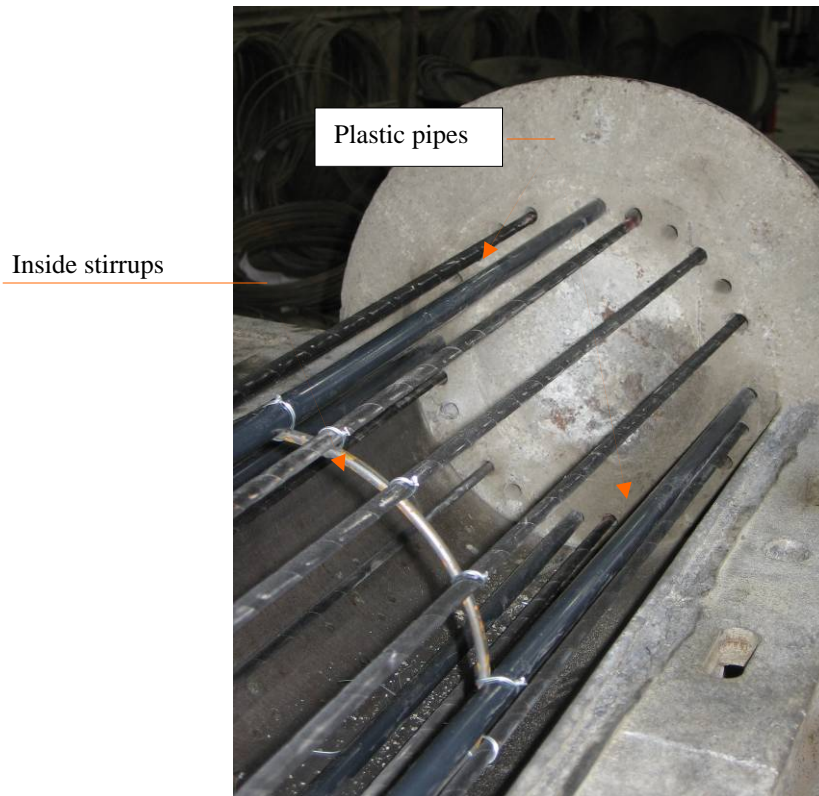


Figure 8. Adding the plastic pipes and the inside stirrups

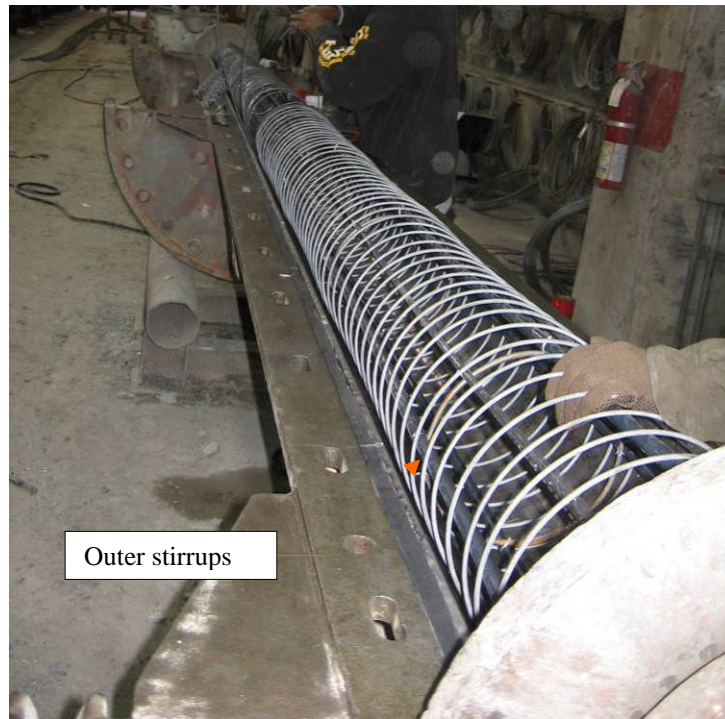


Figure 9. The outer spiral stirrups with a pitch of 3.0 in

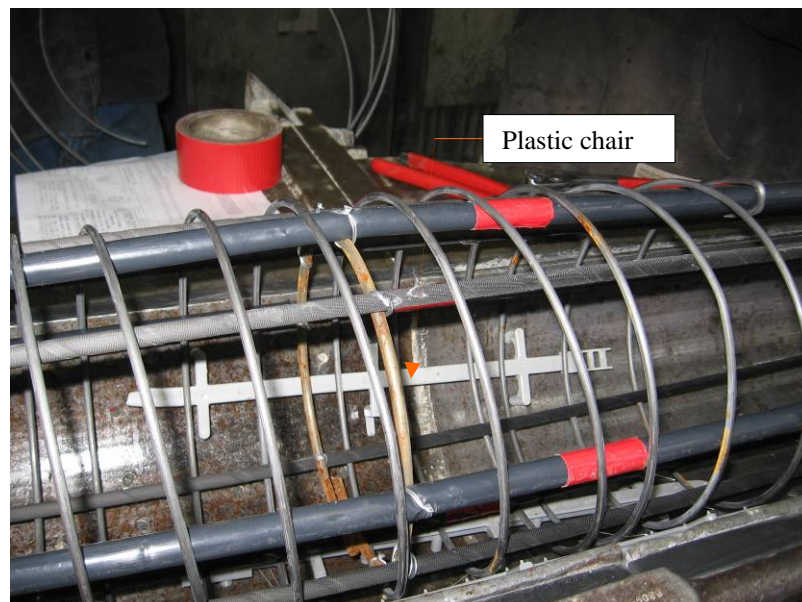


Figure 10. Plastic chairs to provide the required concrete cover



Figure 11. Concrete batch plant



Figure 12. Placing concrete into the open mold



Figure 13. Making the concrete cylinders for quality control testing



Figure 14. Placing the upper part of the mold and bolting it to the lower part



Figure 15. The steel mold on the spinner being spun

The remaining two poles were manufactured in the same way, except for the stirrups, where the CFRP C-GRID was used instead of steel wires. The C-GRID is available in rolls 42 in wide, representing the transverse direction, and 500 yards in length, representing the longitudinal direction. The roll was cut into six parts of variable length (Figure 16). Five parts were 42 in wide, while the last part was only 30 in wide. Table 5 shows the details of each part. The length of each part was calculated by subtracting two concrete covers from the outer diameter of the cross-section of the pole where the part starts, and the result was increased by 25% development. 25% was a conservatively estimate, to avoid bond failure of CFRP GRID. As shown in Figure 17, the C-GRID was placed into the mold where the longitudinal direction coincides with the circumferential

direction of the mold, whereas the transverse direction of the grid coincided with the longitudinal direction of the mold. The grid was placed in this way to have the longitudinal direction of the grid with the higher strength resist any force that might occur during spinning. The grid was then tied to the bars using plastic ties, as shown in Figure 17.

Table 5

Details of the C-GRID cutting list

Part Number	Bending Diameter (in)	Width (in)	Length (in)	No. of Pieces
1	8.06	42	31	2
2	8.70	42	34	2
3	9.50	42	37	2
4	10.22	42	40	2
5	11	42	43	2
6	11.73	30	46	2
Total		240	231	12



Figure 16. Cutting the C-GRID into six parts

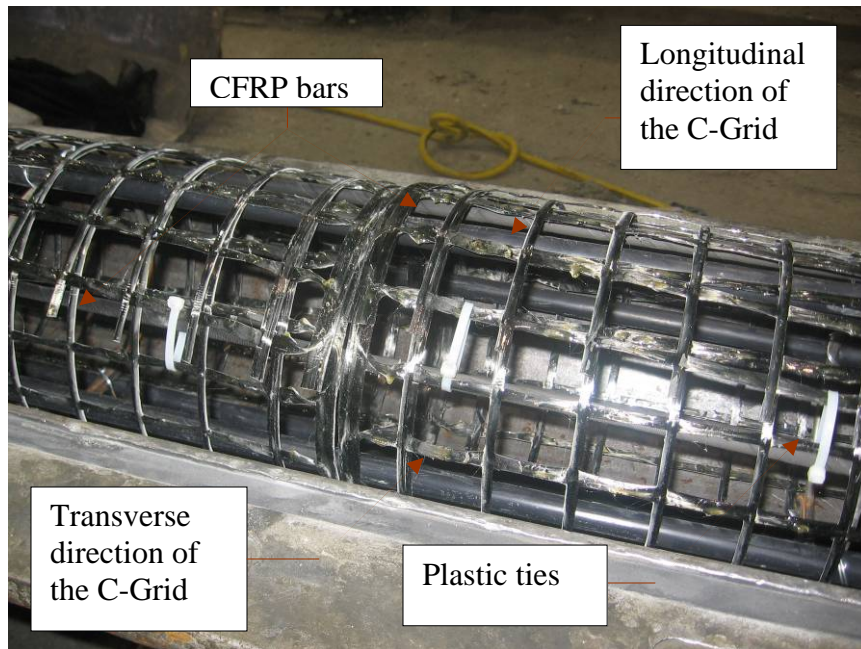


Figure 17. Tying the C-GRID to the bars using plastic ties

3.3 Test Setup and Instrumentation

The flexural behavior of the CFRP pole was evaluated in terms of load deflection curves, cracking moment, ultimate moment capacities, and strains in the concrete and reinforcement. A schematic diagram for the test setup is shown on Figure 18. The actual setup is shown in Figure 19 and Figure 20. The pole specimen rested on two supports. The first support was located at the pole's butt, and the second support worked as the fulcrum, located 3.0 ft from the pole's butt. This distance, 15% from the overall length of the pole, was chosen to represent the typical embedment length used in practice. The supports were designed and manufactured specifically to sustain the reactions from the load applied to the pole. The second support was fixed to the test frame through eight rated clamps, with four on each side, to prevent the support from moving upward during the

test, as shown in Figure 21. The two supports were equipped with two semicircular collars, on which the poles were placed and clamped (Figure 20) to restrain the poles against lateral movement.

The load was applied at a distance of 1.0 ft from the tip of the pole. The lever arm was 16.0 ft. The load was applied using a manual hoist chain connected to a tension load cell and hooked to the trolley crane of the laboratory, as shown in Figure 22.

Two groups of strain gages were installed along the circumference of the pole at distances of 6 in and 18 in from the second support, as shown in Figure 23. Each group of strain gages consisted of four strain gages located at the quadrants of the pole to measure the strain of the concrete during test life and up to the failure of the specimen.

The strain gages were purchased from Vishay Micro-measurements and designated as N2A-06-20CBW-120. The first three letters represent the gage series; the N2A series has a strain range $\pm 3\%$ and is recommended for stress analysis applications employing large gage patterns. Large gage patterns are recommended by the manufacturer for concrete structures and, in our case, were designated as 20CBW. The gage length is 2.0 in, and the gage resistance is 120 ohms, as indicated by the last three digits of the designation. The self-temperature compensation is a factor, depending on the type of alloy used in the manufacturing of the strain gages, and is represented by the fourth and fifth digits.

The deflection was recorded manually by means of a scale that was attached to the test frame near the tip of the pole, as shown in Figure 24, and the crack width was measured manually using concrete comparators, as shown in Figure 25. The strain gages

and the load-cell readings were recorded via a data acquisition system and transferred to the structural laboratory computer for analysis (Figure 26).

The data acquisition system is a System 5000 Data Acquisition System from Vishay. The System 5000 is a complete data system for stress analysis and structural materials testing and features unique operating software.

Data sheets were prepared before testing, one to record the deflection reading and the other was to record the crack width.

Two dial gages were installed at the supports of the poles' as shown in Figure 27, to record the movement of the poles' at the supports. This movement results from the support's lack of total fixation. The readings were used to correct the measured deflection at the tip of the pole.

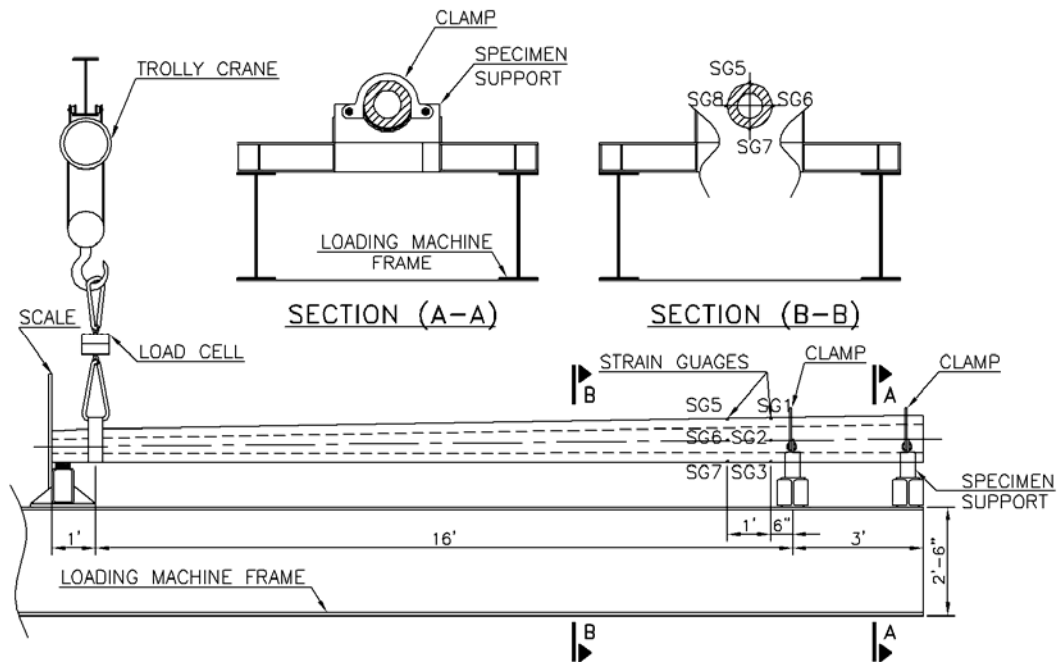


Figure 18. Schematic diagram showing the test setup



Figure 19. Test setup

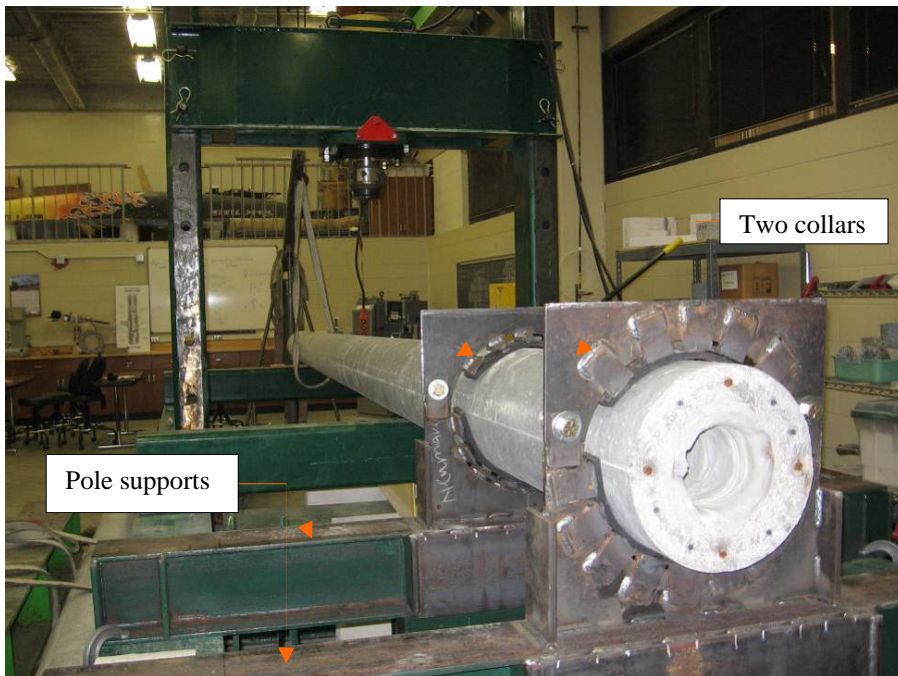
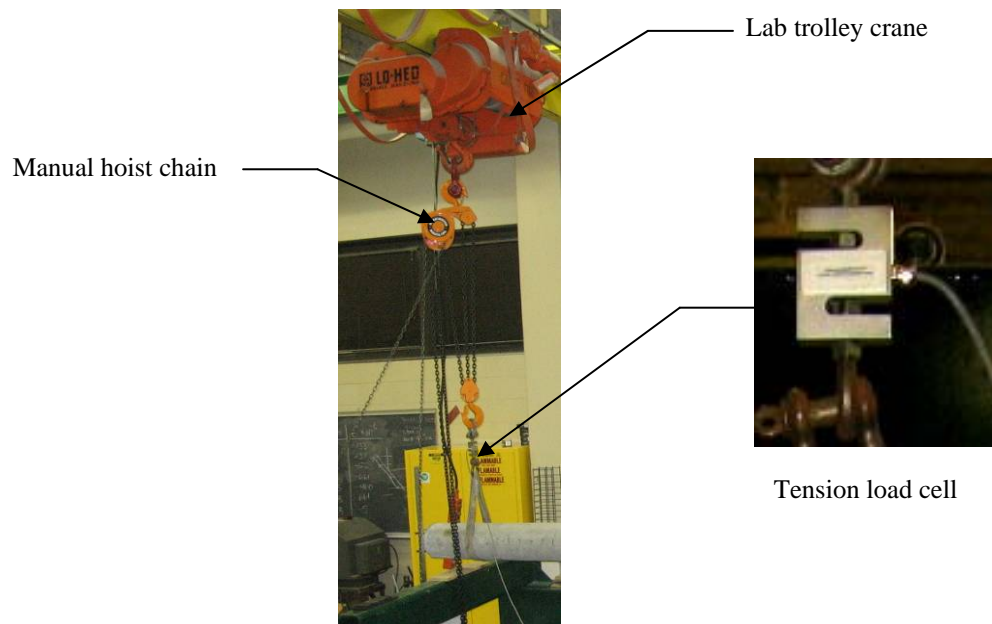


Figure 20. Details of pole end supports



Rated clamps to fix the beam to the loading machine while testing

Figure 21. The clamp fixation of the supporting beams



Manual hoist chain

Lab trolley crane

Tension load cell

Figure 22. The loading system at pole tip end



Figure 23. Strain gages location at 6 in and 18 in from the support

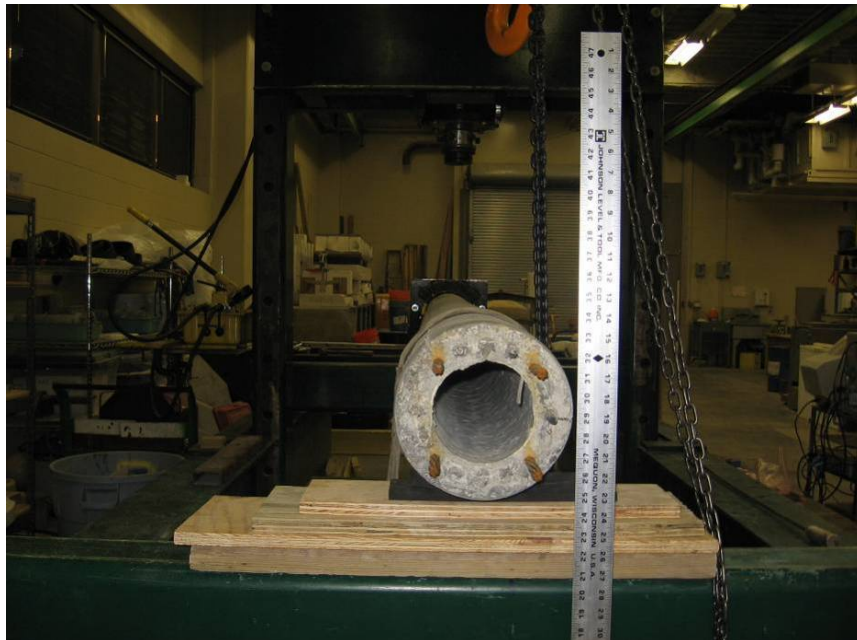


Figure 24. Deflection measurement scale at pole tip end



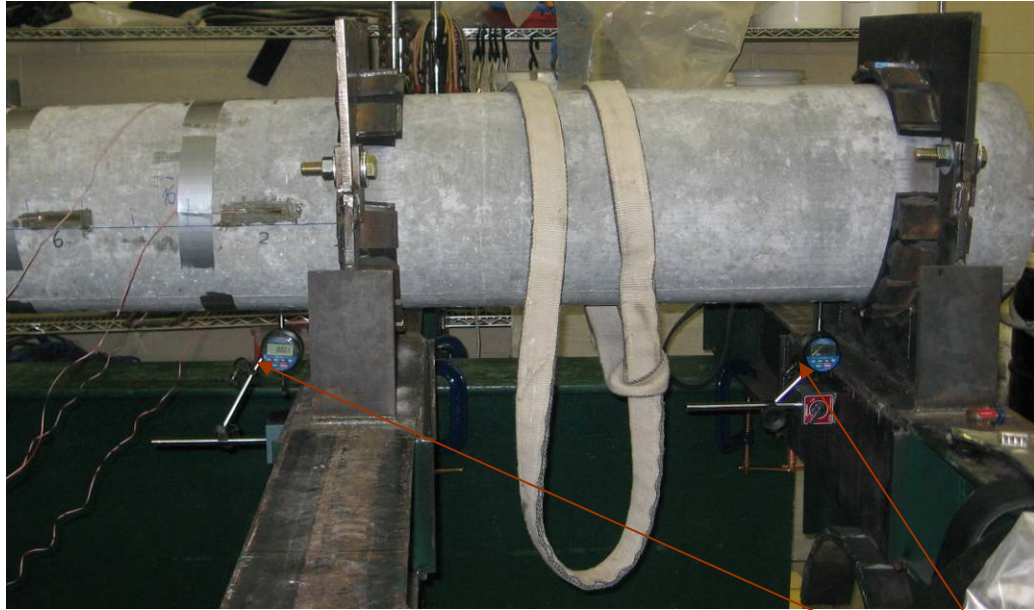
Figure 25. Concrete comparator for crack measurement

Desk top to
read and store
the data from
the DAS



Data Acquisition System
Vishay System 6000 DAS

Figure 26. Data recording system



Dial gages for deflection measurements

Figure 27. Dial gages locations for deflection measurements near the supports

3.4 Test Procedure

The first test was performed on the first specimen of the first group, having six CFRP bars as the main reinforcement and labeled as G01-01. The first step in the procedure was to make sure that all instrumentation was working and that the data acquisition system was able to recognize the data transferred. The various testing activities included applying the load, monitoring the data acquisition system, recording the deflection, recording the crack width, and monitoring the overall performance of the pole during testing. Several individuals were present, and each was assigned one of the tasks. The load was applied in increments of 100 lbs. There was a pause after each load increment appli-

cation to allow time to read the deflections and to inspect any structural distress that might have occurred.

The second test was performed on the first specimen of the second group, having 12 CFRP bars as the main reinforcement and labeled as G02-01. The same procedure was used for the second test, with only one difference in the test setup. In this test, the deflection was recorded manually using a tape that was connected to the pole, as shown in Figure 28, rather than the scale shown on Figure 24, that was used for the first test.

The third test was performed on the second specimen of the first group, having six CFRP bars as the main reinforcement and labeled as G01-02. The test setup and procedures were slightly changed from the previous two tests. As per the second test, the tap measure shown in Figure 28 was used to measure the deflection; however, the two dial gages shown in Figure 27 were replaced by two LVDTs, as shown in Figure 29. The LVDTs were connected to the data acquisition system to report any movement in the support during the loading and unloading of the pole. In this test, one cycle of loading and unloading was performed to check the elastic and plastic deformations of the tested pole. The load was applied in increments of 100 lbs, up to 80% of the expected failure load, then the load was totally unloaded to zero, and the pole was loaded again in increments of 100 lbs up to failure. There was a pause after each load increment application to allow time to read deflections and inspect any structural distress might have occurred.

The fourth and final test was performed on the second specimen of the second group, having 12 CFRP bars as the main reinforcement and labeled as G02-02. The test setup used for the third test was applied to the final test, but with extra gages applied between the supports to measure the strain in this area. Three strain gages were applied to

form a rosette, as shown in Figure 30. The main reason for these gages was to determine the flexural shear strain in this region.

In the third test two cycles of loads were applied prior to failure. In the first cycle, the load was applied up to 50% of the expected failure load, then the load was released up to zero, reloaded again up to 80% of the expected failure load, unloaded up to zero, and then reloaded up to failure. In each cycle, the load was applied in increments of 100 lbs, while for unloading the load was released in increments of 500 lbs. There was a pause after each increment of loading and unloading to allow time for reading deflections, measuring the crack width, and to permit for the inspection of any structural distress might have occurred.



Figure 28. Deflection measuring tape at the tip of the pole



Figure 29. LVDTs for deflection measurements and corrections



Figure 30. Strain gage rosette

3.5 Test Results

A brief summary of the test results is presented in Table 6, and a detailed description follows in the next sections. Table 7 shows the compressive strength of the cylinders tested at 28 days. From this table, it can be seen that there is a discrepancy between the results of the cylinders tested at the UAB laboratory and those tested at the plant. Some of the factors that might have caused this discrepancy were the handling and shipping of the specimens to the laboratory, the rate of loading of the cylinders, the difference in the temperature of the curing tanks, the eccentric loading of the cylinders, and the testing caps. To eliminate the discrepancies, the results of the cylinders from the plant were used in calculating the average compressive strength of the specimens G01-02 and G02-02.

Table 6

Summary of test results

Specimen ID.	No. of Bars	Cracking Load (lbs)	Tip Deflection at Cracking (in)	Cracking Strain (10^{-6})	Failure Load (lbs)	Corrected Tip Deflection at Failure (in)	Concrete Compressive Failure Strain (10^{-4})	Max. Concrete Compressive Strain (10^{-4})
G01-01	6	568	0.59	97	3790	25.84	32.06	35.58
G01-02		1025	1.54	170	4102	25.91	NA	24.96
G02-01	12	545	1.08	96	4247	20.465	NA	23.05
G02-02		904	0.92	106	5251	21.99	26.44	26.44

Table 8 shows the average compressive strength at 28 days for the concrete used in casting the poles. The second column of the table represents the strength at which the concrete cylinders were broken. Fouad (1988) showed that spinning increases the compressive strength by about 20% to 30%; therefore, a factor of 1.2 was used to represent

the actual compressive strength of the pole. This factor is shown on the third column of the table, and the last column represents the actual compressive strength used in this study.

Table 7

Compressive strength readings of concrete cylinders at 28 days

Specimen ID	No. of Bars	No. of Cylinders	Compressive Strength at 28 days (psi)				Average (psi)
			Cylinders tested at plant	Cylinders tested at plant	Cylinders tested at UAB lab	Cylinders tested at UAB lab	
G01-01	6	2	9500	9500	--	--	9500
G02-01							
G01-02	12	4	8790	9109	7697	7634	8950*
G02-02			4	9030	9070	6768	7403

The numbers marked with * is the average compressive strength on 28 days calculated using the cylinders tested at the plant only.

Table 8

Average 28-day compressive strength of concrete including spinning factor

Group No.	Specimen ID	No. of Bars	Average Compressive Strength at 28 days (psi)	Spinning Factor	Actual Compressive Strength at 28 days (psi)	Average Actual Compressive Strength at 28 days (psi)
Group 1	G01-01	6	9500	1.2	11500	11120
	G01-02		8950	1.2	10740	
Group 2	G02-01	12	9500	1.2	11500	11180
	G02-02		9050	1.2	10860	

3.5.1 Cracking Loads

The cracking loads of the two groups are shown on Table 9. From this table, it can be seen that the first cracking load for pole G01-01 was recorded at a load of 1298 lbs.

The crack load was determined by the naked eye and by hearing a cracking noise, and it was assured or adjusted by the strain reading. By observing the strain readings, it was seen that there was a sudden change in the readings, either at this load or at a slightly lower load.

When the load was applied to pole G01-01, there was no deflection observed or strain reading detected by the data acquisition system up to a load of 730 lbs. This load was considered the force needed to counteract the effect of the pole's own weight. Therefore, the cracking load of 1298 lbs recorded during the test can be broken into two components; the first component of 730 lbs represents the load needed to counteract the effect of the own weight of the pole, and the second component of 568 lbs is the actual cracking load.

For pole G01-02, there was no deflection observed or strain reading detected by the data acquisition system when the load was applied up to 346 lbs. Similar to the first pole, this load was considered to be the force needed to counteract the effect of the pole's own weight. The first cracking load was recorded at 1371 lbs, and after subtracting the pole's own weight, the actual cracking load became 1025 lbs.

For the second group of poles, the first cracking load was recorded at a load of 1203 lbs for pole G02-01 and, after eliminating the pole's own weight, the actual cracking load became 545 lbs. For pole G02-02, the first cracking load was recorded at 1211 lbs, and after the pole's own weight was eliminated, the actual cracking load became 904 lbs.

In comparing the numbers representing the pole's own weight in each group, a significant difference could be observed. This difference was due to a slight change in the

test setup between the first two poles tested (G01-01 and G02-01) and the other ones (G01-02 and G02-02). During the test of the last two poles, a box steel beam was placed under the pole near the loading point. The existence of this beam decreased the lever arm for the moment, and therefore, decreased the load required to counteract the effect of the pole's own weight. Another issue was the support. In the first group (G01-01 and G02-01), there was a gap between the pole and the collar that acted as a support, while in the second group this gap was totally filled with rubber. The existence of the gap resulted in increasing the load required to lift the pole up from rest.

Table 9

Cracking load of the poles

Group No.	Specimen ID	No. of Bars	Recorded Cracking Load (lbs)	Own Weight Effect (lbs)	Actual Cracking Load (lbs)	Average Cracking Load (lbs)
Group 1	G01-01	6	1298	730	568	796.5
	G01-02*		1371	346	1025	
Group 2	G02-01	12	1203	658	545	724.5
	G02-02*		1211	307	904	

Specimens marked with * were reinforced with C-GRID

3.5.2 Failure Loads

The failure loads of the two groups are shown on Table 10. From this table, it can be seen that the failure loads for the first group were recorded to be 4520 lbs and 4448 lbs for poles G01-01 and G01-02, respectively, and after subtracting the pole's own weight, the failure loads became 3790 lbs and 4102 lbs, respectively, making an average failure load of 3946 lbs for the first group.

For the second group, the failure loads were recorded to be 4905 lbs and 5558 lbs for poles G02-01 and G02-02, respectively, and after eliminating the pole's own weight, the failure loads became 4247 lbs and 5251 lbs for poles G02-01 and G02-02 respectively, making an average failure load of 4749 lbs for the second group.

Table 10 shows that the failure load for G01-02 and G02-02 was higher than the failure load for G01-01 and G02-01 by 8% and 24%, respectively. The 24% difference in the failure load for poles G02-01 and G02-02 is significant. To understand where the difference came from, we have to study the variables and uncertainties that might cause it. Failure load is a function in the cracked cross-section area of the pole, the cross-section area of the reinforcement, and the concrete compressive strength. The concrete compressive strength is a function in the spinning factor.

The cross-section area of the G02 specimens was checked prior to testing, and there was no significant difference. The cross-section area of the reinforcement was checked before casting, and there was no significant difference. Concrete cylinders were prepared and tested to determine the compressive strength of concrete at 28 days. The results of the cylinders showed that the compressive strength at 28 days of pole G02-01 was 6% higher than pole G02-02. Failure load is directly proportioned to the compressive strength of concrete; therefore, theoretically speaking, the failure load for pole G02-01 should be higher than the pole G02-02, which was not the case. Concrete compressive strength is increased by spinning, by about 20% to 30%, as shown by Fouad (1998). If we consider that the compressive strength of the pole G02-01 was improved by only 20% due to spinning, and the compressive strength of the pole G02-02 was improved by 30% due to spinning, then we have a concrete compressive strength of 11,765 psi and 11,500

psi for poles G02-01 and G02-02, respectively. Now we have a concrete compressive strength for pole G02-01 3% lower than pole G02-02; accordingly, the failure load of pole G02-02 will be higher than pole G02-01. We can conclude that spinning is one of the factors that cause the significant difference in the failure load between the poles G02-01 and G02-02.

Another factor that causes the significant difference in the failure load between poles G02-01 and G02-02 is the use of the C-GRID in the pole G02-02. The C-GRID provided two things: a confining pressure on the poles, resulting in an increase in the ultimate compression force of the poles, allowing them to carry more loads, and a slightly increases in the reinforcement ratio of the pole, thereby increasing its capacity.

Table 10

Failure loads of the poles

Group No.	Specimen ID	No. of Bars	Recorded Ultimate Load (lbs)	Own Weight Effect (lbs)	Actual Ultimate Load (lbs)	Average Ultimate Load (lbs)
Group 1	G01-01	6	4520	730	3790	3946
	G01-02*		4448	346	4102	
Group 2	G02-01	12	4905	658	4247	4749
	G02-02*		5558	307	5251	

Specimens marked with * were reinforced with C-GRID

Figure 31 shows the ultimate capacities of the two groups tested. It can be seen that although the difference in the reinforcement ratio between the two groups was doubled, there was only a 20% increase in the ultimate capacity, and this is because the ultimate moment capacity equation is a function not only of the number of bars used, but of

the location of the neutral axis, the orientation of the bars around the cross-section, and their relationship to the neutral axis.

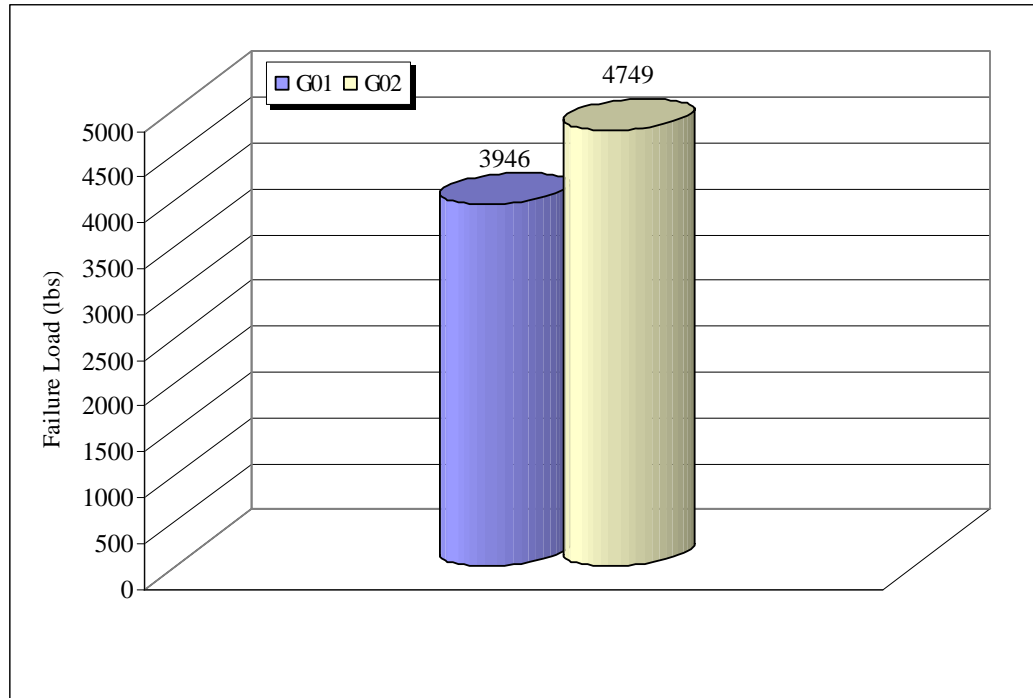


Figure 31. Failure load of the two groups

3.5.3 Deflection

As the load was applied to specimen G01-01, there was no deflection observed or strain reading detected by the data acquisition system up to the load of about 730 lbs. Afterward, deflection was observed to increase linearly, as shown in Figure 32. At a load of 1298 lbs, the first crack was formed at a strain of 97×10^{-6} , recording a tip deflection of 0.59 in. After the first cracking, the deflection rate increased, and the deflection increased non-linearly with the load. At a load of 1457 lbs, the second crack was formed, recording

a tip deflection of 2.58 in. This increase in the deflection rate is due to the reduction in the pole stiffness due to cracking. At a load of 1576 lbs, the third crack was formed, recording a tip deflection of 4.43 in, and then several cracks started to form, keeping the non-linear behavior of the deflection versus the load up to a load of 1674 lbs. After this load, the deflection again started to increase linearly with the load up to failure. At a load of 4504 lbs, the maximum concrete strain of 35.58×10^{-4} was recorded, and at a load of 4520 lbs, the pole failed recording a deflection of 25.84 in and a strain of 32.06×10^{-4} (Figure 33).

For pole G01-02, there was no deflection observed or strain reading detected by the data acquisition system as the load was applied up to 346 lbs. Afterward, deflection was observed to increase linearly up to a load of 900 lbs, as shown in Figure 32. Between the loads of 900 lbs and 1500 lbs, crack formation started; however, the first crack was reported at a load of 1371 lbs, making a strain of 167×10^{-6} and recording a tip deflection of 1.54 in. The difference between the first crack reported and the actual crack formation is due to the formation of small, internal cracks prior to the external crack being reported. It was obvious during this test that there were not too many cracks formed, especially when compared to pole G01-01; the crack width was also much smaller than that of pole G01-01. As shown in Figure 32, the pole started to deflect linearly again between the load of 1500 lbs to the load of 3700 lbs but with a different slope. No more cracks were formed; however, the existing cracks widened up especially the first crack. Upon reaching 3700 lbs, the load was released to zero, reporting a residual deflection of 0.75 in, and all the cracks were closed. The pole was reloaded again and, as shown in Figure 32, the pole started to deflect linearly with the load, but with a different slope, up

to a load of 3700 lbs, and after that the pole deflected with almost the same slope as the slope of the first cycle up to failure. At a load of 4062 lbs, the maximum compressive strain was recorded to be 24.96×10^{-6} , and the tip deflection was recorded to be 22.50 in. The failure load was reported at 4448 lbs, where the deflection was 25.90 in.

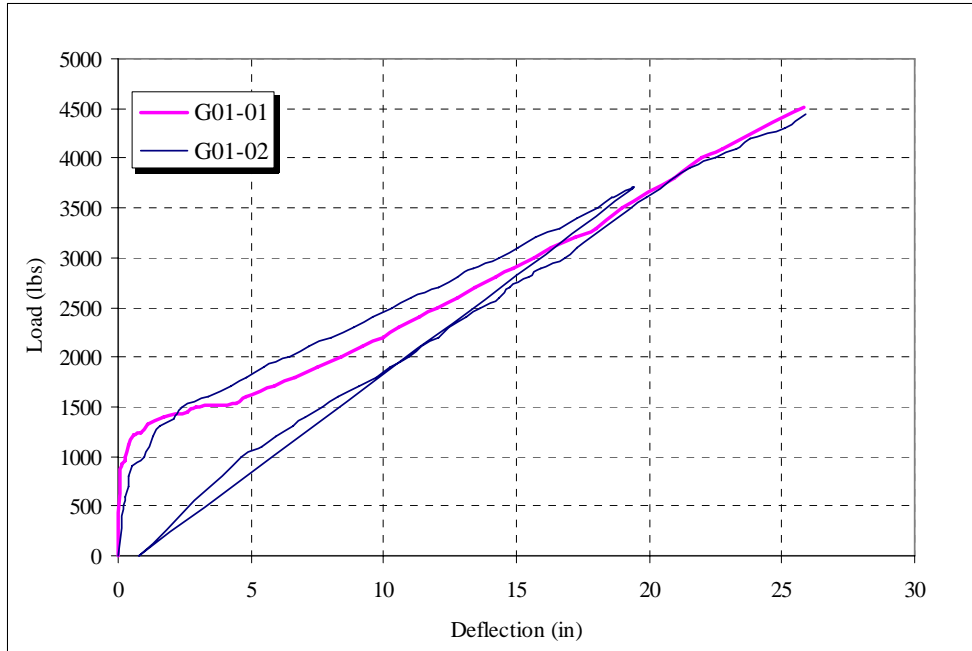


Figure 32. Load deflection curves for the first group

It can be seen in Figure 32 that the load deflection curves of the poles G01-01 and G01-02 are very similar, with no significant difference between them. However, it can be seen that pole G01-02 had a slightly higher stiffness than pole G01-01. This is because pole G01-02 was reinforced with the C-GRID instead of spiral steel stirrups. The C-GRID was able to provide the pole with an increase in its stiffness because the C-GRID had strands in both directions; however, the steel stirrups are acting in only one direction.

The load deflection curves of the two poles started linearly up to a load of 1000 lbs, and then, between the loads of 1000 lbs and 1500 lbs, the two poles were nonlinearly deflecting. This is the range where the poles started cracking and adjusting their new stiffness; after that, the two poles started deflecting linearly again up to failure. Although pole G01-02 had a higher stiffness than pole G01-01, subjecting the pole G01-02 to a loading cycle resulted in the two poles failing at almost the same load and reporting the same deflection, as can be seen in Figure 32.

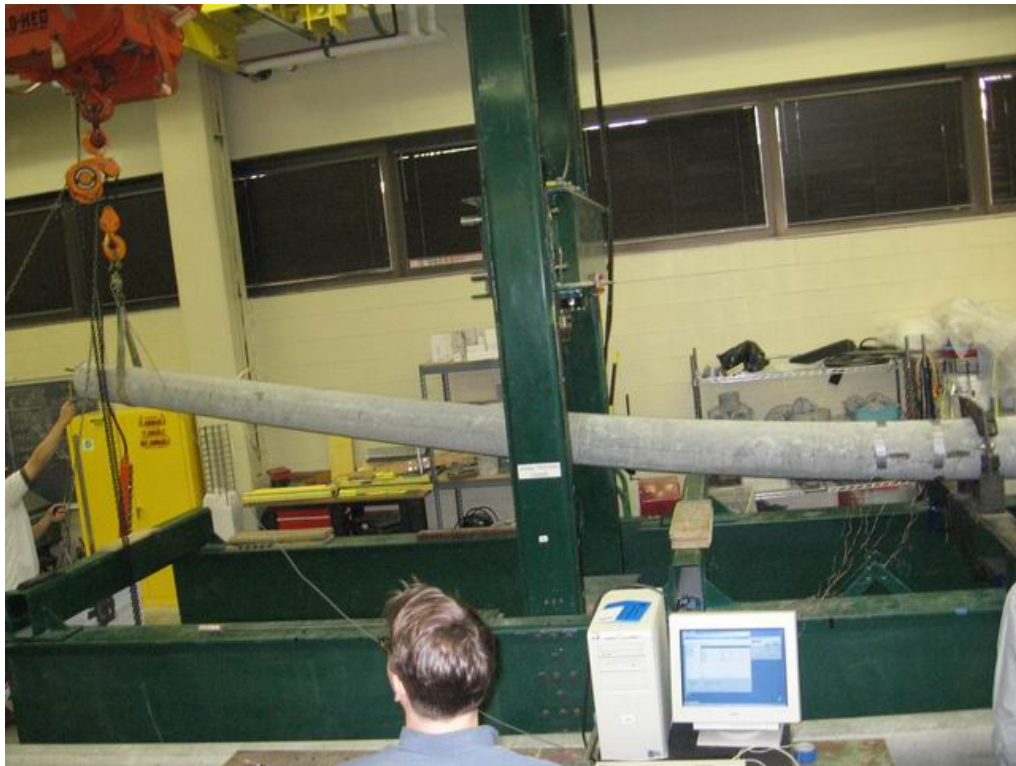


Figure 33. Deflection of pole G01-01 prior to failure

When the load was applied on pole G02-01, there was no deflection observed or strain reading detected by the data acquisition system up to 658 lbs. This load was con-

sidered the force needed to counteract the effect of the pole's own weight. As the load on the pole was increased afterward, deflection was observed to increase linearly, as shown in Figure 34. At a load of 1203 lbs, the first crack was formed at a strain of 96×10^{-6} , recording a tip deflection of 1.08 in. After the first cracking, the deflection kept increasing linearly but with a higher rate. This increase in the deflection rate was due to the reduction in pole stiffness due to cracking. At a load of 1392 lbs, several hair cracks started forming, recording a tip deflection of 1.96 in. Cracks continue to form up to a load of 2400 lbs, and at the same time the previously formed hair cracks widened. At a load of 4609 lbs, the maximum concrete strain of 25.05×10^{-4} was recorded, and at the load of 4905 lbs the pole failed, recording a deflection of 20.46 in and a strain of 16.03×10^{-4} .

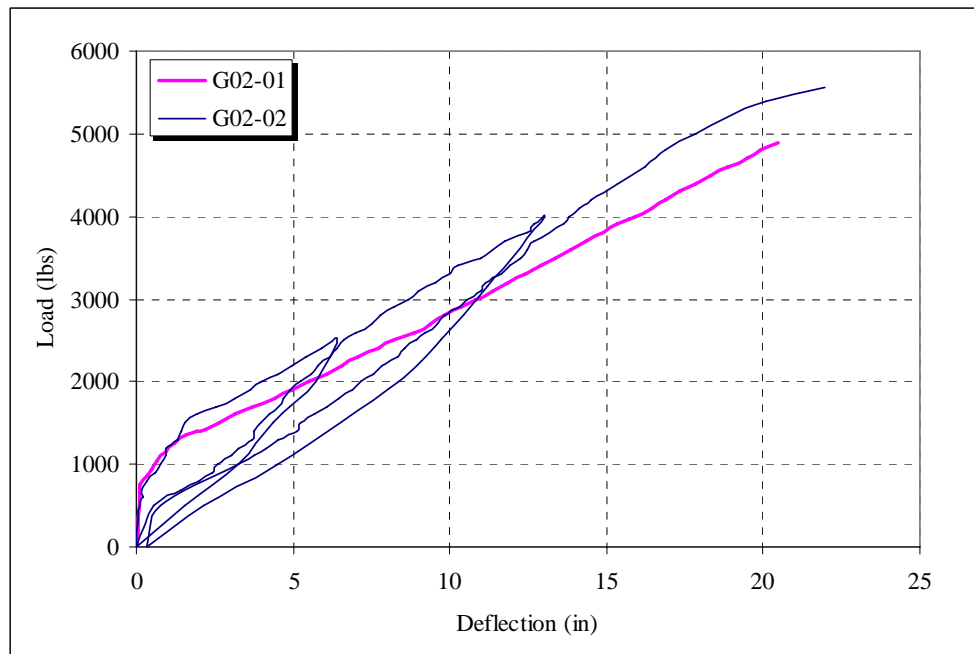


Figure 34. Load deflection curves for the second group

For pole G02-02, the load was applied three cycles. In the first cycle, the load was applied up to 2500 lbs, which was expected to represent about 50% of the failure load, then the load was unloaded to zero. When the load was applied in this cycle, there was no deflection observed or strain reading detected by the data acquisition system up to a load of 307 lbs. Afterward, deflection was observed to increase linearly up to a load of 900 lbs, as shown in Figure 34. Between the loads 900 lbs and 1500 lbs, crack formation started; however, the first crack was reported at the load of 1211 lbs, making a strain of 104×10^{-6} and recording a tip deflection of 0.92 in. The difference between the first crack reported and the actual crack formation is due to the formation of small, internal cracks prior to the external crack being reported. As per pole G01-02, it was obvious during this test that there were not too many cracks formed, especially when compared to pole G02-01; the crack width was also much smaller than that of pole G01-01. As seen in Figure 34, the pole starts to deflect linearly again between the load of 1500 lbs and the end of the first cycle (2500 lbs) but with a different slope, recording a deflection of 6.4 in at a load of 2500 lbs and a compressive strain of 874×10^{-6} , then the load was released to zero, reporting zero deflection. In addition, after unloading, all of the cracks were totally closed.

In the second cycle, the load was applied up to 4000 lbs, which was expected to represent about 80% of the failure load, then the load was unloaded to zero. When the load was applied in this cycle, the pole started to deflect linearly up to a load of 500 lbs, and between the load of 500 lbs and 1000 lbs the pole started to deflect nonlinearly; this range is characterized by the reopening of the cracks, and this explains the nonlinear behavior of the deflection. It can be seen in Figure 34 that the pole did not follow the same path of deflection during the second cycle of loading, which means that the pole lost

some of its stiffness due to cracking. After the cracks were reopened and the pole adjusted to its new transformed section, the pole started to deflect linearly again. At a load of 2500 lbs, the pole deflection was recorded to be 6.63 in, which was almost equal to the deflection of the first cycle, and the compressive strain reading was recorded to be 891×10^{-6} , which was also close to the strain of the first cycle. After the loading went beyond 2500 lbs, the deflection slope changed to match the deflection slope of the first cycle. The deflection then continued to increase linearly up to a load of 4000 lbs, representing the end of the second cycle. At this load, the pole deflection was recorded to be 13.04 in, and the compressive strain reading was 17.09×10^{-4} . The pole was then unloaded in increments of 500 lbs down to zero. At zero loading, a residual deflection was recorded to be equal to 0.31 in, while all the cracks closed again.

In the last cycle, the load was applied up to failure. When the load was applied, the pole started to deflect linearly up to a load of 500 lbs and, between the loads of 500 lbs and 1000 lbs, the pole started to deflect nonlinearly due to the reopening of the cracks. From the point where the load started and up to a load of 1000 lbs, the pole behavior was very close to the behavior of the second cycle, and the load deflection path was almost the same; however, afterward, the pole started to deflect linearly, with a different slope than that of the second cycle. At a load of 2500 lbs, the reported deflection was 8.94 in, and the strain reading was 10.32×10^{-4} , making a significant difference from the first two cycles, and at a load of 4000 lbs, the tip deflection was 13.82 in and the strain reading was 17.53×10^{-4} , marking a slight expected difference from the second cycle. It can be seen in Figure 34 that, during the third cycle of loading, the pole did not follow the same path of deflection from the second cycle, which means that the pole lost more of its stiff-

ness due to cracking. The deflection then continued to increase linearly up to failure. The pole failed at a load of 5558 lbs, reporting a tip deflection of 22 in and a maximum failure compressive strain of 26.44×10^{-4} (Figure 35).

In Figure 34, it can be seen that the load deflection curves of poles G02-01 and G02-02 are very similar with no significant difference. Starting from zero loading and up to a load of 1500 lbs, the load deflection curves of the two poles were almost identical. As per the first group of poles, the load deflection curves of the second group started linearly up to a load of 900 lbs, and then, between the loads of 900 lbs and 1500 lbs, the two poles nonlinearly deflected. After that the two poles started deflecting linearly again up to failure.

Figure 34 shows that pole G02-02 had a slightly higher stiffness than pole G02-01, and this is because pole G02-02 was reinforced with C-Grid instead of steel stirrups, which results in increasing its stiffness, as discussed previously. For instance, at the failure load of pole G02-01, the tip deflection was 20.5 in; however, at the same load, the tip deflection of pole G02-02 was 17.8 in, which is about 13% less than the pole G02-01. The C-Grid not only improves the stiffness of the pole, it also increases its capacity. For instance, the failure load of pole G02-01 was 4900 lbs, compared to a failure load of 5558 lbs for pole G02-02 reinforced with C-GRID.

Figure 36 shows the load deflection curves of the four specimens. It shows that all four specimens deflected linearly with the load and had almost the same deflection values starting from a zero load and up to a load of about 750 lbs, which corresponds to the average cracking load of the poles. Following the cracking load and up to a load of 1500 lbs, the poles started to deflect nonlinearly with the load, but still the deflection curves

coincided with each other. After that, the poles started to deflect linearly again, but with different slopes, representing the stiffness of each pole after cracking. The poles of the second group (G02-01 and G02-02) had higher stiffness than the poles of the first group (G01-01 and G01-02), and this is because the second group had more reinforcement than the first group. It could also be noticed that the poles reinforced with C-GRID had higher stiffness than the poles reinforced with steel stirrups, which means that the C-GRID helped to increase the transformed stiffness of the poles after cracking.



Figure 35. Deflection of pole G02-02 prior to failure

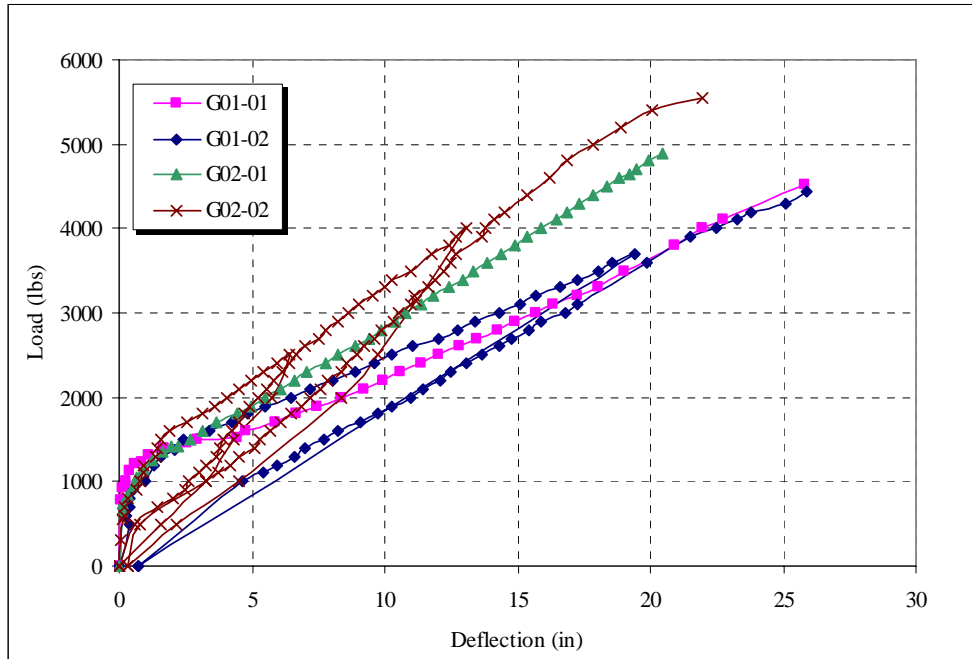


Figure 36. Load deflection curve of the four specimens

3.5.4 Failure Modes

Two types of failure modes were observed, as shown in Table 11. Prior to the failure of pole G01-01, shear cracks formed between the two supports, as shown in Figure 37. At a load of 4520 lbs, the concrete crushed explosively in compression near the second support, as shown in Figure 38. After unloading the pole, it was observed that the pole underwent a permanent cracking and deflection. This permanent cracking and deflection could be due to the low reinforcement ratio used in this pole, which makes the concrete controls the failure mode of the pole.

One of the interesting observations during this test was the slippage of the prestressing steel strands inside the plastic pipes, as shown in Figure 39. These prestressing steel strands were used for the purpose of specimen casting and the pipes were used to

prevent any bonding between these strands and the concrete and, thereby, cancel its effect on the behavior of the specimen. Slippage of the strands proves that we were able to cancel the effect of the steel strands on the behavior of the pole, and the idea of using the plastic pipes was successful.

Table 11

Failure modes of the poles

Group No	Pole No	Failure Mode
Group 1	G01-01	Compression failure
	G01-02	Diagonal tensions shear failure combined with compression shear failure at support
Group 2	G02-01	Compression failure
	G02-02	Diagonal tensions shear failure combined with compression shear failure at support



Figure 37. Shear cracks between supports prior to G01-01 pole failure

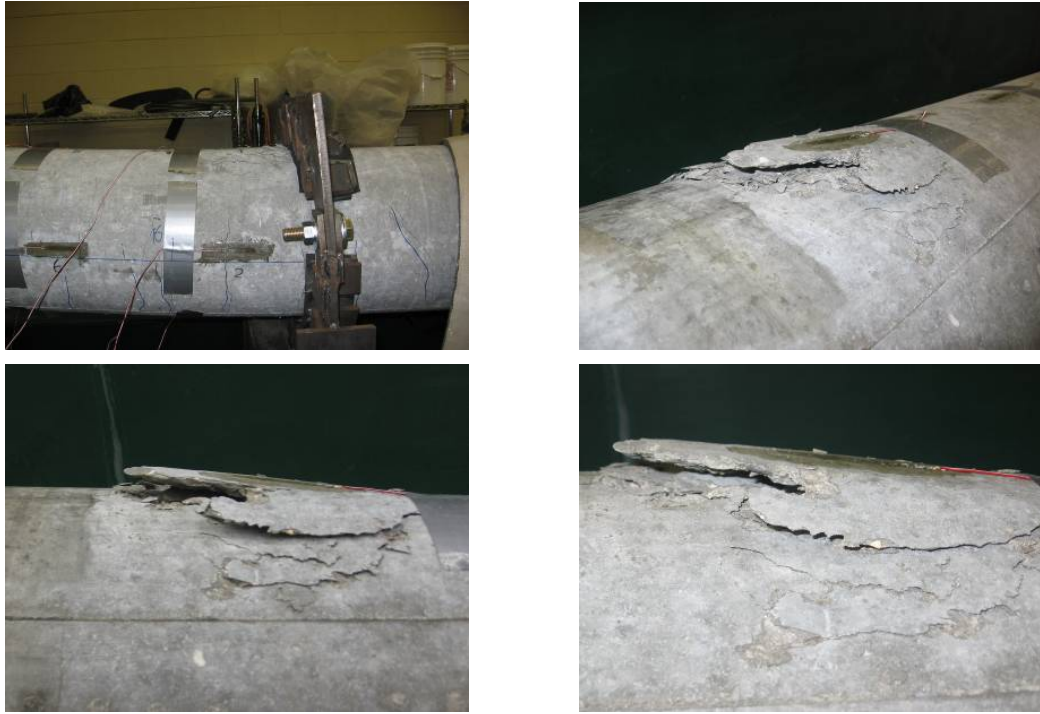
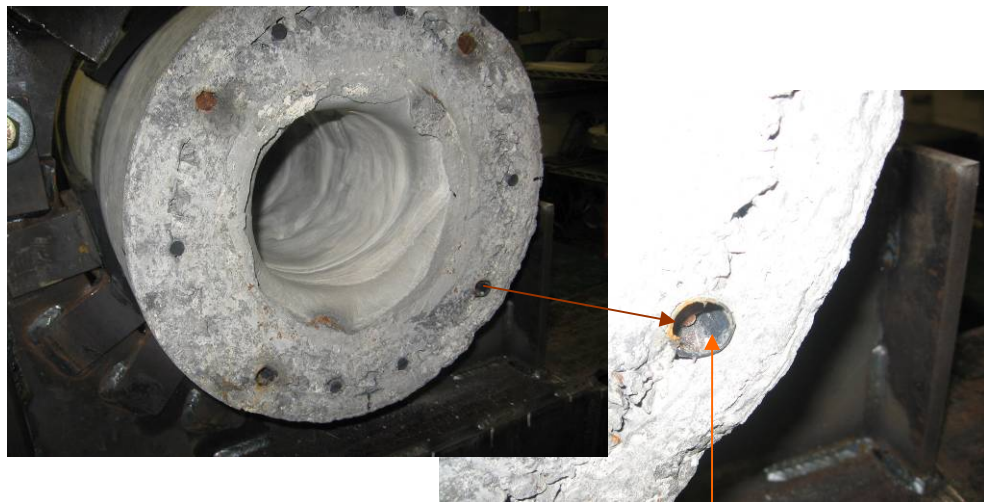


Figure 38. Concrete crushing at failure from different views for G01-01



Slippage of prestressing strands assures its inactivity during pole testing

Figure 39. Slippage of prestressing strands during testing

During the first cycle of loading for pole G01-02 and at a load of 3600 lbs, a diagonal shear crack formed between the two supports, as shown in Figure 40. This crack closed after unloading and at a load of 3000 lbs in the second load cycle, the same crack reopened and began widening up to failure. At a load of 4448 lbs, the diagonal crack widened into a principal diagonal tension crack and extended to the top compression fibers of the pole, and a sudden failure took place as this crack dynamically joined the crushed concrete zone (Figure 41). Unlike pole G01-01, after the pole was unloaded, all the flexure cracks were closed, leaving some hair cracks, and the residual deflection recorded was very low. This was due to the use of the C-GRID in pole G01-02. The C-GRID helps in providing the concrete with an ample amount of confinement, as well as increasing its reinforcement ratio, which accordingly provides the pole with more elasticity than pole G01-01.



Figure 40. Diagonal shear crack for pole G01-02

The failure of the pole was also characterized by the slippage of the CFRP bars at failure, as shown in Figure 42. This slippage is due to the destruction of the bond between the longitudinal bars and the surrounding concrete at the support region, which is a common phenomenon during shear failure mode.

Similar to the pole G01-01, slippage of the prestressing steel strands inside the plastic pipes was observed (Figure 42).



Figure 41. Concrete failure from different views for G01-02

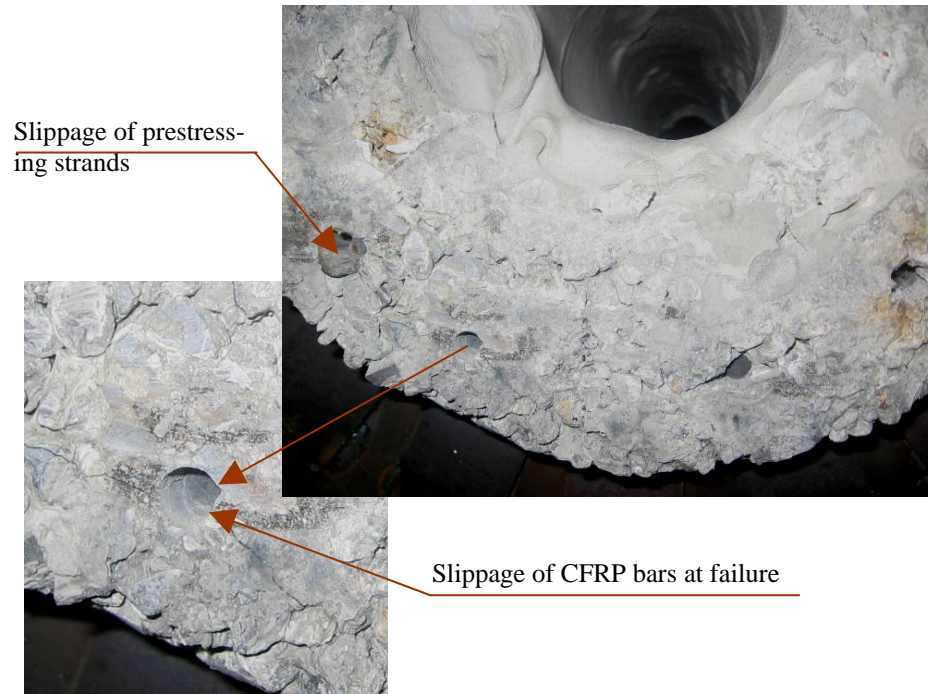


Figure 42. Slippage of CFRP bars and prestressing strands at failure of pole G01-02

The failure modes of the second group of poles were very close to those of the first group. The pole reinforced with steel stirrups as shear reinforcement failed in compression, whereas the poles reinforced with C-GRID failed in diagonal tension shear failure, combined with compression failure at the support. This indicates that the use of the C-GRID had a significant effect on the mode of failure of the poles. It is also interesting to mention that the shear cracks developed in all of the poles prior to failure, but the poles reinforced with C-GRID were not able to sustain the applied shear force and had a shear failure. On the other hand, the poles reinforced with the steel stirrups were able to sustain the applied shear force, resulting in a compression failure. Similar to the poles of the first group, slippage of the prestressing steel strands inside the plastic pipes was observed.

For pole G02-01, shear cracks were formed between the two supports, as shown in Figure 43 prior to failure, and the maximum concrete strain of 25.05×10^{-4} was recorded at the load of 4609 lbs. At a load of 4905 lbs, the concrete crushed explosively in compression near the second support, as shown in Figure 44.



Figure 43. Shear cracks between supports prior to failure of pole G02-01



Figure 44. Concrete crushing at failure of pole G02-01

Since the failure of pole G01-02 reinforced with C-GRID was due to shear and was accompanied by the slippage of the longitudinal CFRP bars, and since we expected to have the same scenario for pole G02-02 of the second group because it was also reinforced with the C-GRID, we were also interested in knowing when the slippage of the CFRP bars happened, so we measured the slippage during this test.

For pole G02-02, the first shear crack occurred during the second cycle of loading at 4000 lbs. The crack formed between the two supports, as shown in Figure 45. At the last cycle of loading, the crack widened and, at a load of 5558 lbs, it widened into a principal diagonal tension crack and extended to the top compression fibers of the pole, and sudden failure took place as this crack dynamically joined the crushed concrete zone (Figure 46). Slippage of the CFRP bars happened only at failure, when the bond between the longitudinal CFRP bars and the surrounding concrete was destroyed.

The failure of the pole was also characterized by the failure of the CFRP bars and the C-GRID, as shown in Figure 47 and Figure 48. This type of failure can best be explained using the truss and tie model analogy. In this model, the concrete acting in compression represents the top chord of the truss, the C-GRID acting in tension represents the vertical members of the truss, the longitudinal CFRP bars acting in tension represent the bottom chord of the truss, and the concrete between the top and bottom chords represents the diagonal member. When the shear force exceeds the ultimate capacity of the truss, it results in the failure of the diagonal member, the compression chord, and the vertical members, as shown in Figure 47 and Figure 48, and the bottom tension chord failed due to the debonding of the longitudinal bars from the surrounding concrete.

By means of the strain readings of the rosette, the principal strains and their angle of inclination were calculated. It was found that, prior to failure and at a load of 5065 lbs, just before we lose the strain readings of the rosette, the pole was subjected to orthogonal principal strains equal in magnitude but opposite in direction. In such a case, the shear stress is equal in magnitude to the principal stress and occurs at 45 degree diagonal planes, which was the case in our poles. It is noteworthy to mention that the principal strain calculated at a load of 5065 lbs was 0.012, which exceeds the ultimate strain of the C-GRID used and explains the failure of the C-GRID, as shown in Figure 48.

Similar to pole G02-01, after the pole was unloaded, all of the flexure cracks were closed, leaving some hair cracks, and the residual deflection recorded was very low. Slippage of the prestressing steel strands inside the plastic pipes was also observed.



Figure 45. First shear crack for the pole G02-02



Figure 46. Failure of Pole G02-02 from different views

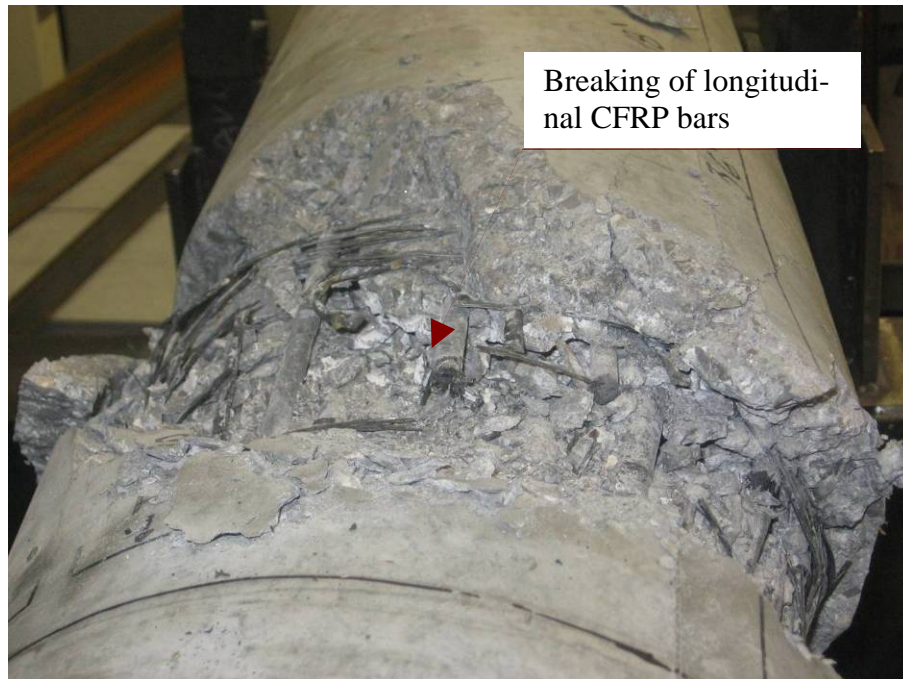


Figure 47. Failure of concrete and longitudinal CFRP bars

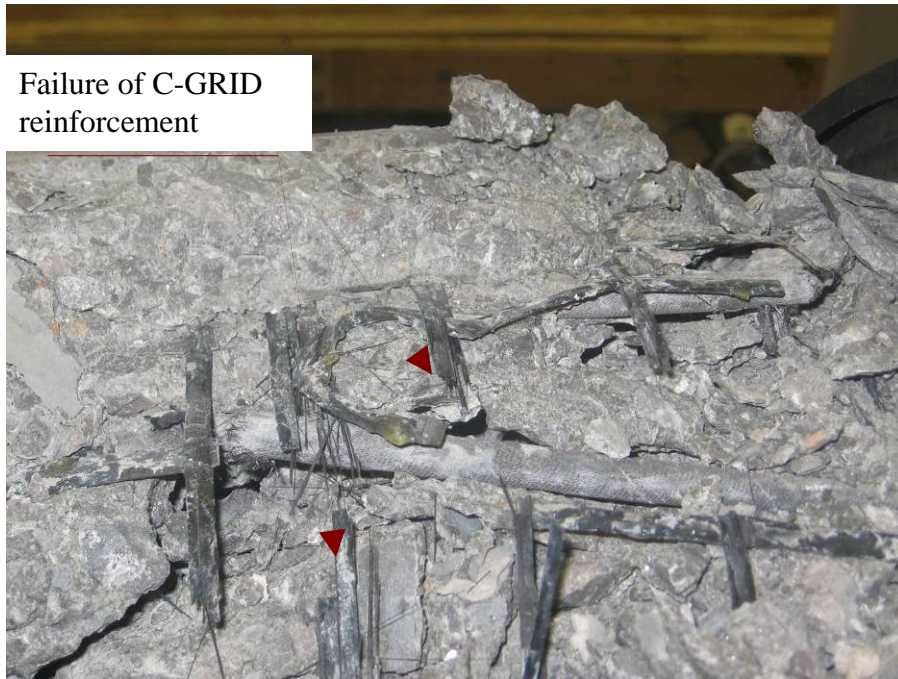


Figure 48. Failure of C-GRID reinforcement

3.5.5 Compressive Strain Readings

Figure 49 and Figure 50 show the load compressive strain at the supports for the poles of the two groups. We can see that the poles had a very good agreement between each other.

Figure 49 shows that, for the first group, there were no strains detected up to loads of 730 lbs and 346 lbs for poles G01-01 and G01-02, respectively. The difference between these reading was due to the difference in the test setup between the two poles as discussed previously. It can also be seen that the first portion of the two curves representing the linear elastic stage are parallel to each other. At a load of 1298 lbs, pole G01-01 cracked recording a strain of 97×10^{-6} , whereas at a load of 1355 lbs, pole G01-02 cracked recording a strain of 170×10^{-6} . The difference between the two cracking loads

and their corresponding strain was due to using the C-GRID as shear reinforcement, which results in improving the performance of pole G01-02. At a load of about 2500 lbs, the two curves coincide with each other, up to the end of the first cycle for pole G01-02. After unloading a permanent strain of 231×10^{-6} was reported, and after reloading the strain increased linearly with the load up about 720 lbs. The strain then started to increase nonlinearly with the load up to 1000 lbs. After that the strain increased linearly again till we lost it at a load of 4062 lbs, recording a strain of 24.96×10^{-4} .

Figure 50 shows that, for the second group, there were no strains detected up to loads of 658 lbs and 307 lbs for poles G02-01 and G02-02, respectively. The difference between these readings was due to the difference in the test setup between the two poles, as discussed. It can also be seen that the first portion of the two curves representing the linear elastic stage is coinciding with each other. At a load of 1203 lbs, pole G02-01 cracks, recording a strain of 96×10^{-6} , whereas at a load of 1211 lbs, pole G01-02 cracks, recording a strain of 106×10^{-6} . The difference between the two cracking loads and their corresponding strain is due to using the C-GRID as shear reinforcement, which results in improving the performance of pole G01-02. The strains continued to increase linearly as the load increased, but with a different slope than the initial slope up to the end of the first loading cycle. After unloading, a permanent strain of 53×10^{-6} and 32×10^{-6} for the first and second loading cycles, respectively, was reported. After the pole was reloaded, the strains increased linearly up to failure, except for a very small portion between the loads of 375 lbs and 900 lbs. Pole G02-02 failed at a load of 5558 lbs, reporting a failure strain of 26.44×10^{-4} .

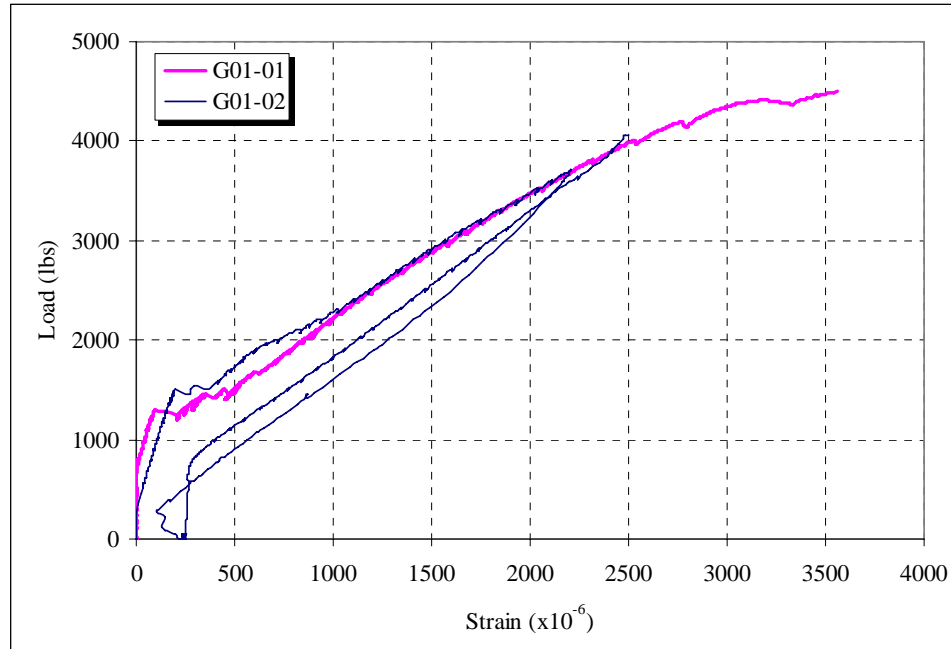


Figure 49. Load versus compressive strain for G01 specimens

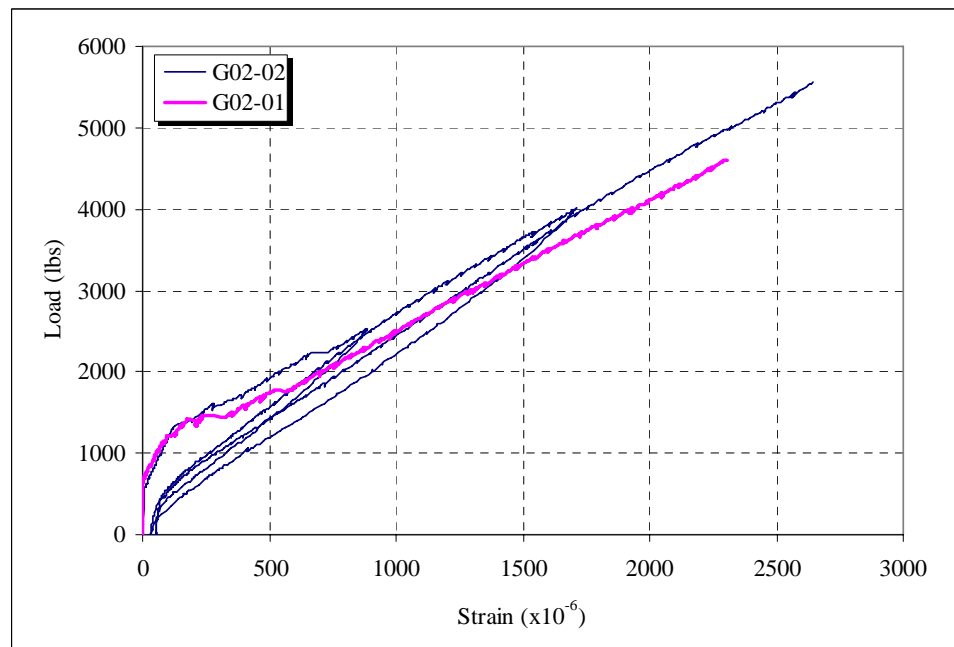


Figure 50. Load versus compressive strain for G02 specimens

3.5.6 Crack Width and Spacing

Figure 51 shows the crack pattern along the length of the pole G01-01 after unloading. The maximum crack width for this pole was 0.04 in and the crack was located at one foot from the second support. Other cracks in this region were about 0.035 in and were spaced at 4 in. Moving toward the middle of the pole up to 10 ft from the butt, the crack width decreased measuring an average of 0.02 in; however, the crack spacing ranged from 3 to 4 in. For the second half of the pole, starting at 10 ft from the butt and up to five feet from the tip, the crack width measured an average of 0.007 in, with crack spacing of 6 in. There was no cracking observed for the rest of the pole.



Figure 51. Cracking pattern for pole G01-01

Figure 52 shows the crack width versus loading for the pole G01-02 at two feet from the second support where the first crack was formed. At a load of 1700 lbs, the crack width was about 0.02 in and increased to a width of 0.025 in at a load of 1900 lbs. At a load of 2100, the crack width reached 0.03 in and, prior to the end of the first cycle

at a load of 3200, the crack width was 0.06 in. After unloading, all of the cracks closed, leaving only hair cracks. After reloading, the crack reopened and started widening as the load increased, so the crack width was about 0.02 in at a load of 1000 lbs. The crack width increased almost linearly during the second stage of loading, recording a crack width of 0.06 in at a load of 3000 lbs, after which we were not able to measure the crack due to safety issues. After failure, all of the cracks were closed again, leaving only hair cracks. Although there were not as many cracks as with pole G01-01, the cracks for pole G01-02 was spaced every 4.0 in, starting from the second support and up to the middle of the pole.

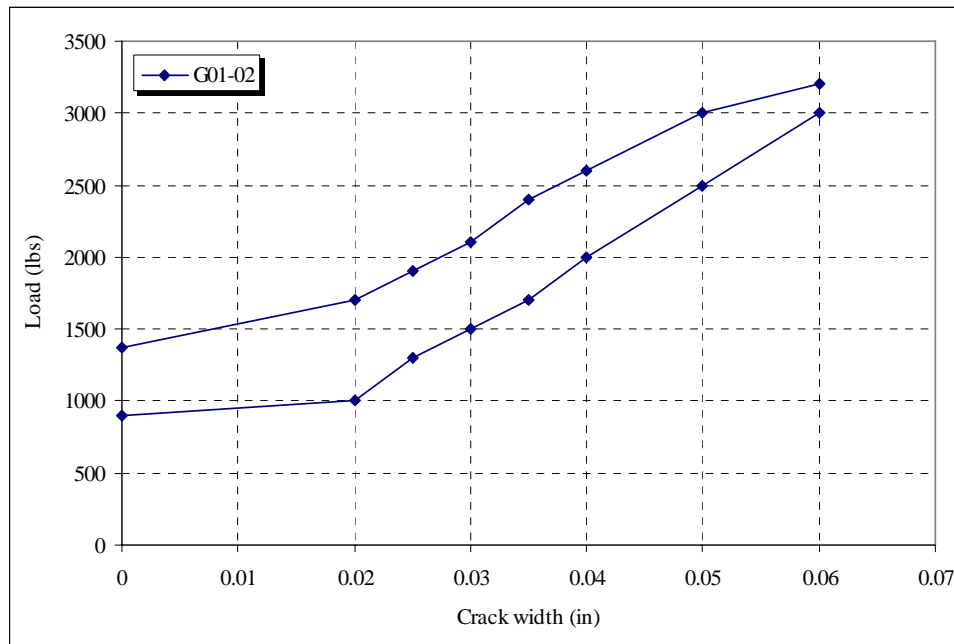


Figure 52. Crack width versus loading for the pole G01-02

Figure 53 shows the crack pattern along the length of pole G02-01 after unloading. All of the cracks left after unloading were hair cracks that were hardly seen, and they were distributed at 4 in, starting from the second support and up to the middle of the pole. For the second half of the pole, there was no cracking observed. The crack distribution for pole G02-02 was similar to the crack distribution of pole G02-01.



Figure 53. Cracking pattern for pole G02-01

Figure 54 shows the crack width versus loading at one foot from the second support for the second group of poles (G02-01 and G02-02). For pole G02-01, at a load of 2100 lbs, the crack width at one foot from the second support was about 0.02 in and increased to a width of 0.025 in at a load of 3100 lbs. At a load of 3800 lbs the crack width reached 0.03 in, and prior to failure, at a load of 4000 lbs, the maximum crack width measured was 0.035 in.

For pole G02-02, at a load of 2000 lbs, the crack width was about 0.01 in and increased to a width of 0.013 in by the end of the first load cycle at a load of 2500 lbs. After unloading, all of the cracks closed leaving only hair cracks. After reloading, the crack reopened at a load of 1300 lbs and started widening as the load increased reporting the same crack widths as for the first load cycle, which indicates that the pole was still in its elastic range. It can be seen in Figure 54 that the crack width increased almost linearly during the second stage of loading, recording a crack width of 0.016 in at a load of 3000 lbs, and at the end of the second load cycle, at a load of 3700 lbs, the crack width was 0.02 in. After reloading, the crack reopened at a load of 1100 lbs and started widening as the load increased reporting the same crack widths as for the second load cycle.

It is obvious from Figure 54 that the crack width for pole G02-02 is much less than for pole G02-01; for instance at a load of 2000 lbs, the crack widths were 0.017 in and 0.01 in for poles G02-01 and G02-02, respectively, and since the pole G02-02 was reinforced with the C-GRID as shear reinforcement, it can be concluded that the C-GRID significantly decreased the crack width of the pole.

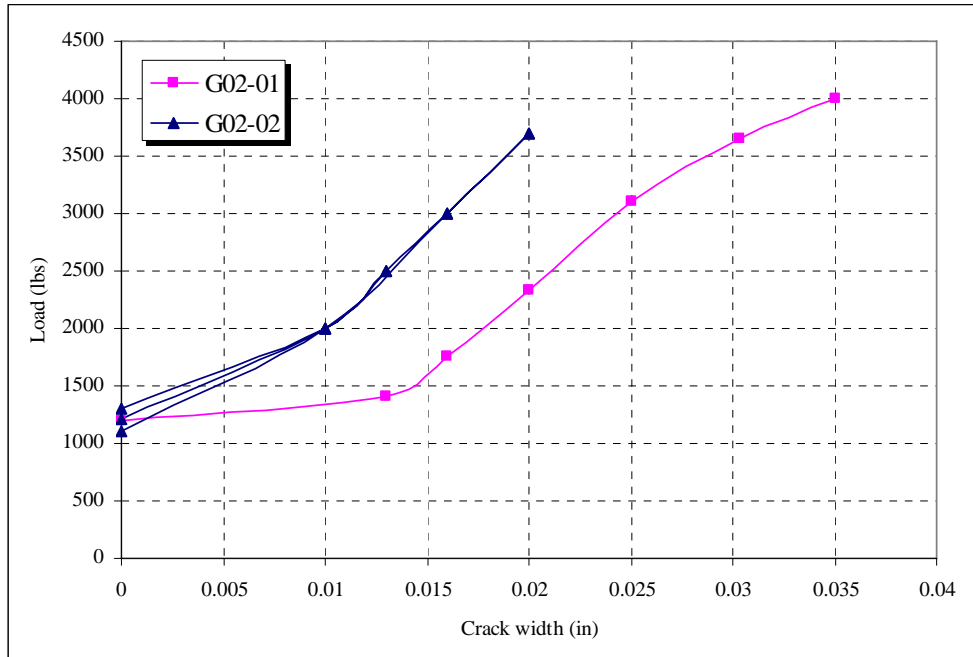


Figure 54. Crack width versus loading for G02 specimens

3.6 Summary

Four full-scale poles were manufactured using a spinning process and high strength concrete, and CFRP bars served as their reinforcement. The poles were tested to ultimate failure under a cantilever load test to study the flexural behavior of spun concrete poles reinforced with CFRP bars. The conclusions drawn can be summarized as follows:

1. Concrete poles reinforced with CFRP bars showed satisfactory flexural behavior, as they were able to produce a significant amount of deflection of about 12% from the free length of the pole prior to failure to overcome the brittle nature of the CFRP bars.

2. The reinforcement ratio significantly affected the failure mode of the poles. For pole having low reinforcement ratio, it resulted in permanent cracking and deflection after unloading. For other pole with a higher reinforcement ratio, all of the flexure cracks were closed after unloading, leaving hair cracks, and the residual deflection recorded was very low.
3. The reinforcement ratio did not significantly affect the flexural capacity of the poles. Although the difference in reinforcement ratio between the two poles was doubled, the ultimate capacity was increased by only 20%. This is because, the ultimate moment capacity equation is not only a function of the number of bars used, but also a function of the location of the neutral axis, the orientation of the bars around the cross-section, and their relationship to the neutral axis.
4. The reinforcement ratio does not have a significant effect on crack spacing. Although the two groups had different reinforcement ratios, the crack spacing at failure load was about 4.0 in, starting from the support and up to the middle of the poles.
5. The use of the C-GRID as a shear reinforcement significantly affected the failure mode of the poles. The C-GRID was not able to resist the high shear forces developed between the supports because of its small cross-section area and ultimate strain compared to steel spirals. The poles reinforced with C-GRID failed in compression shear mode between the supports due to shear. The poles reinforced with steel spirals underwent compression failure at the support due to flexure with comparable failure loads. Moreover, one pole, having a low reinforcement ratio and being reinforced with steel spirals, underwent permanent cracking and deflec-

tion after unloading. For the other pole with the same reinforcement ratio but reinforced with the C-GRID for shear reinforcement, all of the flexure cracks were closed after unloading, leaving some hair cracks, and the residual deflection recorded was very low.

6. The use of the C-GRID as a shear reinforcement significantly decreased the crack width of the poles. With the poles having the same reinforcement ratio, the crack width for the poles reinforced with the C-GRID was decreased by about 40% prior to failure, as compared to the poles reinforced with traditional steel stirrups.

CHAPTER 4

ANALYTICAL STUDY

4.1 General

The main objective of the theoretical analysis was to predict the behavior of the spun concrete poles reinforced with CFRP prior to testing and compare the results obtained from this study with the experimental results and results from the finite element analysis. Design formulations to estimate the flexural capacity, deflection, crack width, and ductility of the poles were developed based on equations available in the literature on the design of concrete poles and concrete structures reinforced with CFRP.

4.2 Flexural Design Equations

An analytical investigation was performed to study the behavior of the test specimens under loading conditions. The ultimate and cracking moment capacities were calculated for each group of specimens. The following assumptions were made in calculating the ultimate and cracking moments. These assumptions are based on the assumptions and the provisions of the ACI 440.1R (2003).

- Strain in the concrete and CFRP is proportional to the distance from the neutral axis.
- The CFRP and concrete are adequately bonded.
- The behavior of CFRP is linearly elastic until failure.

- The tensile concrete strength is neglected in flexural computations.
- The ultimate concrete strain is 0.003

4.2.1 Ultimate Moment Capacity Equation

Based on these assumptions, the assumed rectangular compressive stress distribution in the concrete is used for simplification and is represented by a statically equivalent concentrated force, defined by the cylinder compressive strength f'_c , the parameter β_1 , and the quantity Kc , which locates the centroid of the stress block, as shown in Figure 55.

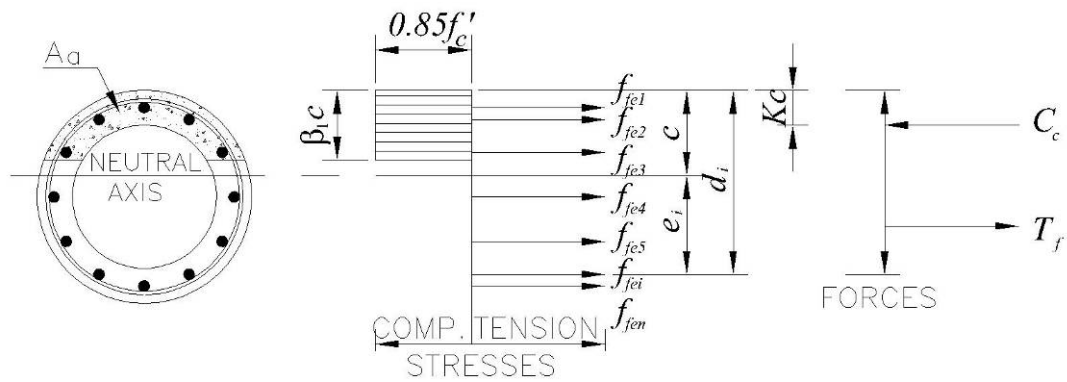


Figure 55. Concrete stress area and assumed stress distribution in pole section

The ultimate moment capacity of a pole section is determined based on the strain compatibility and the internal force equilibrium as follows:

$$M_u = \sum_{i=1}^n e_i A_{fi} f_{fei} + C_c (c - Kc) \quad (1)$$

$$e_i = d_i - c \quad (2)$$

$$f_{fei} < f_{fu} \quad (3)$$

Where A_{fi} and f_{fei} are the area and stress of the i^{th} reinforcement, respectively. c is the location of the neutral axis measured from the extreme compression fiber of the pole, Kc is the position of the centroid of the stress block, d_i is the distance of the i^{th} reinforcement from the extreme compression fiber, e_i is the distance of the i^{th} reinforcement to the neutral axis, and f_{fu} is the ultimate strength of the CFRP bars. It should be also noted that the quantity $e_i A_{fi} f_{fei}$ is positive when the i^{th} reinforcement is located below the neutral axis and negative when it is located above.

Unlike traditional steel reinforcement, CFRP is a linearly elastic material up to failure and does not have a yielding point, as shown in Figure 56.

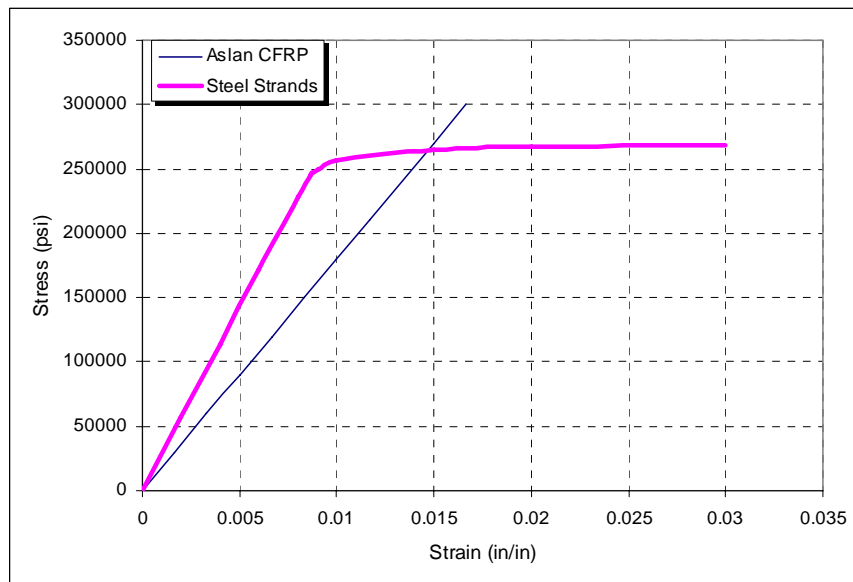


Figure 56. Stress-strain curves of CFRP bars and steel strands

This means that if a CFRP bar reaches its ultimate strength, failure will be sudden and catastrophic; therefore, in calculating the ultimate capacity of the poles reinforced with CFRP bars, the stress in the CFRP bars should always be less than the ultimate strength to avoid the catastrophic failure of the pole. In other words, the pole section should be designed as an over-reinforced section in which failure will be due to crushing of concrete. This condition is satisfied by using equation (3).

4.2.2 Cracking Moment

Cracking starts when the tensile stress in the extreme fiber of the concrete reaches its modulus of rupture. The cracking moment can be computed by elastic theory to predict the behavior of poles using the following relationship:

$$M_{cr} = \frac{f_r I_g}{y_t} \quad (4)$$

$$f_r = 7.5\sqrt{f'_c} \quad (5)$$

The first equation represents the cracking moment due to reaching the modulus of rupture of concrete f_r , which is calculated as a function of the concrete compressive strength of the pole using equation (5), as proposed by ACI 318-05. I_g is the gross moment of inertia of the section, and y_t is the distance from the centroidal axis to the extreme tensile fiber of the section.

4.2.3 Deflection

Deflection of concrete poles is calculated using the virtual work method as follows:

$$\Delta = \int_0^L \frac{M \cdot x}{E_c I} dx \quad (6)$$

Where M is the applied moment, x is the distance from the support, E_c is the modulus of elasticity of concrete, I is the moment of inertia, and L is the length of the pole. Before the cracking of the concrete section, the gross moment of inertia (I_g) is used to calculate the deflection; however, after cracking, the effective moment of inertia (I_e) is used. It is worthy of mention that concrete poles are tapered structures, so their moment of inertia is variable along the pole length.

Several researches have studied the deflection of rectangular concrete structures reinforced with CFRP bars, and the results of these studies show that the use of Branson's equation in calculating the effective moment of inertia underestimates the deflection of concrete structures reinforced with CFRP. These studies proposed several modifications to Branson's equation to account for the difference between the CFRP bars and traditional steel reinforcement. The factors thought to have an effect on Branson's equation were the difference between the modulus of elasticity of traditional steel reinforcement and CFRP bars, bond strength, and reinforcement ratio. According to ACI 440.1R-03, the effective moment of inertia (I_e) for concrete structures reinforced with FRP bars was calculated as follows:

$$I_e = \left(\frac{M_{cr}}{M_a} \right)^3 \beta_d I_g + \left(1 - \left(\frac{M_{cr}}{M_a} \right)^3 \right) I_{cr} \leq I_g \quad (7)$$

Where

$$\beta_d = \alpha_b \left[\frac{E_f}{E_s} + 1 \right] \quad (8)$$

In equation (7), β_d is a reduction coefficient that was multiplied to the first term of Branson's equation to reduce the gross moment of inertia and, accordingly, reduce the calculated effective moment of inertia in a trial to make Branson's equation work for concrete structures reinforced with CFRP bars. This reduction coefficient incorporates two of the factors that were thought to represent the difference in behavior between concrete structures reinforced with traditional steel reinforcement and concrete structures reinforced with CFRP bars. The first factor is the bond coefficient α_b , which accounts for the differences in bond strength between traditional steel reinforcement with concrete and CFRP bars with concrete. A bond coefficient of 1.0 means that the CFRP bars have the same bond traditional steel reinforcement, a higher value for the bond coefficient means higher bond, and a less value means less bond. In this study, the bond coefficient was taken to equal 0.5, as recommended by previous studies. The second factor is E_f/E_s , where E_f and E_s are the modulus of elasticity of the FRP bars and the steel, respectively, M_{cr} is the cracking moment, M_a is the maximum moment subjected to the pole, and I_{cr} is the cracking moment of inertia calculated as follows:

$$I_{cr} = I_{A_a} + \sum_{i=1}^n n_f \cdot A_{f_i} \cdot e_i^2 \quad (9)$$

In this equation, I_{A_a} is the moment of inertia of annulus at the neutral axis calculated, as discussed later in this chapter, n_f is the modular ratio between CFRP and con-

crete, A_{f_i} is the area of the i^{th} reinforcement, and e_i is the distance of the i^{th} reinforcement to the neutral axis.

The ACI 440.1R-03 committee report recommends having more experimental data so that the value of the bond-dependent coefficient α_b can be comprehensively evaluated. Yost et al. (2003) claimed that the accuracy of equation (7), for the calculation of the effective moment of inertia for concrete structures reinforced with FRP bars, primarily relied on the reinforcement ratio of the member, and proposed a new formula for the bond-dependent coefficient α_b that is a function of the ratio of the reinforcement ratio used and the balanced reinforcement ratio of the section. The coefficient is calculated as follows:

$$\alpha_b = 0.064 \left(\frac{\rho}{\rho_b} \right) + 0.13 \quad (10)$$

Where ρ is the reinforcement ratio used, and ρ_b is the balanced reinforcement ratio of the section.

The ACI 440.1R-06 committee report also proposed revisions to the design equation in the ACI 440.1R-03 committee report. The reduction coefficient β_d was modified. The key variable in the equation was changed from the modulus of elasticity of FRP reinforcement to the relative reinforcement ratio, as shown in the following equation:

$$\beta_d = \frac{1}{5} \left(\frac{\rho}{\rho_b} \right) \leq 1.0 \quad (11)$$

Bischoff and Scanlon (2007) concluded that equation (7) under-estimates the deflection of concrete members reinforced with FRP because the ratio I_g/I_{cr} is typically

much greater than three, and proposed a new equation to calculate the effective moment of inertia based on a weighted average of flexibility rather than stiffness. The proposed equation is as follows:

$$I_e = \frac{I_{cr}}{\left(1 - \eta \left(\frac{M_{cr}}{M_a}\right)^2\right)} \leq I_g \quad (12)$$

$$\eta = 1 - \frac{I_{cr}}{I_g} \quad (13)$$

From this discussion, it can be seen that there are different thoughts regarding the calculation of the effective moment of inertia for concrete structures reinforced with CFRP bars. In this study, for the sake of comparison and the best formulation of the equation that calculates the deflection of concrete poles reinforced with CFRP bars under service and ultimate load, the effective moment of inertia of concrete poles reinforced with CFRP bars was calculated every one foot along the length of the pole using the modified Branson's equation proposed by the ACI 440.1R-03 report, the bond coefficient proposed by Yost et al. (2003), the updated reduction coefficient proposed by the ACI 440.1R-06 committee report, and the new equation proposed by Bischoff and Scanlon (2007).

To draw the theoretical load deflection curve for the poles, several points were required; therefore, the deflection was calculated at load intervals of 150 lbs, starting from zero and going up to the cracking load. The load interval was increased to 500 lbs after cracking. For ease of calculation, the tip deflection was calculated for a unit load acting one foot from the tip of the pole, and then multiplied by the load increment to get the required deflection. The deflection was calculated as follows:

- a. The pole was divided from the tip to the support in equal segments 1.0 foot long.
- b. The moment at the end of each load segment was calculated. The moment at the end of each segment is equal to the length of the pole from the loading point up to the end of each segment, and this is because the applied load is a unit load.
- c. The bending moment diagram was drawn for each segment, and the area under the bending moment diagram was calculated. The result was multiplied by the distance from the tip to the centroid of each segment. In our case, the bending moment diagram is zero for the first segment, triangle for the second segment, and trapezoidal for the rest of the segments.
- d. For each segment, the result from step “c” was divided by the moment of inertia calculated at the end of the segment. Prior to the cracking load, the moment of inertia used was the gross moment of inertia and, after cracking, the moment of inertia used was the effective moment of inertia calculated as described previously.
- e. The results from step “d” were summed all together and divided by the modulus of elasticity of concrete.
- f. The result from step “e” was multiplied by each load interval to determine the deflection.

The load deflection curves shown in Figure 70 and Figure 71 of chapter 6 and developed as discussed were compared with the results from the experimental study, result-

ing in the development of a modified design equation for the calculation of the effective moment of inertia of concrete poles reinforced with CFRP bars, as shown in Chapter 6.

4.2.4 Crack Width

The ACI 440.1R-03 equation was used to calculate the crack width of spun concrete poles reinforced with CFRP. The equation is as follows:

$$w = \frac{2200}{E_f} \beta \cdot k_b \cdot f_{f_{ei}} \cdot \sqrt[3]{d_c \cdot A} \quad (14)$$

$$\beta = \frac{e_t}{e_i} \quad (15)$$

Where w is the crack width in mils, d_c and A are as shown in Figure 57, and k_b is a bond coefficient assumed to be 1.0 for this study. A bond coefficient of 1.0 means that the CFRP bars have the same bond as the traditional steel reinforcement, a higher value for the bond coefficient means higher bond, and a smaller value means less bond. E_f is the tensile modulus of elasticity of CFRP bars, and $f_{f_{ei}}$ is the stress on the i^{th} reinforcement.

This equation was developed for a rectangular concrete section with single layer of reinforcement; however, spun concrete poles are round, and the reinforcement is aligned around the cross-section, therefore, the definition of the effective tension area of concrete A was modified to account for the shape difference and reinforcement alignment between rectangular and circular concrete sections. In rectangular concrete sections with single layer of reinforcement, the effective tension area of concrete A is defined as the area of concrete having the same centroid as that of tensile reinforcement, divided by the

number of bars. In this study, however, it is proposed to define the effective tension area of concrete A as the area of concrete having the same centroid as that of the tensile reinforcement farthest from the neutral axis, as shown in Figure 57.

Since the poles are reinforced with CFRP bars rather than traditional steel reinforcement, the crack width seems to have no significant effect on the pole durability; however, cracks need to be controlled for serviceability.

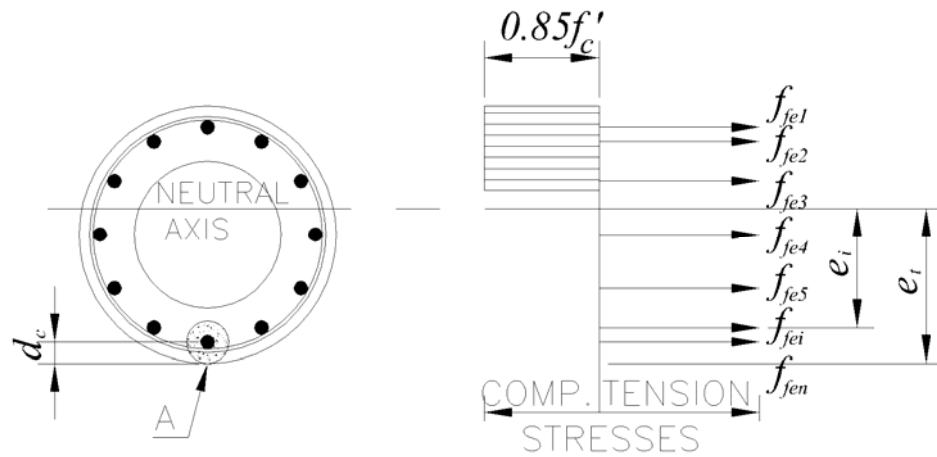


Figure 57. Crack width parameters for pole specimens

4.3 Spreadsheets Design and Verification

Since the design process of poles depends mainly on trial and error iterations in solving for the equilibrium equation, spreadsheets were developed to facilitate the analysis and design process. The flow charts for the spread sheets are shown in appendices A through C.

Since FRP concrete poles are not yet widely used, it was difficult to compare the results obtained from the CFRP spreadsheet. In the literature, one paper by Terrasi et al

(2001) was found dealing with this subject. The results presented in Terrasi et al (2001) were compared with the spreadsheet calculations, as shown in Figure 58. The concrete dimensions, reinforcement, and material properties are shown in Table 12. The ultimate moment capacities shown in Figure 58 are for six different sections of a 26-ft-high CFRP pole. From this figure it can be seen that the spreadsheet conservatively estimates the ultimate capacity of the poles. For poles 1, 2, and 3, the reduction in the ultimate moment capacity calculated using the spreadsheet is 4%, 5%, and 4%, respectively, while for poles 4, 5, and 6, the reduction is about 1%, 0.6%, and 0.6%, respectively. These results show that there is an average reduction in the ultimate moment capacities of about 2.5% when using the spreadsheet. This percentage indicates that the results from the spreadsheet correlate very well with the results obtained from Terrasi et al (2001).

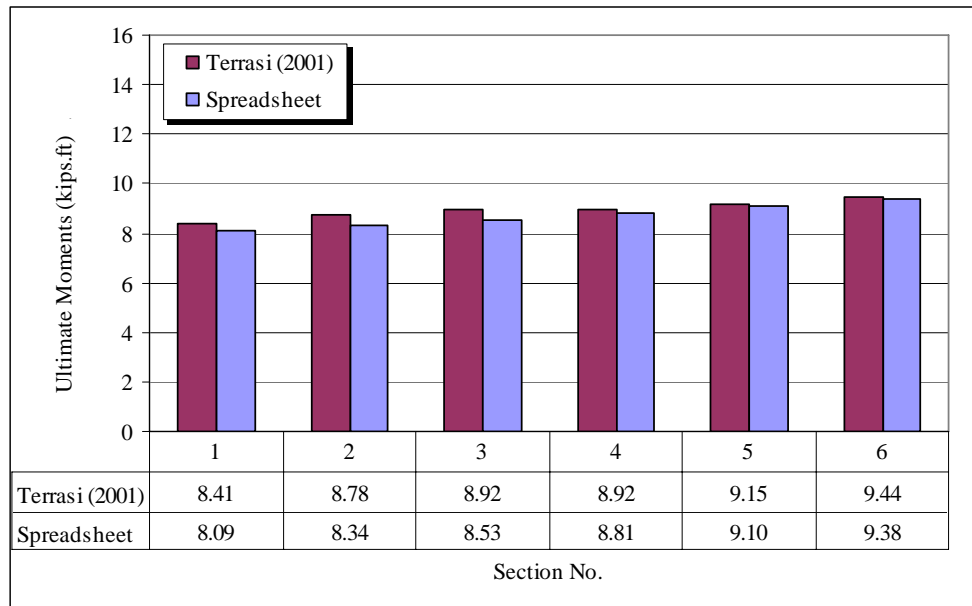


Figure 58. Ultimate moment capacities of CFRP prestressed spun concrete pole

Table 12

Concrete and reinforcement details of six different sections of a CFRP pole (Terrasi et al. 2002)

Section Number	1	2	3	4	5	6
Pole Outer Dia. (in)	7.00	7.17	7.28	7.48	7.68	7.87
Pole Inner Dia. (in)	3.82	4.02	4.13	4.33	4.53	4.72
f_c (ksi)	13.05	13.05	13.05	13.05	13.05	13.05
f_{pu} (ksi)	332	332	332	332	332	332
E_s (ksi)	23350	23350	23350	23350	23350	23350
Conc. Cover (in)	0.80	0.80	0.80	0.80	0.80	0.80
No. of Strands	6	6	6	6	6	6
Tendon Dia. (in)	0.16	0.16	0.16	0.16	0.16	0.16
P_i (kips)	3.73	3.73	3.73	3.73	3.73	3.73

In Table 12, f_c is the average concrete compressive strength, f_{pu} is the ultimate tensile strength of the prestressing strands, E_s is the elastic modulus of the prestressing strands, and P_i is the effective prestressing force applied to the strands.

4.4 Summary

This chapter presents the analytical study that was performed to estimate the behavior of spun concrete poles reinforced with CFRP under loading conditions. Equations to calculate the ultimate moment capacity, cracking moment, deflection, and crack width were presented. Spreadsheets were developed and verified to help in calculating the cracking and ultimate moment capacities of the spun concrete poles reinforced with CFRP bars, calculate the cracking moment of inertia of the poles, and develop the load deflection points needed to draw the load deflection curve of the poles.

CHAPTER 5

FINITE ELEMENT MODELING

5.1 Introduction

Finite element modeling was conducted using the ANSYS software, to model the tested specimens and compare the results from the experimental and analytical programs with the results of the finite element modeling. In addition to improving our understanding of the behavior of poles reinforced with CFRP bars under loading conditions, finite element modeling allows for performing parametric studies through which the effect of different variables, such as concrete strength, wall thickness, concrete cover, flexural, and shear reinforcement ratios, can be investigated.

5.2 Finite Element Model

Modeling of concrete poles using finite element software involves defining the element types and material properties used to model the concrete and the CFRP reinforcement. This section discusses the two element types used to model the concrete and CFRP reinforcement, and presents the mechanical properties of concrete and CFRP that were used in the model.

5.2.1 Element Types

SOLID65 of the ANSYS software was used to model the concrete. This solid element has eight nodes with three degrees of freedom at each node. Each node can accept translational movement in the x, y, and z directions, but none of them can accept rotational movement. This element was designed by ANSYS especially to model concrete structures, as it is capable of crushing in compression, cracking in tension, and plastic deformation.

Link8 of the ANSYS software was used to model the CFRP reinforcement; this is a 3D element that has two nodes with three degrees of freedom at each node. Each node can accept translational movement in the x, y, and z directions. The element is also capable of plastic deformation.

5.2.2 Real Constants

Real constants are used by ANSYS to input the data that are required for the calculation of the element matrix but cannot be determined from the node locations or material properties. Typical real constants include area, thickness, inner diameter, and outer diameter.

Real constant set 1 is used for the Solid65 element. It requires real constants for rebar, assuming a smeared model. Values can be entered for material number, volume ratio, and orientation angles. The material number refers to the type of material for the reinforcement. The volume ratio refers to the ratio of steel to concrete in the element. The orientation angles refer to the orientation of the reinforcement in the smeared model. ANSYS allows the user to enter three rebar materials in the concrete. Each material cor-

responds to x, y, and z directions in the element. The reinforcement has uniaxial stiffness, and the directional orientation is defined by the user. In the present study, the poles were modeled using discrete reinforcement; therefore, a value of zero was entered for all real constants, which turned off the smeared reinforcement capability of the solid 65 element off.

Real constant set 2 was defined for the Link8 element. Values for the cross-sectional area of the CFRP bars and initial strain were entered. A value of zero was entered for the initial strain, because there was no initial strain applied to the CFRP reinforcement. Real constants for Link8 are shown in Table 13.

Table 13

Real constants for Link8 element

Real Constants	
Cross-sectional Area (in ²)	0.101
Initial Strain	0

5.2.3 Material Properties

The materials used in this study are the concrete and the CFRP reinforcement. For reinforced concrete structures, the material properties are defined by the compressive and tensile strengths, and by the modulus of elasticity of the material.

5.2.3.1 Concrete

The concrete used in this study was a specially formulated, high strength concrete mix for spun concrete poles designed and produced by the batch plant. This mixture was designed to produce a concrete with an average compressive strength of about 11,000 psi at 28 days (Table 14).

Different equations have been used to calculate the elastic modulus of concrete; however, it was found by Nunez (2002) that the equation used by Nawy (2001) falls within the upper and lower bound expressions for the estimation of modulus of elasticity, and, it was used in this study. The modulus of elasticity of concrete is calculated as follows:

$$E_c (psi) = \left[40000\sqrt{f'_c} + 10^6 \left(\frac{w}{145} \right)^{1.5} \right] \quad (16)$$

Where,

f'_c = The average compressive strength of concrete

w = Unit weight of concrete in lb/in³

In concrete with normal compressive strength and up to strength of 6000 psi the peak strain ε_0 in compression is equal to 0.002; however, for high strength concrete, the peak strain in compression was calculated as follows (Nunez 2002):

$$\varepsilon_0 = 0.001306 + 1.3789 \times 10^{-7} f'_c \quad (17)$$

The following equations (Nunez 2002) were used to construct the uniaxial compressive stress-strain curve for concrete in this study (Figure 59):

$$f = \frac{f'_c \beta \left(\frac{\varepsilon}{\varepsilon_0} \right)}{\beta - 1 + \left(\frac{\varepsilon}{\varepsilon_0} \right)^\beta} \quad (18)$$

$$\beta = \frac{1}{1 - \frac{f'_c}{\varepsilon_0 E_0}} \quad (19)$$

Where,

f = Stress at any strain ε

ε = Strain at any stress f

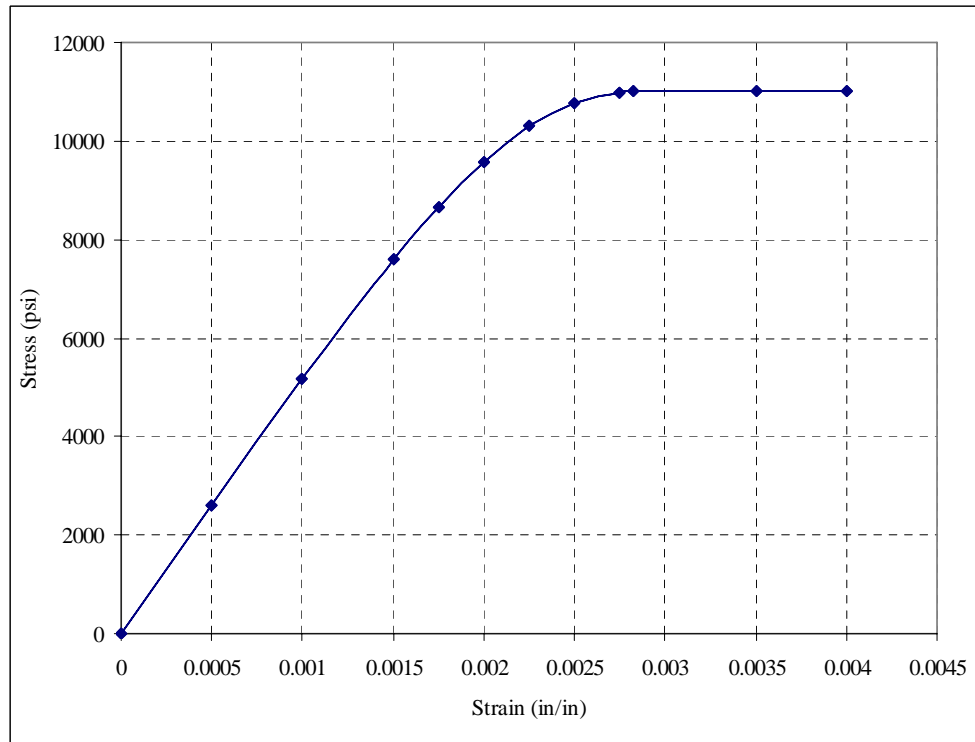


Figure 59. Concrete stress-strain curve adopted in the FE model

ANSYS software uses the smeared crack approach (William and Warnke 1974) to model the cracks in concrete, which requires the definition of a number of constants. These constants are the shear transfer coefficient, the uniaxial tensile cracking stress, and the uniaxial crushing stress. The shear transfer coefficient range from a value of 0 to 1.0, with zero representing a smooth crack and 1.0 representing a rough crack. As reported by Kachlakev et al (2001), the value of the shear transfer coefficient for open cracks varied between 0.05 and 0.25. In this study, a number of preliminary analyses were tried with different values for the shear transfer coefficient within this range, and a value of 0.125 was used, as it was able to closely predict the behavior of the poles. The uniaxial tensile stress was entered as per the experimental records, while the uniaxial crushing stress capability was disabled as recommended by previous research (Kachlakev et al 2001, and Barbosa and Ribeiro 1998). Poisson's ratio for concrete was assumed to be 0.20. Table 14 shows a summary of the concrete properties.

Table 14

Summary of Material Properties for Concrete

Modulus of Elasticity, E_c (psi)	Peak Strain, ϵ_0	Compressive Strength, f'_c (psi)	Tensile Strength, f_r (psi)	Poisson's Ratio, ν
5195235	0.00282	11000	585	0.20

5.2.3.2 CFRP Bars

As indicated in the experimental program, the CFRP bars used in this study were provided by Hughes Brothers Inc. under the commercial name of Aslan 200, and its physical properties are listed in Table 1. CFRP behaves linearly up to failure and was

modeled as a multi-linear elastic material. The stress-strain curve for the CFRP bars used in this study is shown in Figure 60.

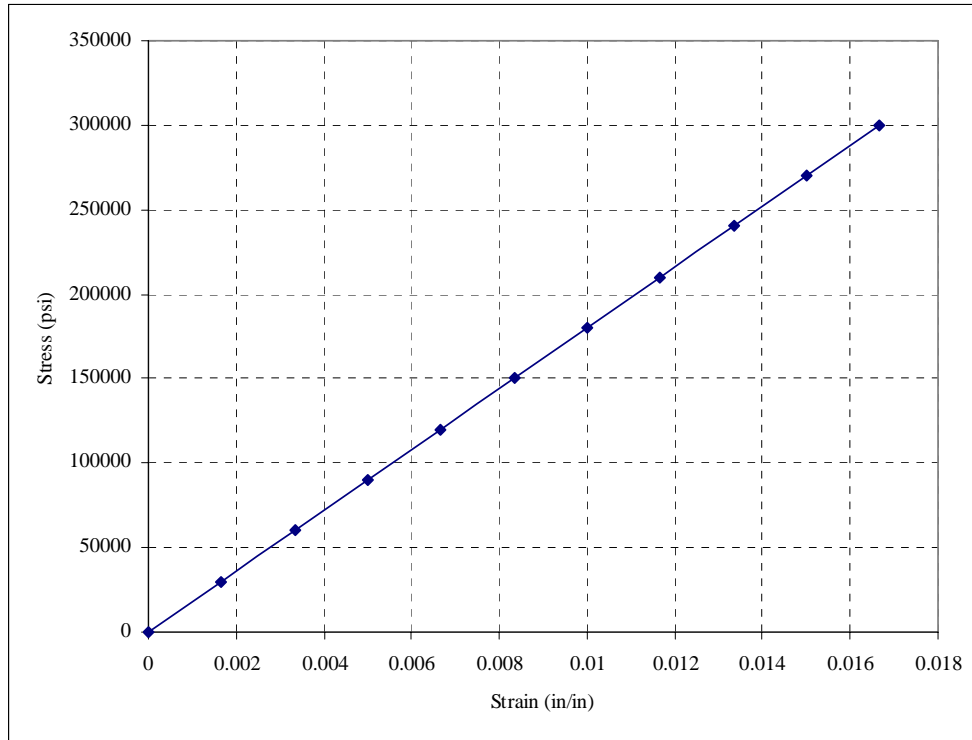


Figure 60. Stress-strain curve for CFRP bars

5.2.4 Structure Modeling

Two poles were modeled using the ANSYS software. The poles were identical to each other, and the only difference was in the number of CFRP bars, one pole having 6 bars and the other 12. The poles were modeled using the volume option and meshed using the volume sweep option. The mesh size was based on a convergence study that was performed to determine a suitable mesh. The poles were meshed every 2 in. in the longitudinal direction (Figure 61), and in the cross-section they were meshed on an angle of

15°, as shown in Figure 62. Figure 62 also shows the orientation of the CFRP bars in the cross-section. The figure shows that the six CFRP bars of the first pole were not symmetrically distributed around the cross-section. The six CFRP bars were modeled that way to match with the orientation of the actual test specimens. The 6 CFRP bars of the first group in the actual test specimens were oriented as shown in Figure 62 because they were restricted by the available opening in the end plates of the molds where the poles were cast. CFRP bars were added to the model, as Link8 element, so that they share the same nodes for concrete (Figure 63), assuming a perfect bond. Each CFRP bar was divided into 120 Link8 elements, so that each element was 2 in long. A preliminary run was tried to check the effect of the stirrups on the results and was found to be not significant, so they were left out in order to decrease the number of elements and perform faster computations. Both finite element models had 5760 Solid65 elements. The first model where the pole was reinforced with six bars had 720 Link8 elements, and the second model where the pole was reinforced with 12 bars had 1440 Link8 elements.

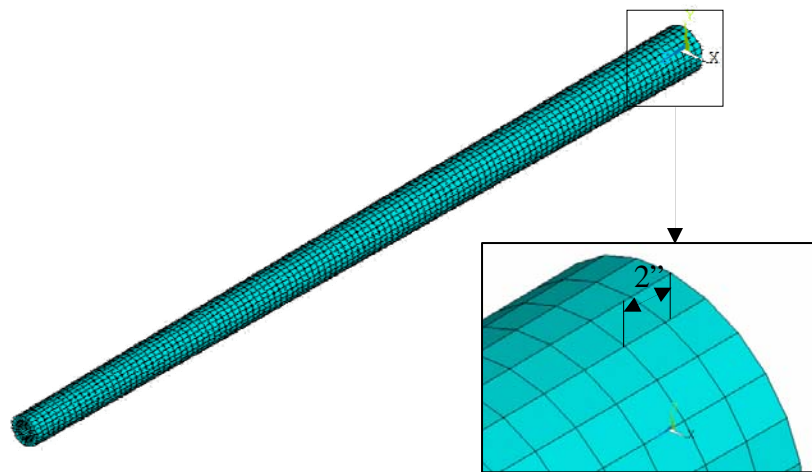


Figure 61. Finite element meshing of the pole in the longitudinal direction

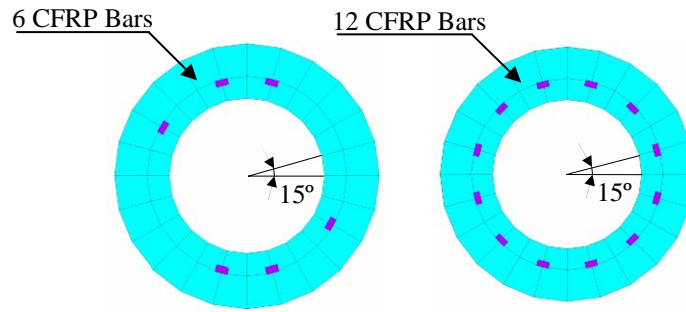


Figure 62. Finite element meshing of the pole in the cross-sectional direction

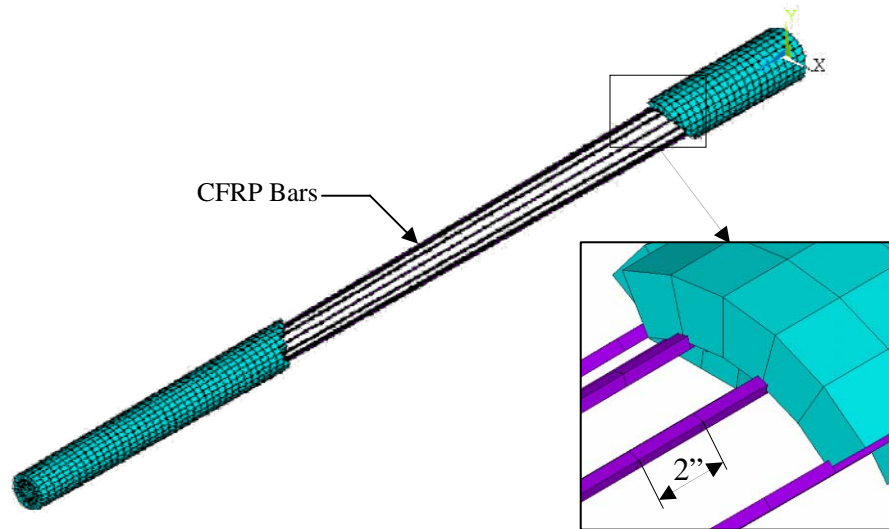


Figure 63. Finite element modeling of the CFRP bars

5.2.5 Loads and Boundary Conditions

Displacement boundary conditions are needed to constrain the model to get a reliable solution for stresses and deformations. Two types of boundary conditions were applied, one was to model the support condition of the poles and the second was to prevent any out-of-plane displacements that might affect the results. The first set of boundary

conditions was applied at two locations, one at the butt end of the pole and the other at 3.00 ft from the butt. These distances were chosen to match the experimental test setup. The supports were modeled as fixed supports, so the displacement in all three directions was prevented, and since the poles were modeled as solid elements, therefore, by constraining the displacement at two nodes of the elements, the rotation will be prevented. The second set of boundary conditions was applied to all of the nodes. All of the nodes were prevented from displacement in the out-of-plane direction by constraining the displacement in the x-direction (Figure 64).

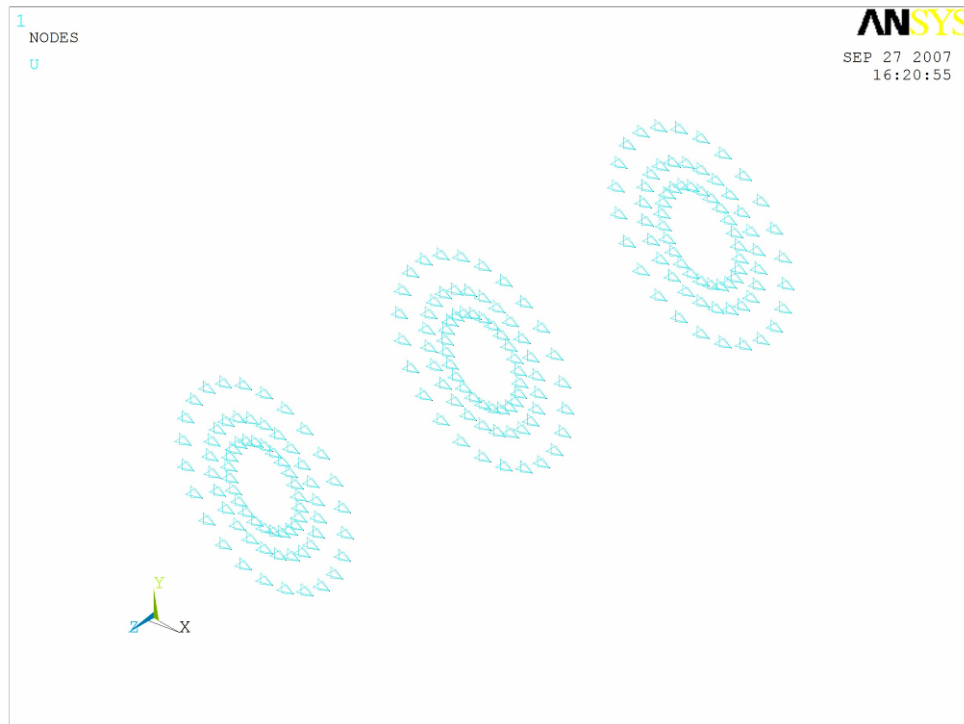


Figure 64. Sample of the out-of-plane joint restraints

During the test, the load was applied at one foot from the tip end of the pole using a strap that surrounded half the circumference of the pole and connected to the hoist chain. In order to match the test setup in our model, the load was also applied at one foot from the tip end of the pole as point loads over the nodes covering half the circumference of the cross-section, as shown in Figure 65. Another reason for distributing the load over the nodes at this section is that if the load was applied on only one node, distortion to the elements connected to this node would happen and the file would not run. The load applied at each node was equal to one over thirteen of the actual load applied.

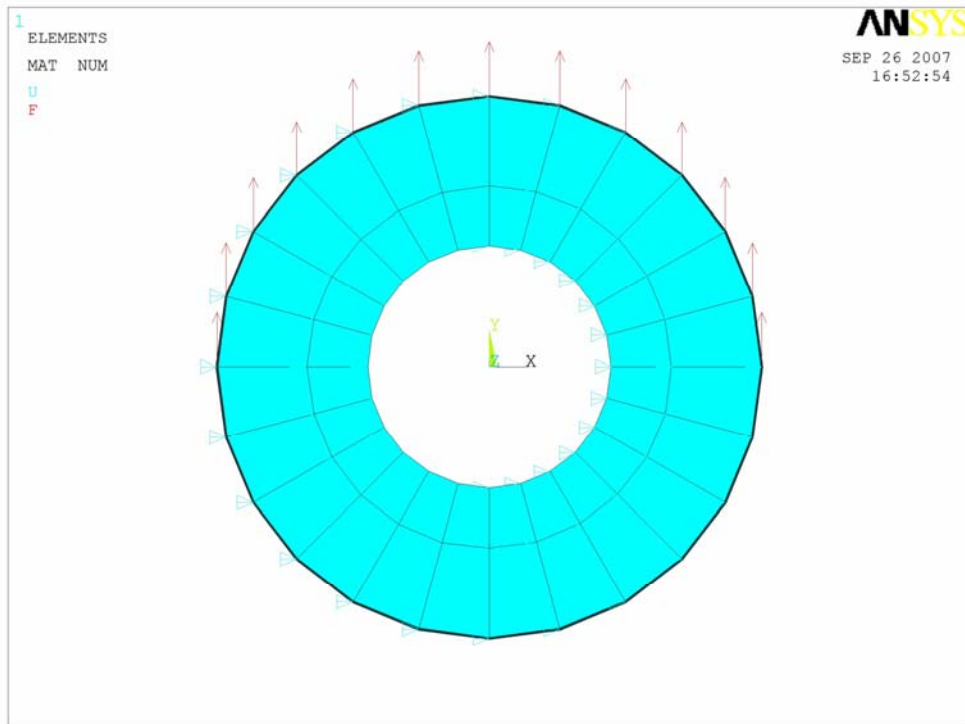


Figure 65. Point loads applied to the pole

5.2.6 Analysis Type

The finite element model for this analysis was a cantilever pole under point loading. For the purpose of this model, the static analysis type was used. Sections 5.2.6.1, 5.2.6.2, and 5.2.6.3 discuss the solution control commands incorporated by the ANSYS and used to perform this analysis.

5.2.6.1 The Newton-Raphson method

The Newton-Raphson method incorporated by the ANSYS was used to compute the nonlinear response. Using this method, the load was subdivided into a series of load increments, and the load increments were applied over several load steps. As per the ANSYS manual, the Newton-Raphson method can be described as follows.

Before each solution, the Newton-Raphson method evaluates the out-of-balance load vector, which is the difference between the restoring forces (the loads corresponding to the element stresses) and the applied loads. The program then performs a linear solution, using the out-of-balance loads, and checks for convergence. If the convergence criteria are not satisfied, the out-of-balance load vector is reevaluated, the stiffness matrix is updated, and a new solution is obtained. This iterative procedure continues until the problem converges (ANSYS Manual, 2005).

Loads were applied in very small increments that sometimes reached 1 lb to avoid any convergence problems that might occur and to fulfill the requirements of the Newton-Raphson method. A listing of the load steps, sub-steps, and loads applied are shown in Table 15 and Table 16.

Table 15

Load increment for the finite element model of the first pole

Load Step	Sub-step	Beginning Time	Time at End of Load Step	Load Increment (lbs)
1	1	0	520	520
2	1	520	526.5	6.5
3	1	526.5	533	6.5
4	1	533	546	13
5	1	546	559	13
6	1	559	572	13
7	1	572	585	13
8	1	585	598	13
9	1	598	611	13
10	39	611	650	1
11	13	650	663	1
12	26	663	689	1
13	1	689	702	13
14	1	702	715	13
15	1	715	728	13
16	1	728	741	13
17	1	741	754	13
18	1	754	767	13
19	1	767	780	13
20	1	780	806	26
21	1	806	832	26
22	1	832	858	26
23	1	858	884	26
24	1	884	910	26
25	13	910	1040	10
26	13	1040	1170	10
27	13	1170	1300	10
28	13	1300	1430	10
29	13	1430	1560	10
30	Auto	1560	2600	Auto
31	Auto	2600	3120	Auto

Load Step	Sub-step	Beginning Time	Time at End of Load Step	Load Increment (lbs)
32	Auto	3120	3250	Auto
33	Auto	3250	3380	Auto
34	130	3380	3510	1
35	65	3510	3640	2
36	65	3640	3756	2

Table 16

Load increment for the finite element model of the second pole

Load Step	Sub-step	Beginning Time	Time at End of Load Step	Load Increment (lbs)
1	1	0	520	520
2	1	520	526.5	6.5
3	1	526.5	533	6.5
4	1	533	546	13
5	1	546	559	13
6	1	559	572	13
7	1	572	585	13
8	1	585	598	13
9	1	598	611	13
10	39	611	650	1
11	13	650	663	1
12	26	663	689	1
13	1	689	702	13
14	1	702	715	13
15	1	715	728	13
16	1	728	741	13
17	1	741	754	13
18	1	754	767	13
19	1	767	780	13
20	1	780	806	26
21	1	806	832	26

Load Step	Sub-step	Beginning Time	Time at End of Load Step	Load Increment (lbs)
22	1	832	858	26
23	1	858	884	26
24	1	884	910	26
25	13	910	1040	10
26	13	1040	1170	10
27	13	1170	1300	10
28	13	1300	1430	10
29	13	1430	1560	10
30	Auto	1560	2600	Auto
31	8	2600	3120	65
32	Auto	3120	3250	Auto
33	Auto	3250	3380	Auto
34	Auto	3380	3510	Auto
35	Auto	3510	3640	Auto
36	Auto	3640	3770	Auto
37	Auto	3770	3900	Auto
38	13	3900	4030	10
39	13	4030	4160	10
40	13	4160	4290	10
41	13	4290	4420	10
42	13	4420	4550	10
43	13	4550	4680	10
44	13	4680	4720	10

In those tables, the time at end of each load step refers to the ending load per load step, and the word “Auto” used in the sub-steps and load increments refers to automatic sub-stepping. Automatic sub-step means that the ANSYS divides the load step into sub-steps based on criteria aimed to achieve a convergence of the solution in the shortest time.

5.2.6.2 Equation solvers

ANSYS incorporates several methods of solving simultaneous equations; however, the sparse direct solver is the default for most of the analyses. The sparse direct solver is based on a direct elimination of equations, as opposed to iterative solvers, where the solution is obtained through an iterative process that successively refines an initial guess to a solution that is within an acceptable tolerance of the exact solution (ANSYS Manual, 2005). In this analysis, the default solver (Sparse Direct) was used as recommended by the ANSYS manual.

5.2.6.3 Convergence criteria

The ANSYS software iterates the equilibrium equations until the convergence criteria are achieved or until the maximum number of equations is reached. The default convergence criteria in the ANSYS is based on the force convergence criteria; however, you still have the choice to define your convergence criteria based on moments, displacements, or rotations, or any combination of these items. ANSYS checks the convergence criteria by comparing the square root sum of squares of the applied load or displacement against the specified criteria after each load step, if the square root sum of squares is greater than the input value, a new iteration will be processed, and if the square root sum of squares is less than the input value, the ANSYS will step to the next load step. In this study, the default force and displacement criteria were used. However, after the concrete cracked, convergence for the non-linear analysis was impossible with the default values, the force criteria were dropped, and the default values for the displace-

ment criteria were changed to reasonable values that can avoid the convergence problem. Table 17 shows the values of the displacement criteria used for this analysis.

Table 17

Displacement convergence criteria

Item	Value
Reference Value	10
Tolerance	0.05

5.3 RESULTS

Figure 66 shows the load versus concrete compressive strain at the support for each of the two test poles. From the figure, we can see that the two poles had the same behavior up to failure. The first part of the two curves was linear and represented the uncracked stage, while the last part of the curves represented the cracked stage after all the cracks had been formed and the stiffness of the section had been adjusted. In between the two parts, there is a transition zone where the cracks developed. We can see from this figure that the ANSYS represent the transition zone with a straight horizontal line. This straight line actually represents two points; the first point is just at the cracking load, while the other point is right after the cracking load. After cracking, the stiffness of the poles changed, so this sudden drop in the strain represented the change in the stiffness of the poles due to cracking. We can also see from this figure a second drop in the strain at a load of 800 lbs and 1000 lbs for the 6-bar pole and the 12-bar pole, respectively. This drop could refer to the stage where all of the cracks have been formed. It could also be seen from this figure that the 6-bar pole fails at a strain of 0.00276, corresponding to a

failure load of 3756 lbs, and the 12-bar pole fails at a strain of 0.0028, corresponding to a failure load of 4720 lbs.

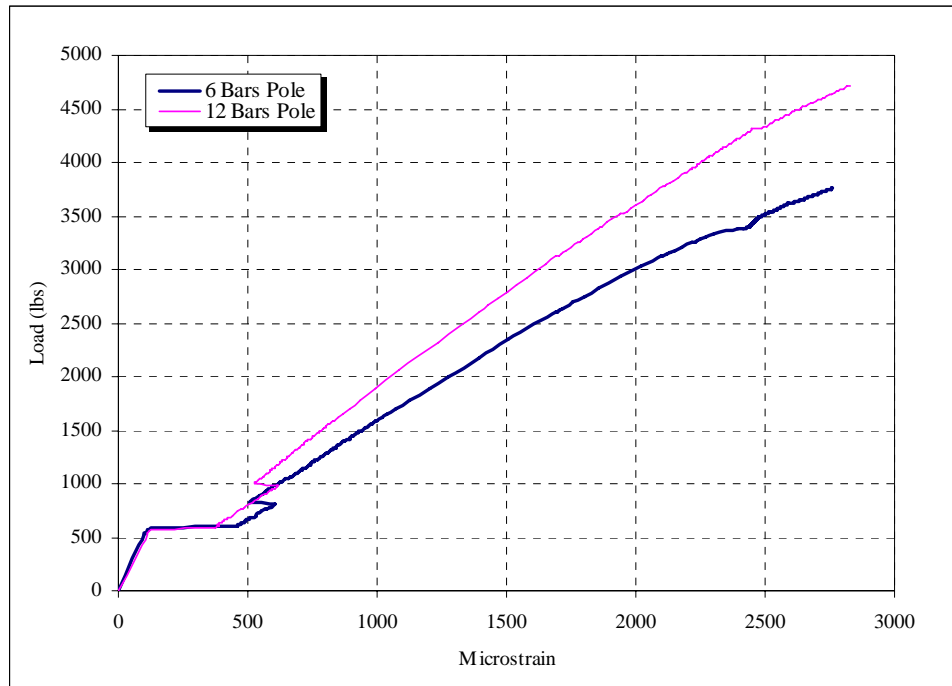


Figure 66. Load-compressive strain plot for the two poles

The load deflection curves for the two poles are shown in Figure 67. The figure shows that the load deflection curve for the two poles is bilinear, with the first part starting from zero and up to the cracking load, and the other part starting from the cracking and up to failure. It can be seen from this curve that the first linear stage for the two poles is coinciding with each other for the two poles, however the second part of the curve is not, and that is because for the first part the two poles were still in the linear stage and both poles were having their entire cross-section resisting the load, while for the other

part the two poles were already cracked, and so the curve was depending upon the stiffness after cracking for the two poles. Since the 12-bar pole has more reinforcement than the 6-bar pole, therefore at the same load the 6-bar pole exhibited more deflection than the 12-bar pole. For instance, at a load of 2600 lbs, the deflection was 16.34 in and 11.56 in for the 6-bar pole and the 12-bar pole, respectively. The gap between the deflection values increases as the load increases, as could be seen from the figure, and this is due to the difference between the effective moment of inertia of each pole. The effective moment of inertia of the pole with the higher number of reinforcement is higher than the other pole because, with more bars, fewer cracks with small widths will form, and higher inertia will develop.

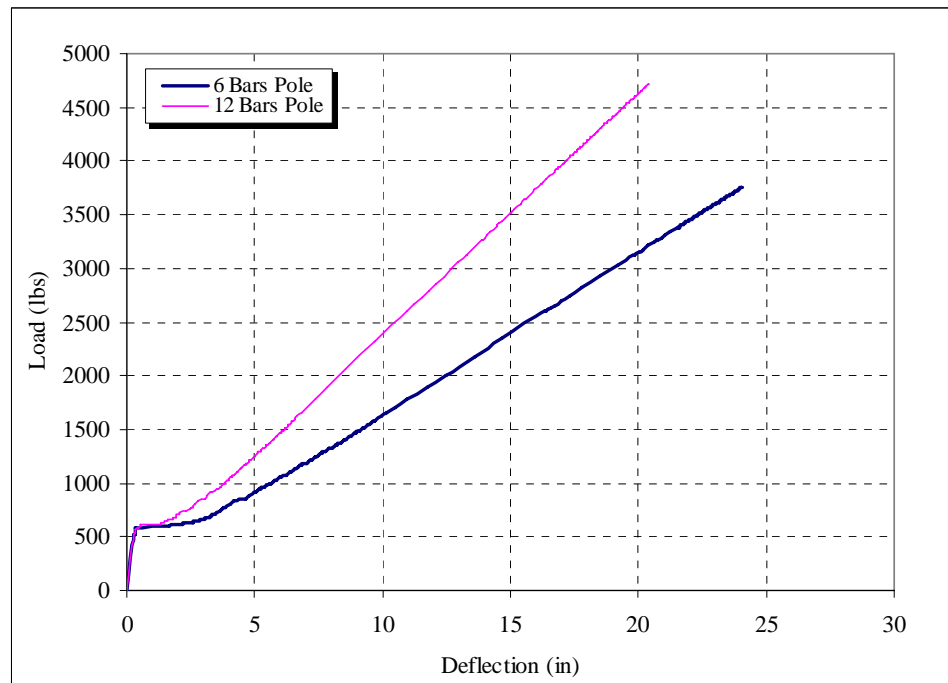


Figure 67. Load-deflection curve for the two poles

5.4 Summary

This chapter provides a finite element model for the spun concrete poles reinforced with CFRP bars using ANSYS finite element software. The types of elements used to model the concrete and CFRP bars as well as the modeling of the material properties of concrete and CFRP bars were presented. A description of how the elements defined to model the concrete and CFRP were combined together to model the whole structure is given. A discussion on the finite element analysis type was also presented where the solution control options used by the ANSYS software to set the nonlinear analysis were presented. Finally, the chapter ends with presenting the results of this analysis.

CHAPTER 6

DATA ANALYSIS AND DISCUSSION

6.1 Introduction

The objective of this chapter is to compare the experimental results with the theoretical results to verify or update the design equations that were proposed in chapter four for the flexural design of spun concrete poles reinforced with CFRP bars. The second objective is to compare the experimental results with the finite element results to verify the finite element model that was used in the analysis. Another objective of this chapter is to compare the flexural behavior of spun concrete poles reinforced with non-prestressed CFRP bars with the flexural behavior of conventional steel reinforced prestressed spun concrete poles. Due to the expensive cost of building the test specimens, we were not able to build a conventional steel reinforced prestressed spun concrete pole specimen. Therefore, we compare the experimental results of the spun concrete poles reinforced with CFRP bars with the theoretical results of conventional prestressed spun concrete poles.

In order to compare the experimental results with the theoretical ones, the experimental records were modified to cancel the effect of the pole's own weight. As discussed in chapter three, the pole's own weight was considered to be the load just before the strain gages start recording. This load was subtracted from all of the experimental data presented in this chapter.

6.2 Experimental Versus Theoretical Data

This section presents a comparative study between the experimental study performed in chapter 3 and the theoretical analysis performed in chapter 4. The comparison focuses on comparing the cracking and ultimate moment capacities, the load deflection curve, and the crack width obtained from the experimental study against the theoretical analysis.

6.2.1 Cracking and Ultimate Loads and Moments

Table 18, Figure 68, and Figure 69 show the theoretical and experimental cracking and ultimate moments of the two groups of this study. The theoretical values are calculated using the spreadsheet described in chapter four. Table 18 shows that the theoretical cracking moments for the two groups show good correlation with the experimental ones. For instance, the theoretical cracking moment for the two groups is 11.46 kips.ft, while the test values are 12.74 kips.ft and 11.59 kips.ft for the first and second groups, respectively. These experimental values are greater by 10% and 1%, respectively. Since the cracking moment depends mainly on the fracture modulus of concrete, and the reinforcement ratio had a minimal effect, we can compare the average cracking moment of the two groups (12.17 kips.ft) with the theoretical cracking moment. By doing so, we found that the theoretical cracking moment differed from the average cracking moment of the two groups by 6%, which is not a significant difference. Based on this discussion, it could be concluded that the basic theoretical equations used to calculate the cracking moment of concrete members reinforced with conventional steel reinforcement is valid for spun concrete poles reinforced with CFRP bars and results in conservative values.

Table 18 also shows that the experimental ultimate moment capacities are 63.14 kips.ft and 75.98 kips.ft for the first and second group, respectively, which corresponds to experimental failure loads of 3946 lbs and 4749 lbs for the first and second groups, respectively as shown in Figure 68 and Figure 69. However, the theoretical ultimate capacities are 59.48 kips.ft and 74.25 kips.ft for the first and second groups, respectively, which corresponds to theoretical failure loads of 3719 lbs for the first group and 4641 lbs for the second group, as shown in Figure 68 and Figure 69. Table 18 shows that there is no significant difference between the theoretical and experimental ultimate moment capacities of the two groups, since the theoretical value is lower by only 6% and 2% from the experimental value of the first and the second groups, respectively. This conclusion verifies the spreadsheet designed for calculating the ultimate moment capacities of spun concrete poles reinforced with CFRP.

Table 18

Theoretical and experimental cracking and failure moments

Group No	Results	Cracking Moment (ft.kips)	% Difference	Failure Moment (ft.kips)	% Difference
Group 1	Theoretical	11.46	(10%)	59.48	(6%)
	Experimental	12.74		63.14	
Group 2	Theoretical	11.46	(1 %)	74.25	(2%)
	Experimental	11.59		75.98	

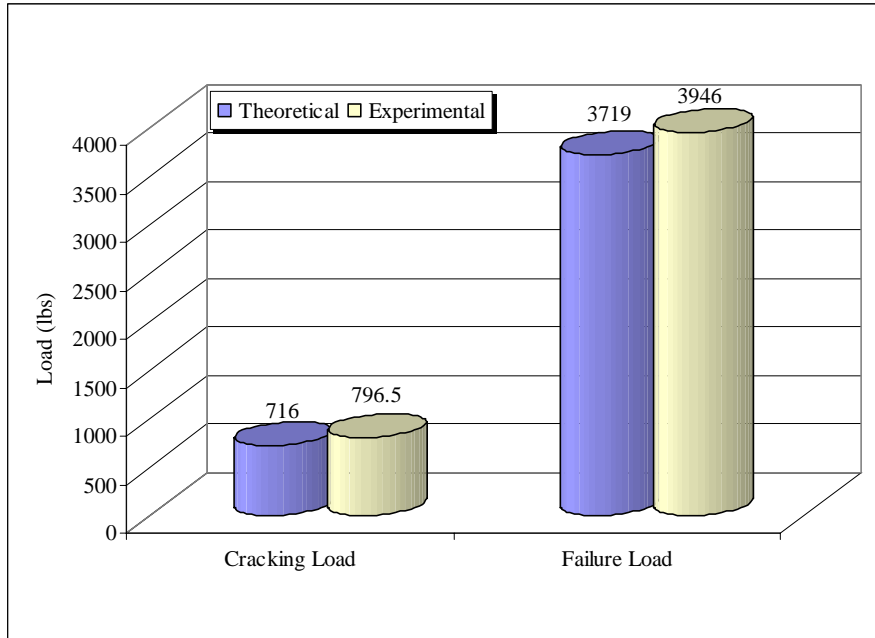


Figure 68. Cracking and failure loads of the G01 specimens

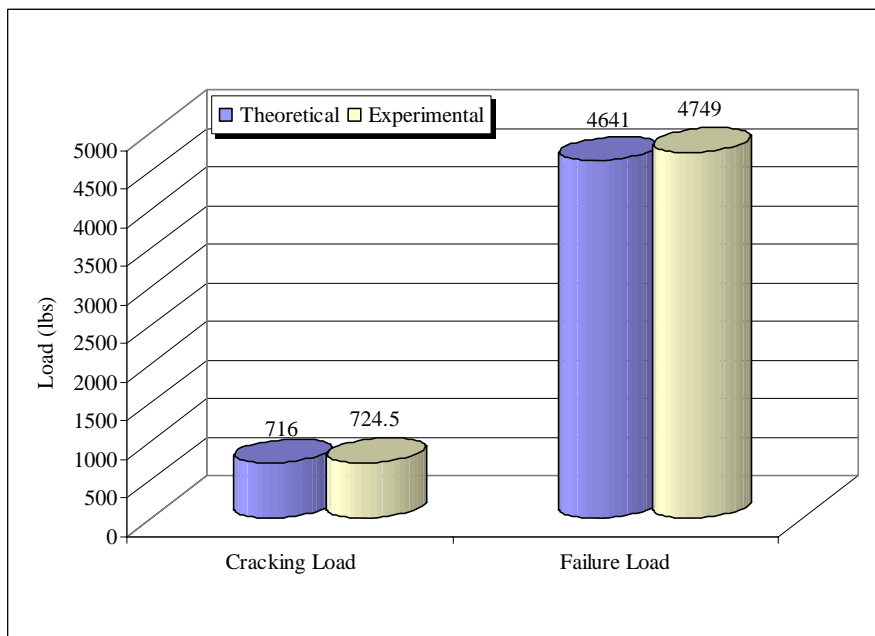


Figure 69. Cracking and failure load of the G02 specimens

6.2.2 Deflection

Figure 70 and Figure 71 show a comparison between the load-deflection curves obtained from the experimental records, and those developed using equations 9 to 15. In Figure 70 we can see that all the curves were identical and coincided with the experimental records starting from zero and up to the cracking load. After cracking, the curves developed using the equations proposed by the ACI 440-03 (2003) significantly diverge from the experimental curve. All of the other curves coincided with the experimental load up to 2000 lbs, and then the curves start diverging upward. At failure load, the lowest deflection was determined by the ACI 440-03 equation to be 23.55 in, underestimating the tip deflection of the pole at failure by 2.31 in, a 9% difference from the experimental records (Table 19).

In Figure 71, all of the curves are identical and coincide with the experimental records starting from zero and up to a load of 3500 lbs, with the curve developed using the equation proposed by Bischoff and Scanlon (2007) slightly overestimating the deflection of the poles between the loads at 1000 lbs and 2000 lbs. At failure load, the lowest deflection was recorded by the Bischoff and Scanlon (2007) equation to be 19.58 in, underestimating the tip deflection of the pole at failure by 1.53 in and making a 7% difference from the experimental records (Table 19).

From this discussion, we can conclude that all of the proposed equations significantly overestimated the deflection at service and ultimate loads for the first group of poles; however, for the second group of poles, the proposed equations were able to predict the deflection of the pole at service load and overestimated the deflection of the poles

at failure. It can be also concluded that the reinforcement ratios affect the prediction of the pole's deflection using the proposed equations.

Table 19

Tip deflection at failure load

Group No.	Experimental (in)	ACI-03 (in)	Yost et al. (in)	ACI-06 (in)	Bischoff (in)
First Group	25.86	23.55	24.11	24.06	23.94
Second Group	21.11	19.64	19.76	19.65	19.58

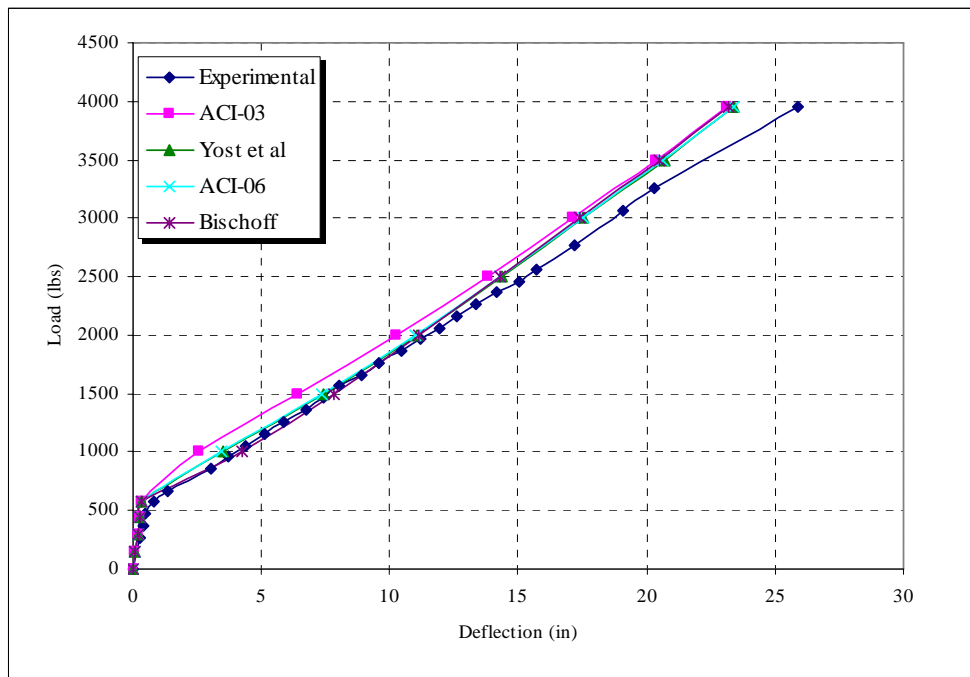


Figure 70. Load-deflection curve for the G01 specimens

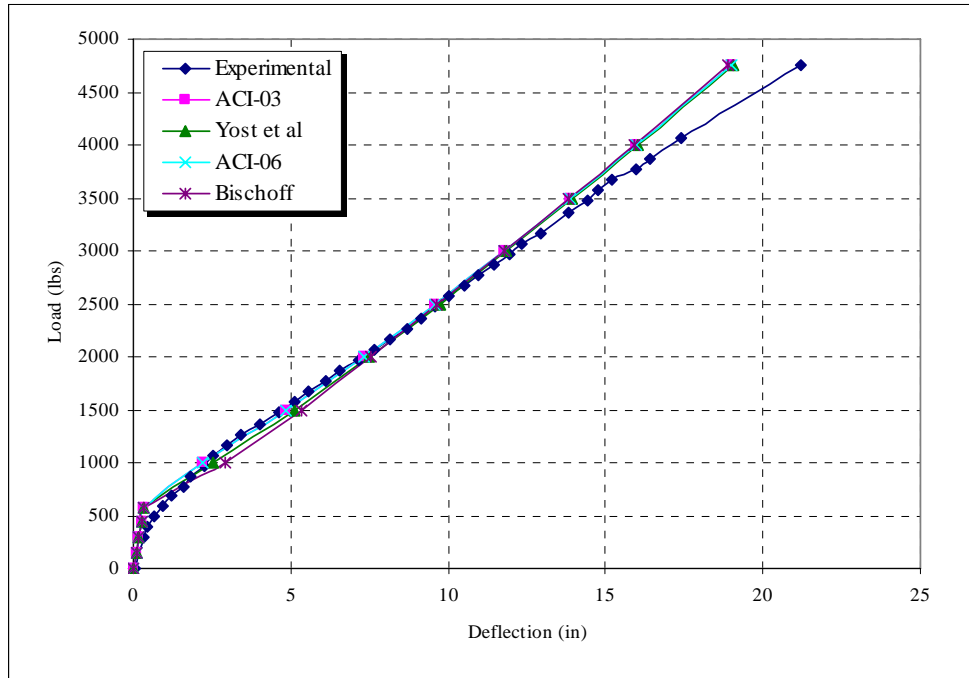


Figure 71. Load-deflection curve for the G02 specimens

This discussion indicates that the proposed equations for the calculation of the effective moment of inertia for concrete structures reinforced with FRP bars need to be revised, at least for spun concrete poles. By trial and error, we were able to find that reducing the calculated cracked moment of inertia by 10% significantly improved the prediction of deflection using any of the proposed equations. This can be seen from the results plotted in Figure 72 and Figure 73. In these figures, the ACI 440-03 is not plotted, as it was not significantly improved compared to others. We can see that we were able to predict the deflection at service and ultimate loads with very high accuracy. For the first group of poles at failure load, the predicted deflection using any of the proposed equations is higher than the experimental values by about 3% (Table 20). At the failure load for the second group, the difference between the predicted and experimental deflection

varied by about 2% to 3% (Table 20), which is a very significant improvement in the results. In Figure 72 and Figure 73 we can see that all of the equations predicted the deflection all over the loading path of the pole with a very good accuracy. The Bischoff and Scanlon (2007) equation is recommended to calculate the deflection of spun concrete poles reinforced with CFRP bars after applying the 10% reduction to the cracked moment of inertia, and this is because of two reasons. First, it conservatively predicts the deflection, and second, it is not a function of the reinforcement ratio and the balanced reinforcement ratio of the pole's cross-section, which is very tedious to calculate for spun concrete poles. The final form for the equation is as follows:

$$I_e = \frac{0.90I_{cr}}{\left(1 - \eta \left(\frac{M_{cr}}{M_a}\right)^2\right)} \leq I_g \quad (20)$$

$$\eta = 1 - \frac{0.90I_{cr}}{I_g} \quad (21)$$

Table 20

Modified tip deflection at failure load after reducing the I_{cr} by 10%

Group No.	Experimental (in)	Yost et al. (in)	ACI-06 (in)	Bischoff (in)
First Group	25.86	26.69	26.63	26.58
Second Group	21.11	21.90	21.77	21.75

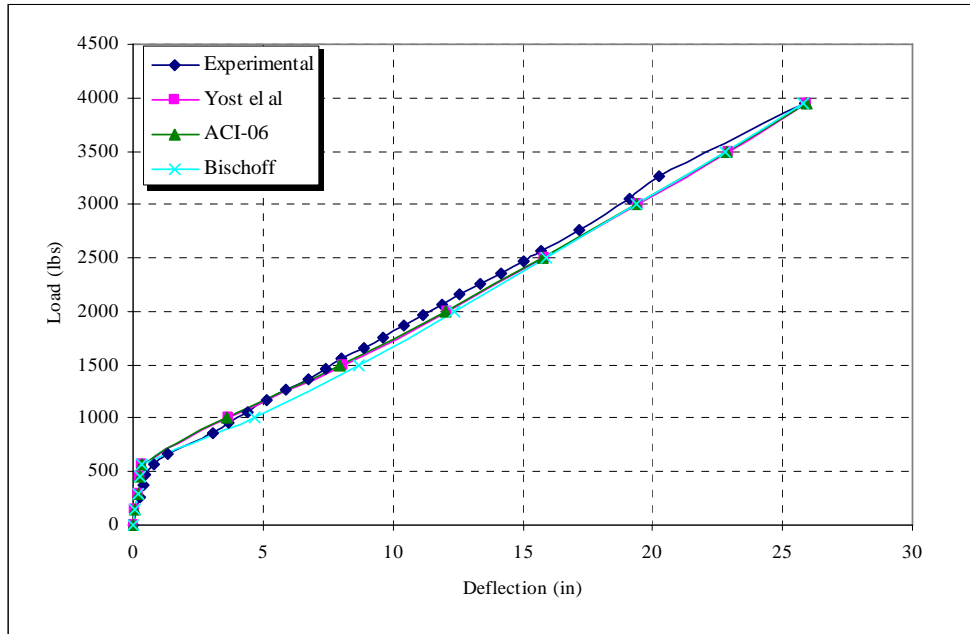


Figure 72. Modified load-deflection curve for the G01 specimens

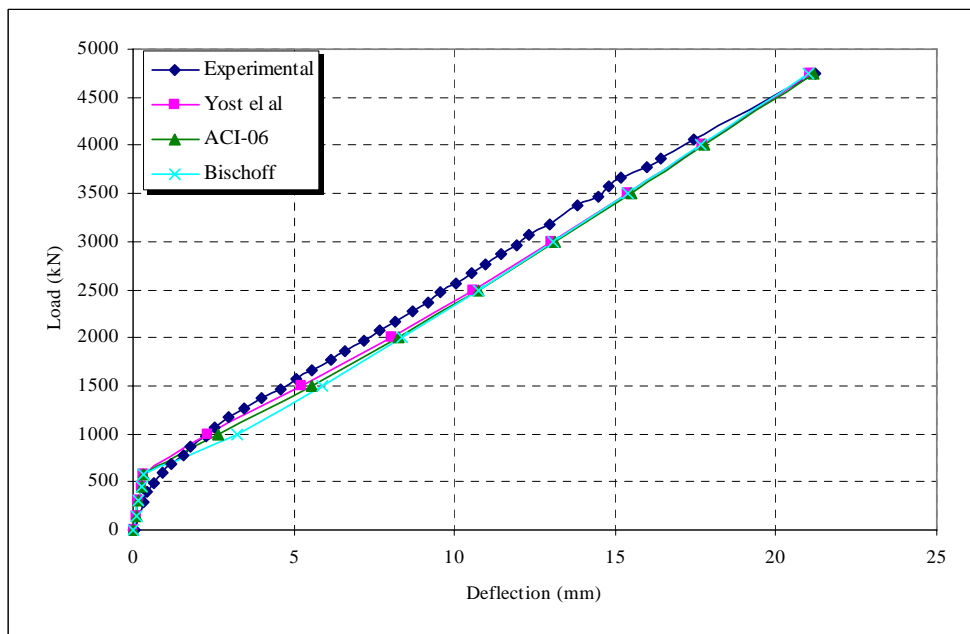


Figure 73. Modified load-deflection curve for the G02 specimens

Table 21 shows the tip deflection of the poles as a percentage from the free length of the pole. We can see that the deflection was 13% and 10% of the pole free length for the first and second groups, respectively. From this deflection percentage we can conclude that the reinforcement ratio has an inversely proportional effect on the deflection of the pole; the higher the reinforcement ratio the lesser the deflection of the pole. We can also conclude that the effect of the reinforcement ratio on the deflection is not that significant, because in our case we are having the reinforcement ratio of the second group double the reinforcement ratio of the first group, but, the tip deflection of the second group was decreased by only 3% of the pole's free length.

Table 21

Tip deflection as a percentage from the free pole length

Group No	Results	Free Length of Pole	Tip Deflection at Failure (in)	Deflection Percentage from the Free length of Pole (%)
Group 1	Experimental	17 ft (204 in)	25.86	13%
Group 2	Experimental	17 ft (204 in)	21.11	10%

6.2.3 Crack width

Table 22 shows the maximum crack width measured during the test compared to that calculated using the ACI-440 equation. From this table we can see that there is a significant difference between the test and calculated values for all of the poles except G02-01. For pole G01-01, the crack width was measured after unloading the pole, and moving it from the test machine, so this crack width is the permanent crack width that remains after unloading, and does not represent the actual crack width during the test. For pole

G01-02, the equation used to calculate the crack width underestimates the crack width of the pole by about 15%; however, Figure 74 shows that at lower loads the calculated crack width is comparable to the crack width measured during the test.

Figure 75 shows the load crack width curve for the second group. We can see that for pole G02-01 the ACI 440 equation correlates well with the experimental results, especially for higher loads. For lower loads, the correlation is not as much as for higher loads, and this contradicts with what we have for pole G01-02 of the first group. For pole G02-02, we can see from Figure 75 that the measured crack width during loading is significantly different from the measured crack width of pole G02-01 and the theoretical calculations.

From this discussion, we can conclude that it is very hard by means of the available information to verify the use of the ACI equation in estimating the crack width of spun concrete poles reinforced with CFRP bars, and we recommend more testing to be performed to help in determining a suitable formula that can be used to calculate the crack width of spun concrete poles reinforced with CFRP bars.

Table 22

Experimental and theoretical maximum crack widths

Group No.	Specimen ID	Load (lbs)	Crack Width (mils)	
			Experimental	Theoretical
Group 1	Pole G01-01	After Unloading	40	50
	Pole G01-02	2854	60	50
Group 2	Pole G02-01	3342	35	35
	Pole G02-02	3393	20	36

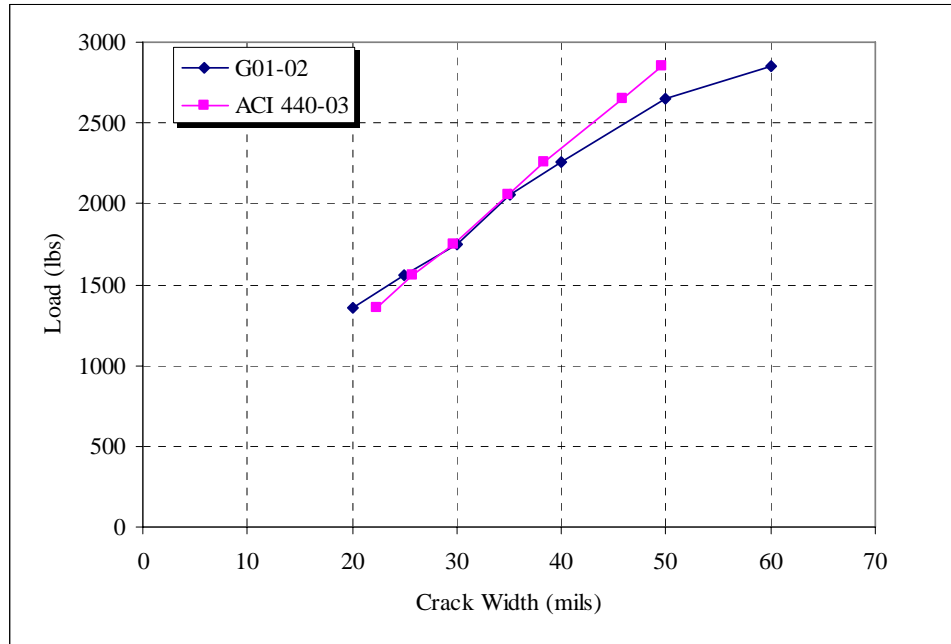


Figure 74. Load-crack width curve for pole G01-02

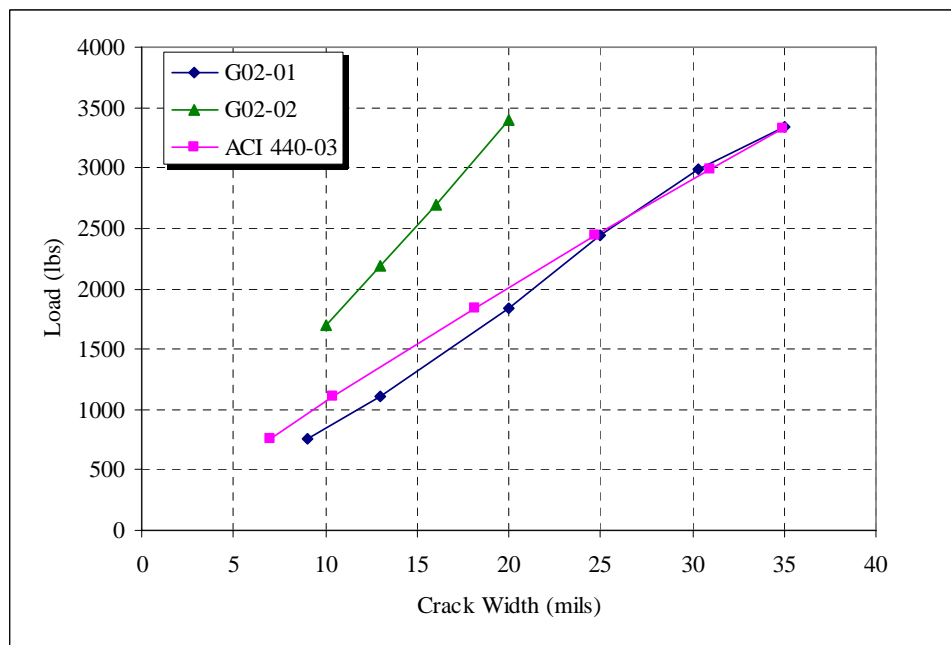


Figure 75. Load-crack width curve for the G02 specimens

6.3 Experimental Versus Finite Element Analysis Poles

This section presents a comparative study of the experimental poles tested as discussed in chapter 3 and the poles modeled using finite element analysis software. The objective of this comparative study is to verify the method by which the finite element model was built and to verify the software used in the analysis. The aim of this verification is to present to the field of structural engineering a finite element model that can help in performing further analysis regarding spun concrete poles reinforced with CFRP bars. Two poles were modeled using the ANSYS software; each pole represented one group of the tested specimens.

6.3.1 Compressive Strains

Figure 76 and Figure 77 compare the load compressive strain at the support from the experimental data with the results from the finite element model for the two groups, using pole G01-01 to represent the first group and pole G02-01 to represent the second group. We can see that the results are in a very good agreement. For the pole of the first group, the curves were identical and coincided with each other up to a load of about 2023 lbs; after this load, a slight divergence occurs between the two curves, with the ANSYS curve overestimating the compressive strain in concrete; however, the two curves were having the same path. This slight divergence is due to the difference between the stress-strain curve used in the finite element model and the actual stress-strain curve of the poles. For the pole of the second group, the two curves coincided with each other up to a load of 3952 lbs, after which we lost the strain gage reading; however, the pole did not reach failure.

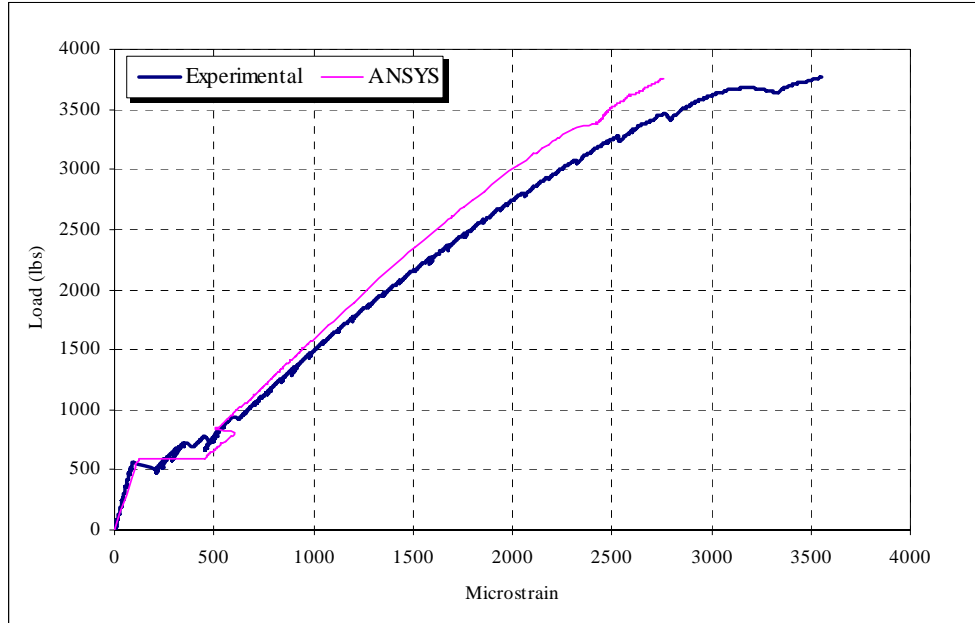


Figure 76. Load-compressive strain for the G01 specimens

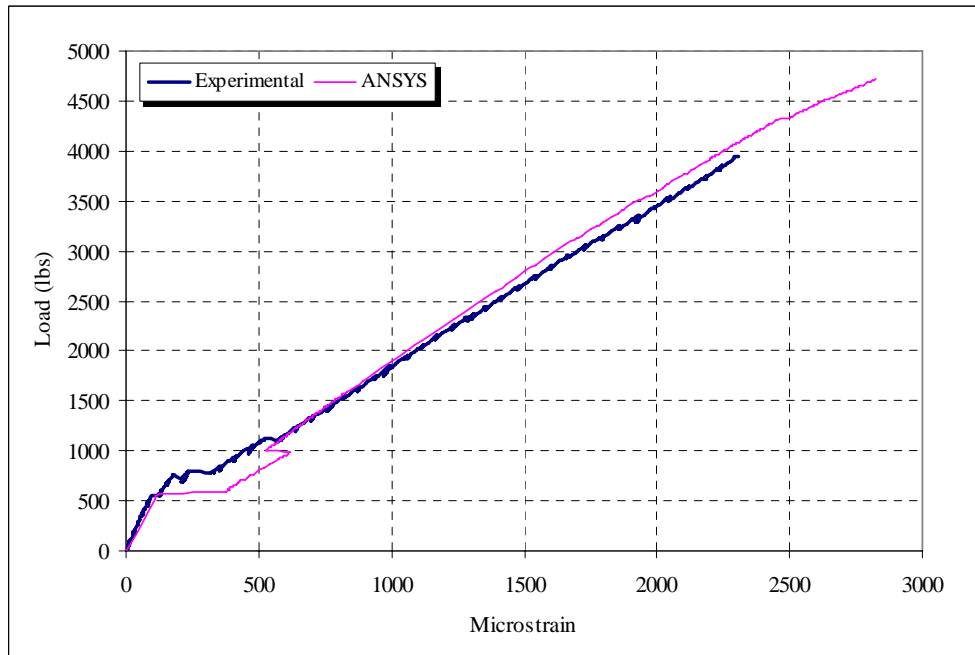


Figure 77. Load-compressive strain for the G02 specimens

6.3.2 Cracking and Ultimate Loads

Table 23 shows the cracking loads predicted by the ANSYS compared to the cracking loads recorded during the test. This table shows that the ANSYS slightly overestimated the values for the cracking loads by 3% and 5% for the first and the second pole, respectively. It is noteworthy to mention here that the cracking strength used in the ANSYS model was the average of the cracking strength that was recorded during the test for the two poles, which explains this slight difference between the cracking loads obtained from the ANSYS and that recorded during the test.

A comparison between the failure load predicted by the ANSYS and the failure load recorded during the test is shown on Table 24. The ANSYS failure loads are the last applied load steps before the solution diverges and the program terminates. Although it could be seen from this table that the ANSYS slightly underestimates the failure load of the first pole, however, the difference between the ANSYS failure load and the experimental failure load is not significant and is on the conservative side. For the second pole, the ANSYS highly overestimated the failure load when compared to the experimental results; however, when comparing this value with the calculated predicted value of 4641 lbs, the difference is only 1.7%, which is not significant. Therefore, this significant difference between the experimental and the ANSYS results might be due to the difference between the actual compressive strength of the pole and the spinning factor used to estimate the compressive strength of the pole.

Table 23

Experimental and finite element model cracking loads

Group No.	Experimental Loads (lbs)	Finite Element Loads (lbs)	% Difference
First Group	568	585	3.0
Second Group	545	572	5.0

Table 24

Experimental and finite element model failure loads

Group No.	Experimental Loads (lbs)	Finite Element Loads (lbs)	% Difference
First Group	3790	3756	-0.90
Second Group	4248	4720	10.50

6.3.3 Deflection

The load deflection curves for the two poles are shown in Figure 78 and Figure 79, and the tip deflection at experimental failure load is presented on Table 25. In general, the ANSYS results agree quite well with the experimental records. For the second pole, we can see in Figure 79 that the ANSYS curve was slightly stiffer than the experimental curve, and this might be due to the difference in the actual modulus of elasticity for concrete for this pole and that used in the ANSYS model. It can also be seen from these figures and from Table 25 that the ANSYS underestimates the tip deflection of the pole at failure, with percentages of 7% and 11% for the first and the second poles, respectively. This could be due to two reasons, the first is the way the ANSYS calculates the effective moment of inertia for the poles, and the second is the assumption of a perfect bond between the concrete and the CFRP bars.

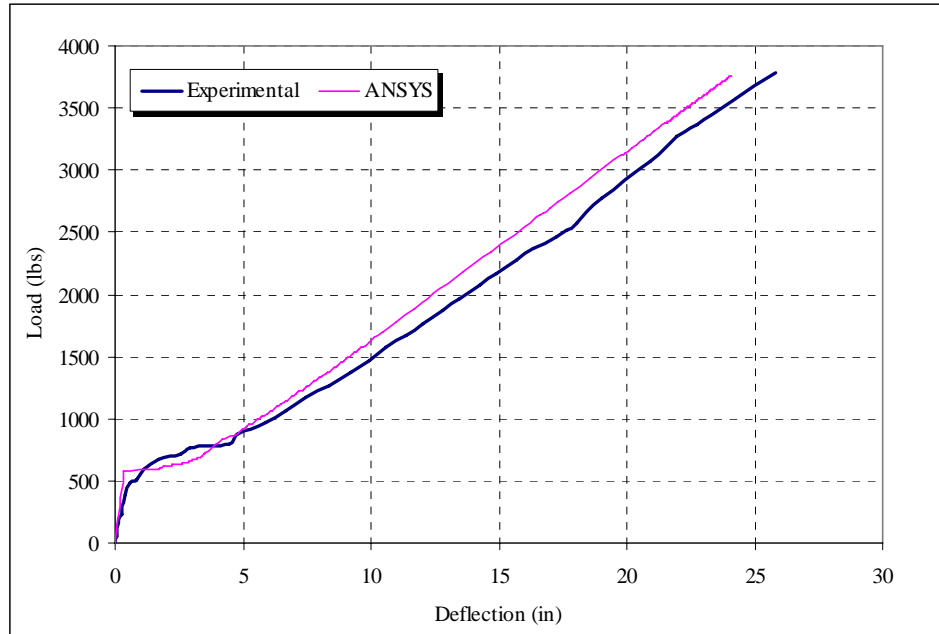


Figure 78. Load-deflection curve for the G01 specimens

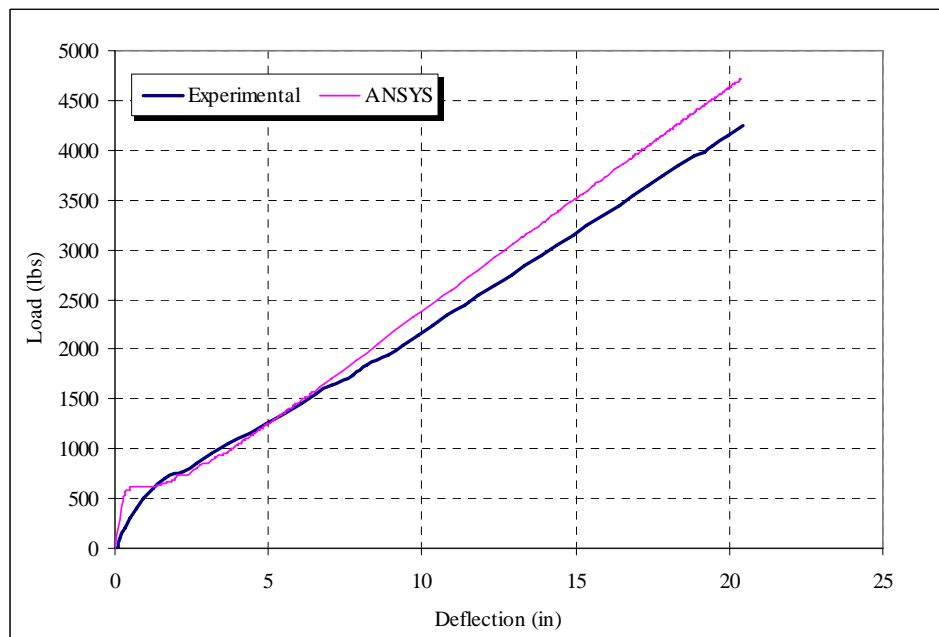


Figure 79. Load-deflection curve for the G02 specimens

Table 25

Experimental and finite element tip deflections at failure load

Specimen ID	Experimental [in]	Finite Element Model [in]	% Difference
First Pole	25.84	24.00	-7.0
Second Pole	20.46	18.28*	-11.0

Deflection values marked with * are the tip deflection at the experimental failure load of 19kN (4248 lbs)

6.4 CFRP Versus Steel Reinforced Prestressed Poles

This section presents a comparative study between the experimental poles tested as discussed in chapter 3 against the traditional poles having the same properties as the tested ones, except that the traditional poles are prestressed with steel strands rather than being reinforced with CFRP bars. The comparison focuses on comparing the cracking and ultimate moment capacities, and the load deflection curve obtained from the experimental study, against the traditional poles. The cracking and ultimate moment capacities, and the load deflection curve for the traditional poles, were calculated theoretically.

6.4.1 Cracking and Ultimate Loads

Figure 80 shows the experimental cracking load compared to the cracking load computed for a traditional, prestressed spun concrete pole reinforced with the same number of bars and having the same bar diameter as the experimental pole, the only difference being the type of reinforcement (CFRP or steel). These figures show that the cracking load for the traditional poles is much higher than for the experimental ones, and this is due to the compression force applied to the traditional poles due to prestressing.

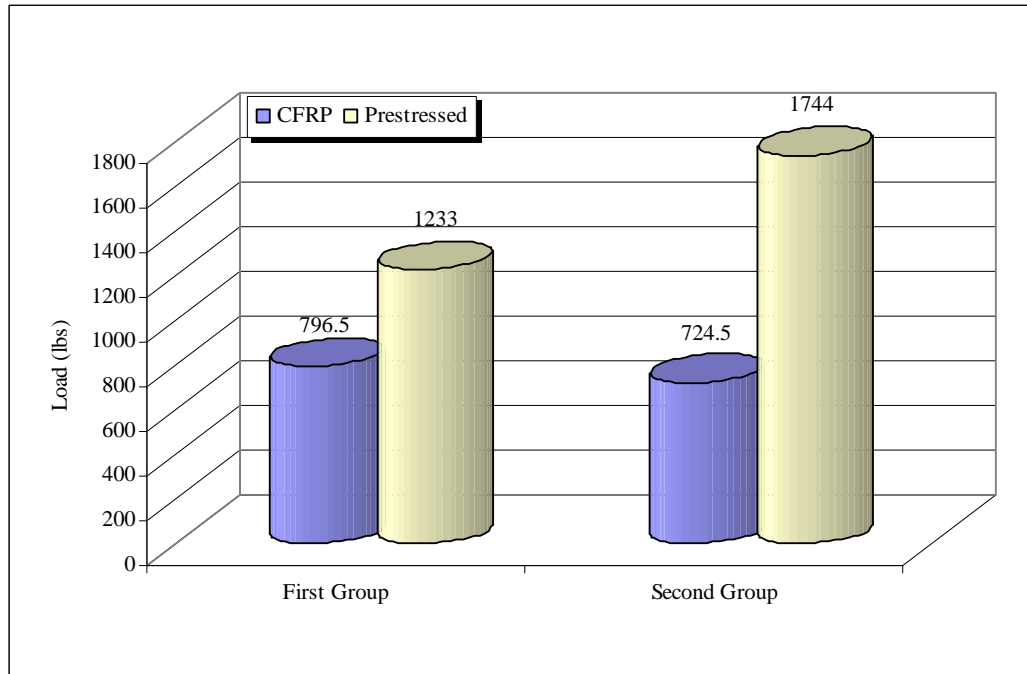


Figure 80. CFRP and prestressed cracking loads

Figure 81 compares the ultimate load of the experimental poles to the computed ultimate load for the traditional poles. It shows that the experimental pole having six bars was able to sustain about 29% more load than the traditional one, and this difference can be increased by prestressing the CFRP bars used to reinforce the experimental poles. However it can be seen in Figure 15 that the ultimate load for the experimental pole having 12 bars was about 13% less than the traditional one and this was due to the prestressing effect of the traditional pole, which can be eliminated and exceeded by prestressing the CFRP bars. We can conclude that the non-prestressing spun concrete poles reinforced with CFRP bars show immense potential as a replacement for traditional steel reinforcement, especially if they are prestressed, as they will provide us with the desired structural characteristics and, at the same time, eliminate the corrosion problem.

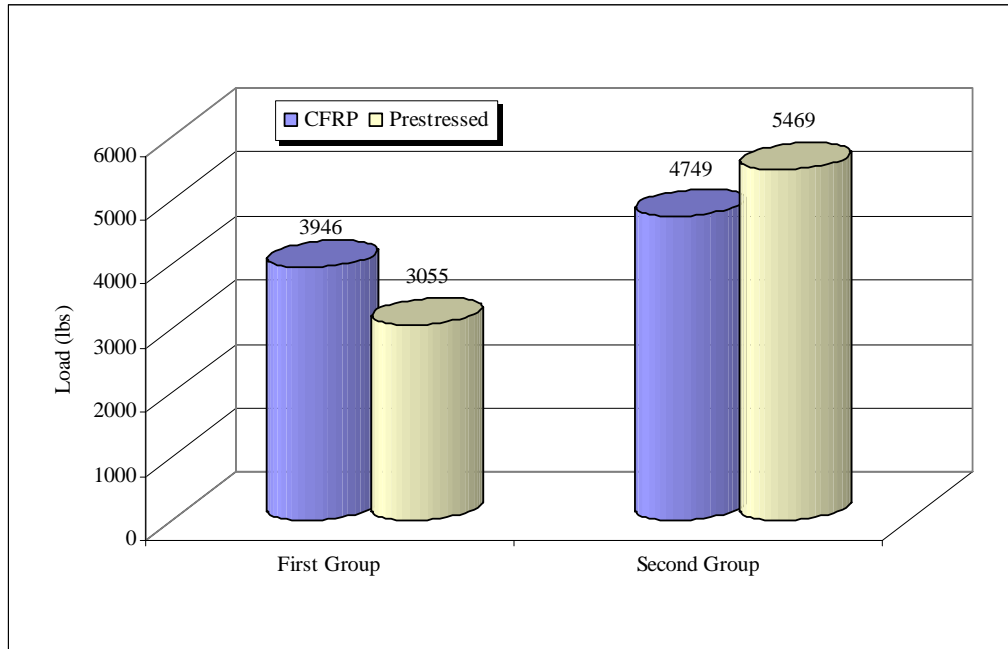


Figure 81. CFRP and prestressed ultimate loads

6.4.2 Deflection

Figure 82 and Figure 83 show the load deflection curves for the two poles compared to the computed load deflection curves of the traditional prestressed ones. The effect of prestressing on the traditional poles is obvious in these figures especially, when compared to the experimental ones. The compression force resulting from prestressing significantly increased the cracking load of the traditional prestressed poles when compared to the experimental poles.

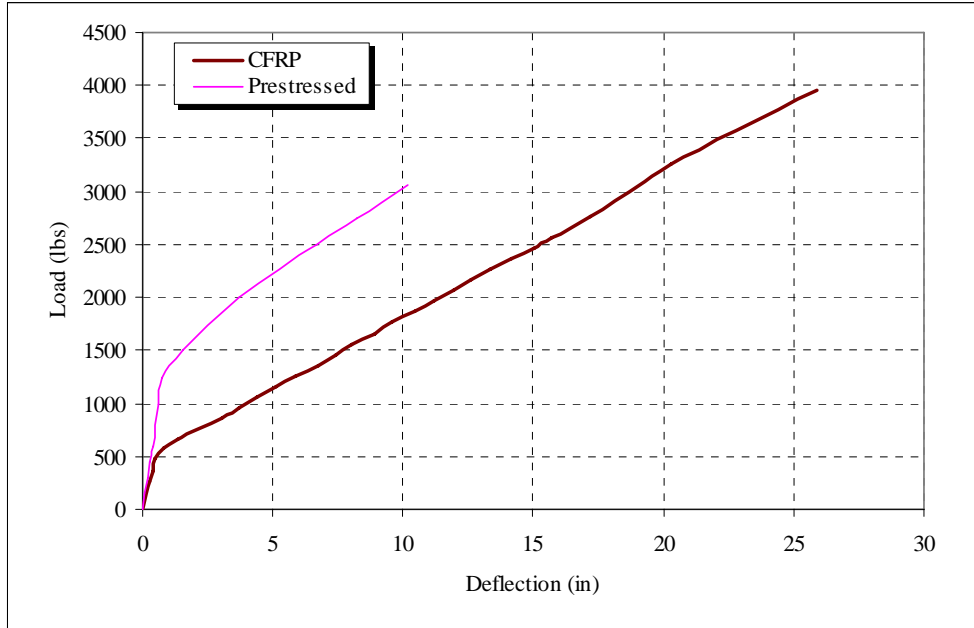


Figure 82. Load-deflection curve for the G01 specimens

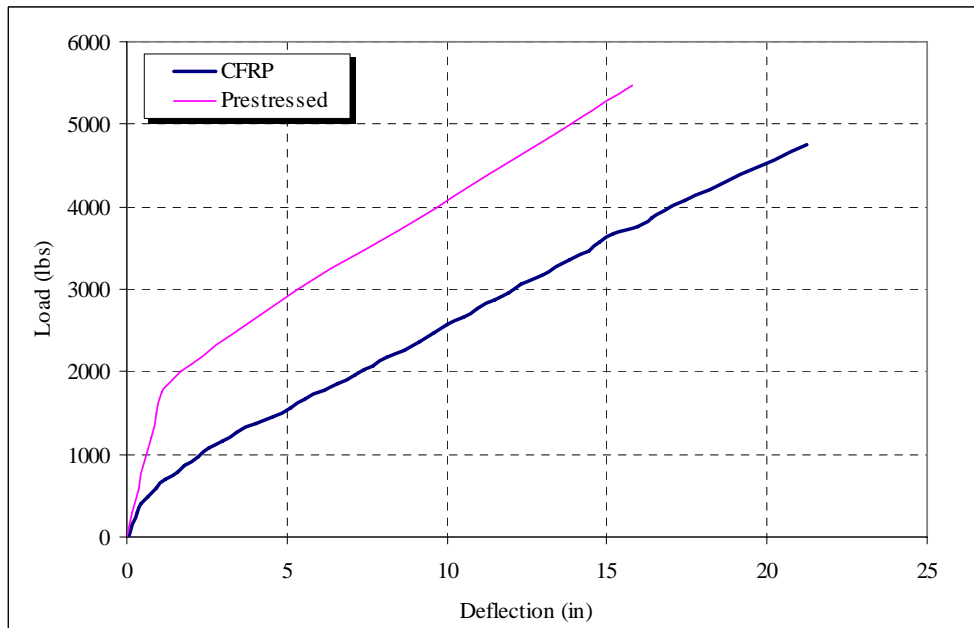


Figure 83. Load-deflection curve for the G02 specimens

CHAPTER 7

SUMMARY AND CONCLUSION

7.1 Summary

This research presented our study of the behavior of spun concrete poles reinforced with CFRP as a replacement for the prestressing steel normally used in concrete poles. The main purpose of this research is to provide a more durable pole that can be used in highly aggressive environments that can affect the reinforcement. Corrosion is a major concern in concrete structures, as it attacks the steel reinforcement, resulting in a decrease of the strength of the structure to the extent that, in some cases, it cannot perform its intended function and may have to be replaced.

Many solutions have been introduced in the literature to overcome the issue of corrosion; however, the solutions are either expensive or impractical. The use of FRP has been introduced in the construction industry to replace the traditional steel reinforcement since mid 1900s, and the literature indicates that the use of this material is gaining more acceptances. Many researchers have studied the performance of FRP in concrete buildings and bridges. Nevertheless, very few studies have investigated the performance of FRP as a replacement to the steel reinforcement in the spun concrete poles in the United States. All these studies were only theoretical.

An extensive literature review was presented to address the current use and design of concrete structures reinforced with carbon fiber reinforced polymers. The literature

review shows that concrete structures reinforced with CFRP have satisfactory flexural behavior and were able to produce sufficient deflection and cracking before failure to account for the lack of plasticity in the brittle FRP material. The literature review also shows that existing equations for the design of concrete structures reinforced with traditional steel may be modified to build new equations for the design of concrete structures reinforced with FRP.

The research work presented analytical study as well as experimental studies to achieve our goals. Moreover, finite element modeling was performed to help us in proofing our results. The conclusion of this research is summarized in the following section.

The experimental study consisted of producing and testing four prototype specimens divided into two groups. The two groups were reinforced with different reinforcement schemes using CFRP bars, while all other variables were kept constant. The poles were manufactured at Valmont Newmark production plant using a specially formulated high strength concrete mix that produced concrete with an average compressive strength of about 11000 psi at 28 days. CFRP bars were provided by Hughes Brothers, Inc. under the commercial name of Aslan 200. The flexural behavior of the poles was evaluated in terms of load deflection curves, cracking moment, ultimate moment capacities, and strains in the concrete. These terms were determined from the cantilever load test. The specimens were supported over the test frame using two supports. The first was located at the pole's butt, and the other support, acting as the fulcrum, was located at 3.0 ft from the pole's butt. The supports used in this study were designed and manufactured especially for this test so that they could sustain the reactions from the load applied to the poles. The load was applied at one foot from the tip of the pole in increments of 100 lbs. There was a

pause after each load increment application to allow time to read deflections and permit the inspection of any structural distress might have occurred.

The analytical study was performed to estimate the behavior of spun concrete poles reinforced with CFRP under loading conditions. Equations to calculate the ultimate moment capacity, the cracking moment, the deflection, and the crack width were presented. Spreadsheets were developed and verified to help in calculating the cracking and ultimate moment capacities of the spun concrete poles reinforced with CFRP bars, calculate the cracking moment of inertia of the poles, and develop the load deflection points needed to draw the load deflection curve of the poles.

Finite element modeling was conducted using the ANSYS software to complete this research study. The tested specimens were modeled, and the results were compared with the experimental results. Solid65 of the ANSYS software was used to model the concrete. This solid element has eight nodes, with three degree of freedom at each node. Each node can accept translational movement in the x, y, and z directions, but none of them can accept rotational movement. This element was designed specially by ANSYS to model concrete structures, as it is capable of crushing in compression and cracking in tension. It is also capable of plastic deformation. Link8 of the ANSYS software was used to model the CFRP bars; this is a 3D element that has two nodes, with three degrees of freedom at each node. Each node can accept translational movement in the x, y, and z directions. The element is also capable of plastic deformation. The material properties for concrete were defined by the compressive strength, tensile strength, and the modulus of elasticity, whereas for the CFRP bars, the material properties were defined by the tensile strength and the modulus of elasticity, and modeled as a multi-linear elastic material. The

poles were meshed every 2 in in the longitudinal direction and they were meshed in the cross-section on an angle of 15°. The CFRP bars were added to the model after meshing so that they would share the same nodes for concrete, assuming a perfect bond. Loads and boundary conditions were then applied to the model. Loads were applied in very small increments that sometimes reach 1.0 lbs to avoid any convergence problem. The Newton-Raphson method incorporated by the ANSYS was used to compute the nonlinear response. Using this method, the load was subdivided into a series of load increments, and the load increments were applied over several load steps.

The data from this research was analyzed and, discussed, and a comparative study was performed. The experimental results were compared against the theoretical results, and the proposed equations for the flexural design of spun concrete poles reinforced with CFRP bars were verified and modified to match the experimental results. The experimental results were also compared against the finite element results, and the method by which the finite element model built was verified. Finally, the experimental flexural behavior of spun concrete poles reinforced with CFRP bars was compared against the theoretical flexural behavior of conventional, prestressed spun concrete poles.

7.2 Conclusion

The conclusions drawn from this study can be summarized as follows:

1. Concrete poles reinforced with CFRP bars showed satisfactory flexural behavior, as they were able to produce a significant amount of deflection, about 12%, from the free length of the pole prior to failure to overcome the brittle nature of the CFRP bars.

2. The reinforcement ratio significantly affected the failure mode of the poles.
For poles having low reinforcement ratio, permanent cracking and deflection resulted after unloading. For the other pole, with a higher reinforcement ratio, all of the flexure cracks were closed after unloading, leaving hair cracks, and the recorded residual deflection was very low.
3. The reinforcement ratio did not significantly affect the flexural capacity of the poles. Although the difference in reinforcement ratio between the two poles was doubled, the ultimate capacity was increased by only 20%. This is because the ultimate moment capacity equation is not only a function of the number of bars used, but of the location of the neutral axis, the orientation of the bars around the cross-section, and their relationship to the neutral axis.
4. The reinforcement ratio does not have a significant effect on crack spacing.
Although the two groups had different reinforcement ratios, the crack spacing at failure load was about 4.0 in, starting from the support and up to the middle of the poles.
5. The use of the C-GRID as a shear reinforcement significantly affected the failure mode of the poles. The poles reinforced with C-GRID failed in compression shear mode between the supports due to shear. The poles reinforced with steel spirals underwent compression failure at the support due to flexure with comparable failure loads. Moreover, one pole, having a low reinforcement ratio and being reinforced with steel spirals, underwent permanent cracking and deflection after unloading. For the other pole, with the same reinforcement ratio but reinforced with the C-GRID for shear reinforcement, all of the flexure

cracks closed after unloading, leaving some hair cracks, and the recorded residual deflection was very low.

6. The use of the C-GRID as a shear reinforcement significantly decreased the crack width of the poles; with the poles having the same reinforcement ratio, the crack width for the poles reinforced with the C-GRID was decreased by about 40% prior to failure, as compared to the poles reinforced with traditional steel spirals.
7. The use of the C-GRID as a shear reinforcement slightly improved the flexural capacity of the poles. Although the compressive strength of the poles reinforced with C-GRID was lower than the other poles, the failure load was almost the same.
8. The ultimate moment capacity of spun concrete poles reinforced with CFRP bars calculated using the proposed equation compared well with the experimental and finite element results.
9. Proposed equations for the calculation of the effective moment of inertia for concrete structures reinforced with FRP bars underestimated the deflection for spun concrete poles reinforced with CFRP bars.
10. The equation proposed by Bischoff and Scanlon (2007) is recommended to use in calculating the deflection of spun concrete poles reinforced with CFRP bars, after multiplying by a 0.90 reduction factor.
11. In general, the finite element model developed can be used for further studies regarding spun concrete poles reinforced with CFRP bars.

12. The finite element model was able to predict the flexural behavior of spun concrete poles reinforced with CFRP bars.
13. The finite element model was able to predict the load versus compressive strain curve of spun concrete poles reinforced with CFRP bars.
14. Cracking loads of the finite element model compared well with that obtained from the experimental data.
15. The load deflection curve predicted using the finite element model compared well to the experimental data.

7.3 Recommendations for Future Work

This research studied the flexural behavior of spun concrete poles reinforced with CFRP bars. The CFRP bars used in this study were provided by Hughes Brothers, Inc. under the commercial name of Aslan 200. The structural characteristics of CFRP bars differ from one manufacture than another, therefore an approach must be developed to study the flexural behavior of spun concrete poles reinforced with CFRP bars provided by another supplier.

The mode of failure of spun concrete poles reinforced with CFRP bars was different when two types of shear reinforcement (CFRP mesh and steel stirrups) were used. An approach is needed to study the effect of shear reinforcement on the behavior of spun concrete poles reinforced with CFRP.

The effect of structural characteristics not included in this study also needs to be investigated. For example, the effect of concrete compressive strength on the performance of spun concrete poles reinforced with CFRP bars should to be studied. The effect of

concrete cover on the bond strength between CFRP bars and concrete also needs to be studied.

Spun concrete poles are tapered structures, so the pole cross-section changes all along its length. An approach is needed to study the geometrical effect on the behavior of spun concrete poles reinforced with CFRP bars.

A parametric study using the finite element modeling verified in this study is needed to so that the effect of different variables, such as concrete strength, wall thickness, concrete cover, and flexural and shear reinforcement ratios, can be tested independently and in pairs to come up with an optimum design for spun concrete poles reinforced with CFRP bars.

More tests are recommended on spun concrete poles reinforced with CFRP bars and with different reinforcement ratios to strengthen the results of this study.

The performance of spun concrete poles reinforced with CFRP bars was comparable to conventional, prestressed spun concrete poles, especially at a lower reinforcement ratio; therefore, an approach is needed to study and compare the effect of prestressing the CFRP bars on the behavior of spun concrete poles.

CFRP has been introduced to the civil engineering industry in several forms, as reinforcement to concrete structures and as a material for repair. In this study, CFRP bars have been used to reinforce spun concrete poles. The repair of conventional prestressed spun concrete poles using CFRP wrapping should also be studied.

REFERENCES

Abdelrahman, A., A., and Rizkalla, S., H., (1999), "Deflection Control of Concrete Beams Pretensioned by CFRP Reinforcements" *Journal of composites for construction*, Vol. 3, No. 2, May, 1999, pp. 55-62.

ACI 318-02, (2002), "Building Code Requirements for Structural Concrete" prepared by the ACI committee 318, Aug. 2002

ACI 363R-92, (2002), "State-of-the-Art Report on High Strength Concrete" prepared by the ACI committee 363, Aug. 2002.

ACI 440.1R-03, (2003), "Guide for the Design and Construction of Concrete Reinforced with FRP Bars" prepared by the ACI committee 440, Mar. 2003.

ACI 440.1R-06, (2006), "Guide for the Design and Construction of Concrete Reinforced with FRP Bars" prepared by the ACI committee 440.

ACI 440.4R-04, (2004), "Prestressing Concrete Structures with FRP Tendons" prepared by the ACI committee 440, Dec. 2004.

ANSYS Manual (2005) ANSYS 10.0A1 Finite Element Analysis System, SAS IP, Inc.

ASCE, (1987), "Guide for the Design and Use of Concrete Poles," Prepared by the Concrete Pole Task Committee of the Committee on Electrical Transmission Structures of the Structural Division of the American Society of Civil Engineers, American Society of Civil Engineers, New York, New York, April, 1987, 52 pp.

ASTM C 150, "Standard Specification for Portland Cement," ASTM International

Barbosa, A. F., Ribeiro, G. O. (1998), "Analysis of Reinforced Concrete Structures Using ANSYS Nonlinear Concrete Model." Proceedings, Computational Mechanics, New Trends and Applications, CIMNE, Barcelona, Spain.

Bischoff, P. H., and Scanlon, A., (2007), "Effective Moment of Inertia for Calculating Deflections of Concrete Members Containing Steel Reinforcement and Fiber-Reinforced Polymer Reinforcement." ACI Structural Journal, Vol. 104, No. 1, pp. 68-75.

Brown V., Bartholomew, C., (1996), "Long-term Deflections of GFRP Reinforced Concrete Beams." Saadatmanesh H., Ehsani M.R., editors. Fiber composites in infrastructure – ICCI'96. Department of Civil Engineering and Engineering Mechanics, University of Arizona, Tucson, AZ, January 1996. pp. 389-400.

Challal O., Benmokrane B., (1993), "Physical and Mechanical Performance of an Innovative Glass Fiber Reinforced Plastic Rod for Concrete and Grouted Anchorages." Rev Can Genie Civ 1993, pp 245-268

Christoffersen, J., Hauge, L., and Bjerrum, J., (1999), "Footbridge with Carbon Fiber Reinforced Polymers, Denmark," Structural Engineering International, Journal of the International Association for Bridge and Structural Engineering (IABSE), No. 4, Nov. 1999, pp. 254-256

Dilger, Walter H., and Rao, S. V., Krishna Mohan, (1997), "High Performance Concrete Mixtures for Spun-Cast Concrete Poles," Journal of the Prestressed Concrete Institute, Vol. 42, No. 4, July-August 1997, pp.82-96.

Dolan, C. W., and Swanson, D., (2002), "Development of Flexural Capacity of FRP Prestressed Beam with Vertically Distributed Tendons," Composites Part B: Engineering, V. 3, No. 1, Elsevier, New York, 2002, pp. 1-6.

Erki, Marie-Anne, (1999), "Fiber-Reinforced Polymers for Structural Engineering in Canada," Structural Engineering International, Journal of the International Association for Bridge and Structural Engineering (IABSE), No. 4, Nov. 1999, pp. 278-280

Fouad H. Fouad, (1988), "Properties of Centrifugally Cast Concrete" Synopsis study sponsored by Sherman Utility Structures, INC. Birmingham, Alabama, June 1988.

Fouad H. Fouad, Scott L. Norman, Calvert Elizabeth, Donovan Michael (1994), "Performance of Spun Prestressed Concrete Poles during Hurricane Andrew" Journal of the Prestressed Concrete Institute, March-April 1994

Fouad, Fouad H.; Sherman, Doug; and Werner, Rolf J, (1992), "Spun Prestressed Concrete Poles - Past, Present, and Future," Concrete International, American Concrete Institute, Volume 14, Number 11, November 1992, pp. 25-29.

Glaser R. E., Moore R.L., and Chiao T. T., (1983), "Life Estimation of an S-glass/epoxy Composite under Sustained Tensile Loading" Comp Technol Rev 1983; pp. 21-26

Grace, N., F., Enomoto, T., Abdel-Sayed, G., Yagi, K. and Collavino, L., (2003), "Experimental Study and Analysis of a Full-Scale CFRP/CFCC Double-Tee Bridge Beam," PCI Journal, Vol. 48, No. 4, July-Aug. 2003, pp. 120-139.

Jeong, S., M., (1994), "Evaluation of Ductility in Prestressed Concrete Beams Using Fiber Reinforced Plastic Tendons," Ph.D. Dissertation, University of Michigan, 1994
Kocer, Y. Fatma, and Arora, S. Jasbir, "Design of Prestressed Concrete Transmission Poles: Optimization Approach" ASCE, Journal of Structural Engineering, Vol.122, No.7, July, pp. 804-814, 1996

Kachlakev, D. I., Miller, T., Yim, S., Chansawat, K., and Potisuk, T. (2001), "Finite Element Modeling of Reinforced Concrete Structures Strengthened with FRP Laminates." California Polytechnic State University, San Luis Obispo, CA and Oregon State University, Corvallis, OR for Oregon Department of Transportation, May. pp.99

Lees, J., M., (2001), "Fiber Reinforced Polymers in Reinforced and Prestressed Concrete Applications: Moving Forward" Progress in Structural Engineering and Materials, Vol. 1, No. 2, 2001, pp. 122-131

Lyons, P., J., (2003), "Feasibility Study of CFRP Prestressed Spun Cast Concrete Poles for Transmission Line Support," M.S. Thesis, University of Alabama, 2003

Nawy, E. G., "Fundamentals of High Performance Concrete" 2nd Edition, Wiley, New York.

Nilson, H. (1987), "Design of Prestressed Concrete" 2nd Ed., John Wiley and Sons, Inc., 1987

Nunez, Edgar, (2002), "Development Of A Flaminated Finite Element for the Analysis of Prestressed Concrete Poles" Ph.D. Dissertation, University of Alabama at Birmingham, 2002

PCI Committee on Prestressed Concrete Poles, (1983), "Guide for Design of Prestressed Concrete Poles," PCI Journal, Vol. 28, No. 3, May-June 1983, pp. 22-87.

PCI Committee on Prestressed Concrete Poles, (1997), "Guide for the Design of Prestressed Concrete Poles," PCI Journal, Vol. 42, No. 6, Nov.-Dec. 1997, pp. 94-134.

Pisani, M., A., (1998), "A Numerical Survey on The Behavior of Beams Prestressed with FRP Cables" Construction and Building Materials, Vol. 12, Elsevier, 1998, pp. 221-232.

Rodgers, Thomas E., Jr, (1984), "Prestressed Concrete Poles: State-of-the-Art," Journal of the Prestressed Concrete Institute, Vol. 29, No. 5, September-October 1984, pp.52-103.

Saafi, M., and Toutanji, H., (1998), "Flexural Capacity of Prestressed Concrete Beams Reinforced with Aramid Fiber Reinforced Polymer (AFRP) Rectangular Tendons" Construction and Building Materials, Vol. 12, Elsevier, 1998, pp. 245-249.

Seible, F., Karbhari, V., M., and Burgueno, R., (1999), "Kings Stormwater Channel and I-5/Gilman Bridges, USA," Structural Engineering International, Journal of the International Association for Bridge and Structural Engineering (IABSE), No. 4, Nov. 1999, pp. 250-253

Sen R., Mariscal D., Shahawy M., (1993) "Durability of Fiber Glass Pretensioned Beams" ACI journal 1993, Vol. 90, No. 5, pp. 525-533

Shahawy, M., A., Beitelman, T., Arockiasamy, M., and Sandepudi, K., S., (1996), "Static Flexural Response of Members Pretensioned with Multiple Layered Aramid Fiber Tendons" Composites: Part B 27B Elsevier, 1996, pp. 253-261.

Stoll, F., Saliba, J., E., and Casper, L., E., (2000), "Experimental Study of CFRP-Prestressed High-Strength Concrete Bridge Beams" Composite Structures, Vol. 49, Elsevier, 2000, pp. 191-200.

Tennyson, R., C., Mufti, A., A., Rizkalla, S., Tadros, G., and Benmokrane, B., (2001), "Structural health monitoring of innovative bridges in Canada with fiber optic sensors," Institute of Physics Publishing, Journal of Smart Material and Structures, Vol. 10, 2001, pp. 560-573

Terrasi G. P., Battig G., Bronnimann R., (2001), "High Strength Spun Concrete Poles Prestressed with CFRP", FRPRCS-5 "Non-Metallic Reinforcement for Concrete Structures" ISBN 07277-3009-6, University of Cambridge, England 16-18 Jul. 2001, Ed. C. Burgoyne, pp. 1103-1112

Terrasi, G. P., Lees, J. M. (2003), "CFRP Prestressed Concrete Lighting Columns" Field Applications of FRP Reinforcement: Case Studies, ACI, 2003 convention, pp. 55-74

Toutanji, H., and Saafi, M., (1999), "Performance of Concrete Beams Prestressed with Aramid Fiber Reinforced Polymer Tendons" Composite Structures, Vol. 44, Elsevier, 1999, pp. 63-70.

Willam, K. J., and Warnke, E. P. (1974), "Constitutive Model for Triaxial Behavior of Concrete." Seminar on Concrete Structures Subjected to Triaxial Stresses, International Association of Bridge and Structural Engineering Conference, Bergamo, Italy, pp.174

Wolff R., Miesslerer H. J., (1993), "Glass Fiber Prestressing System" Fiber reinforced plastic (FRP) reinforcement for concrete structures; properties and applications, 1993, p. 305

Yost, J. R., Gross, S. P., and Dinehart, D. W. (2003), "Effective Moment of Inertia for Glass Fiber-Reinforced Polymer Reinforced Concrete Beams." ACI Structural Journal, Vol. 100, No. 6, pp. 732-739.

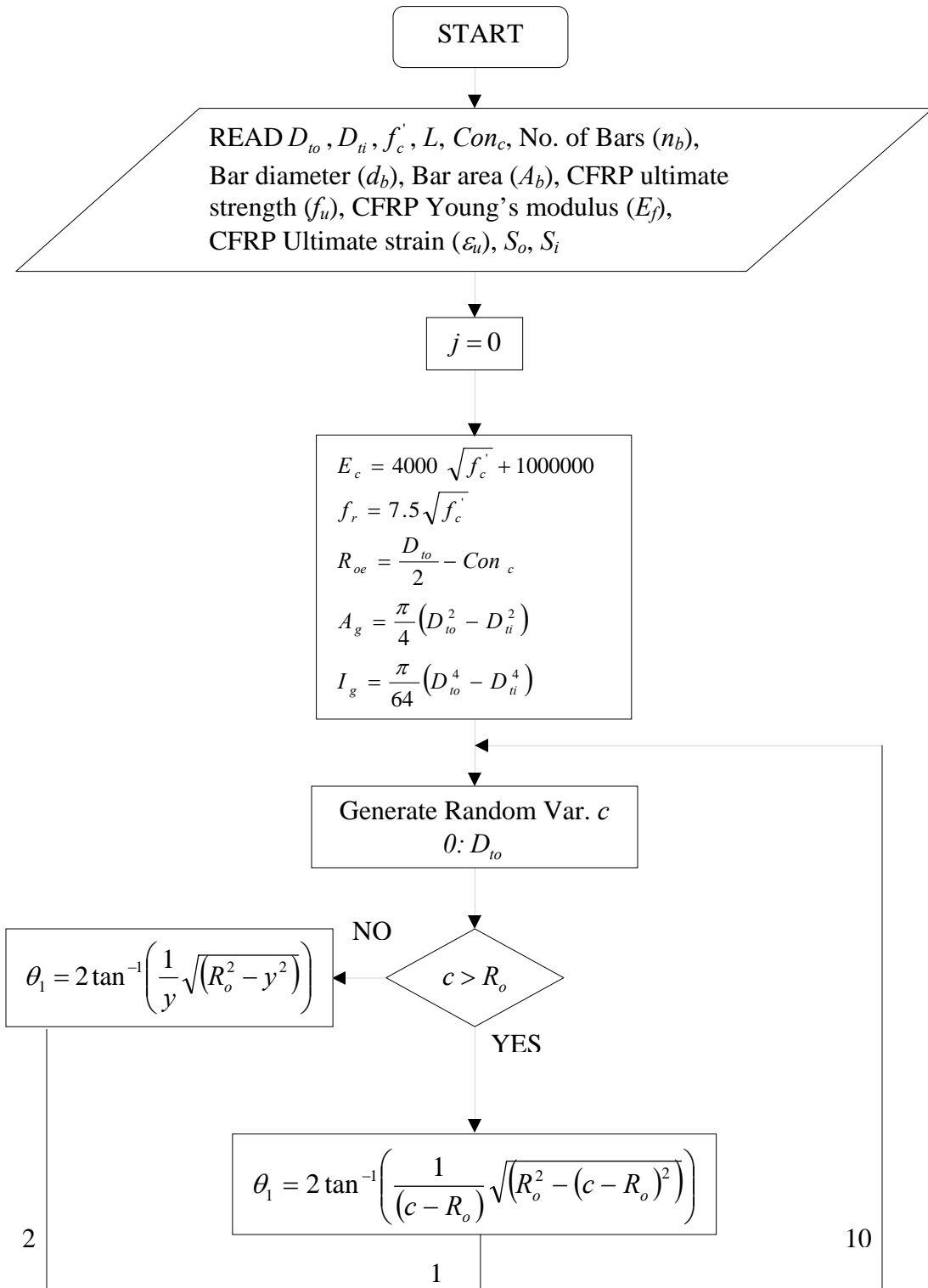
Zou, P., X., W., (2003a), "Flexural Behavior and Deformability of Fiber Reinforced Polymer Prestressed Concrete Beams" Journal of composites for construction, Vol. 7, No. 4, November, 2003, pp. 275-284.

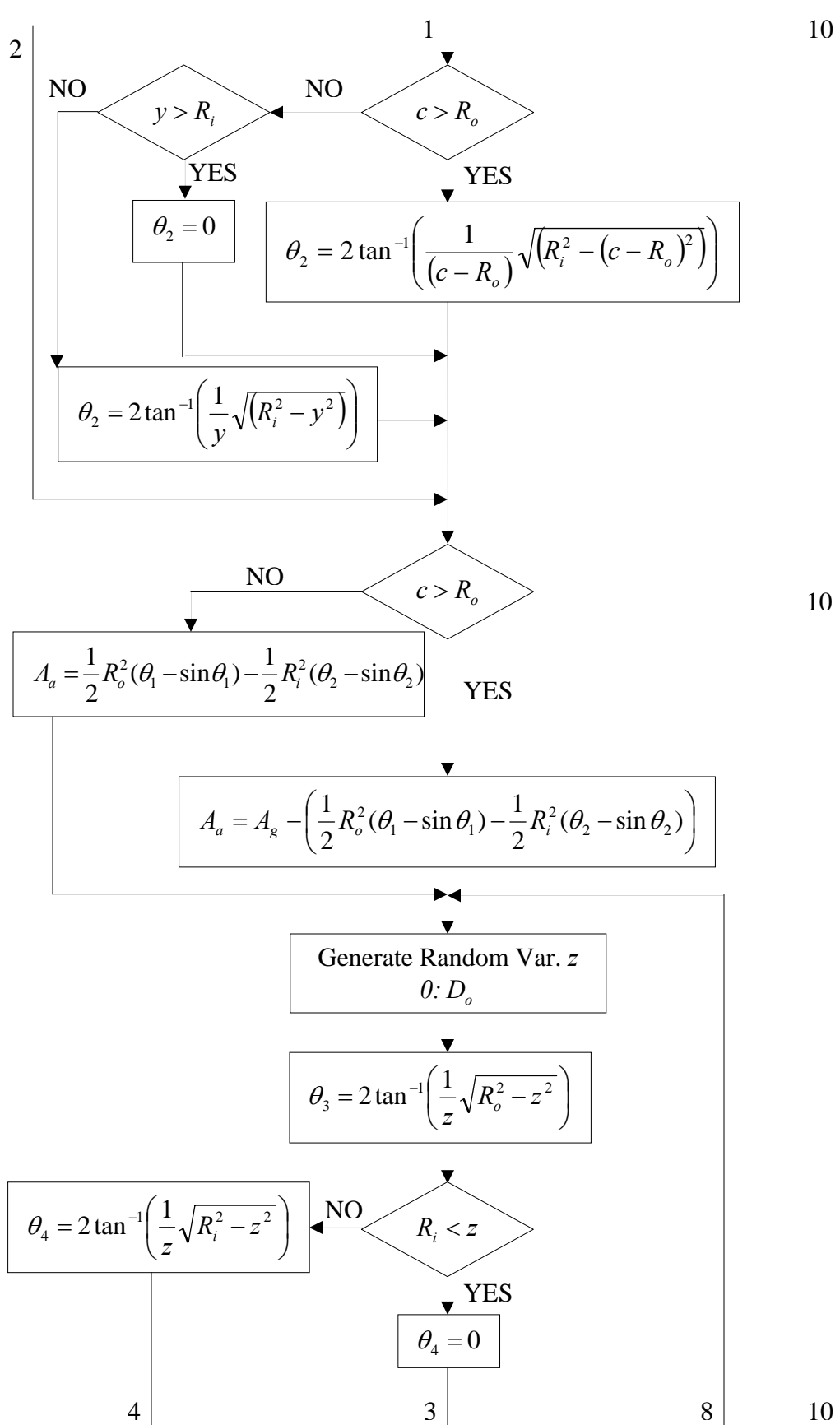
Zou, P., X., W., (2003b), "Theoretical Study on Short-Term and Long-Term Deflections of Fiber Reinforced Polymer Prestressed Concrete Beams" Journal of composites for construction, Vol. 7, No. 4, November, 2003, pp. 285-291.

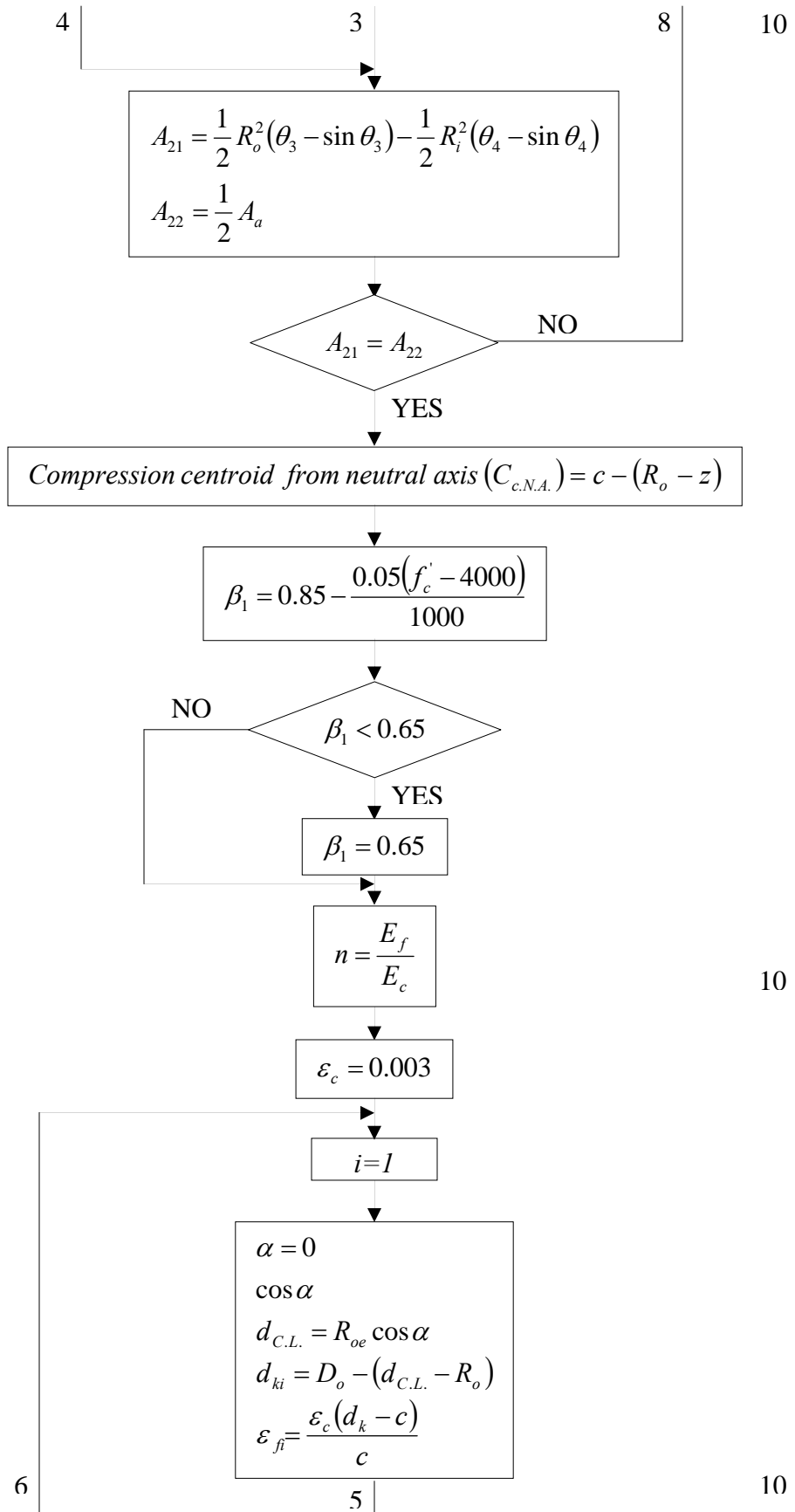
APPENDIX A

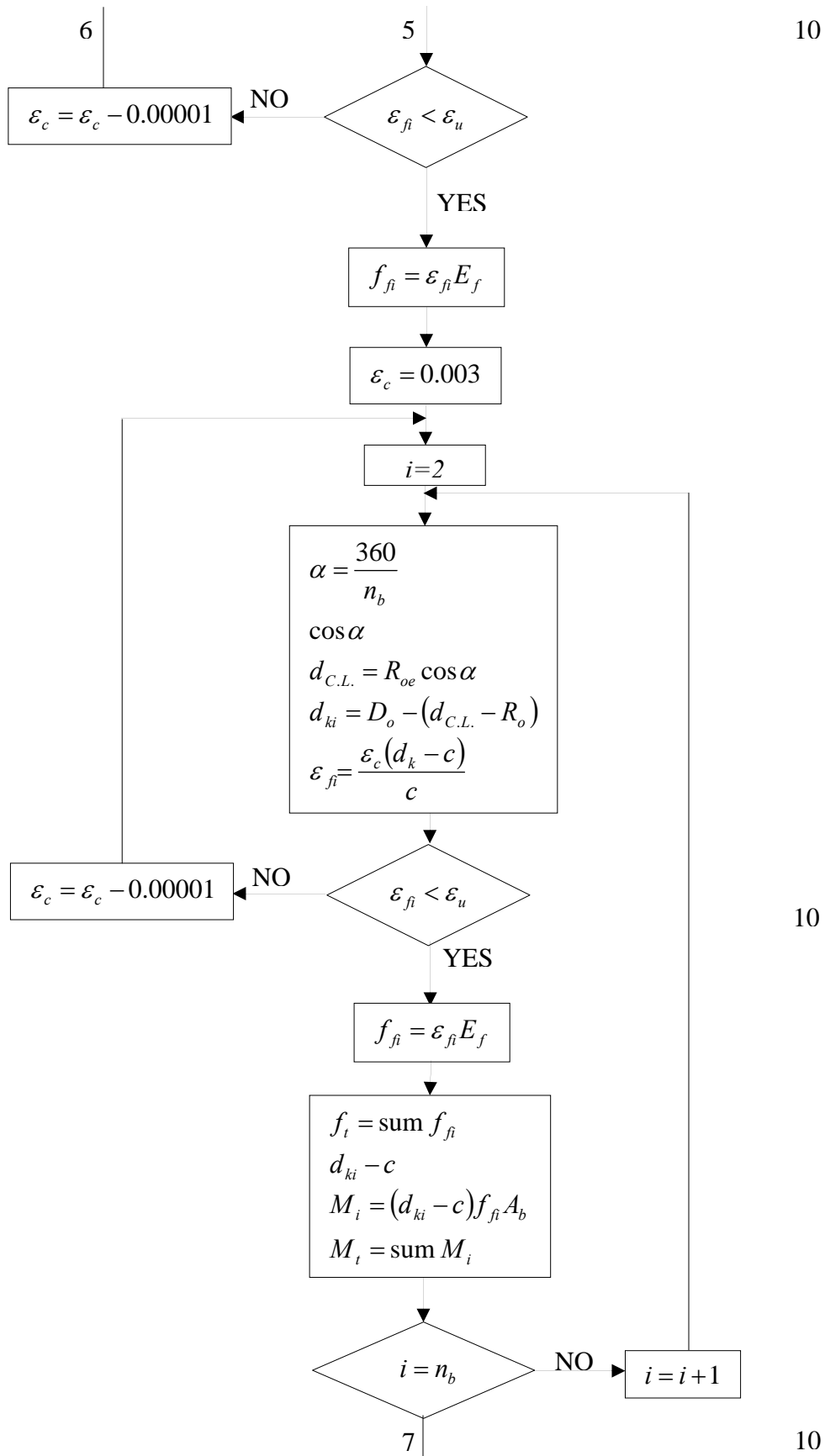
FLOW CHART FOR THE SPREADSHEET DEVELOPED TO DESIGN SPUN CON- CRETE POLES REINFORCED WITH CFRP BARS

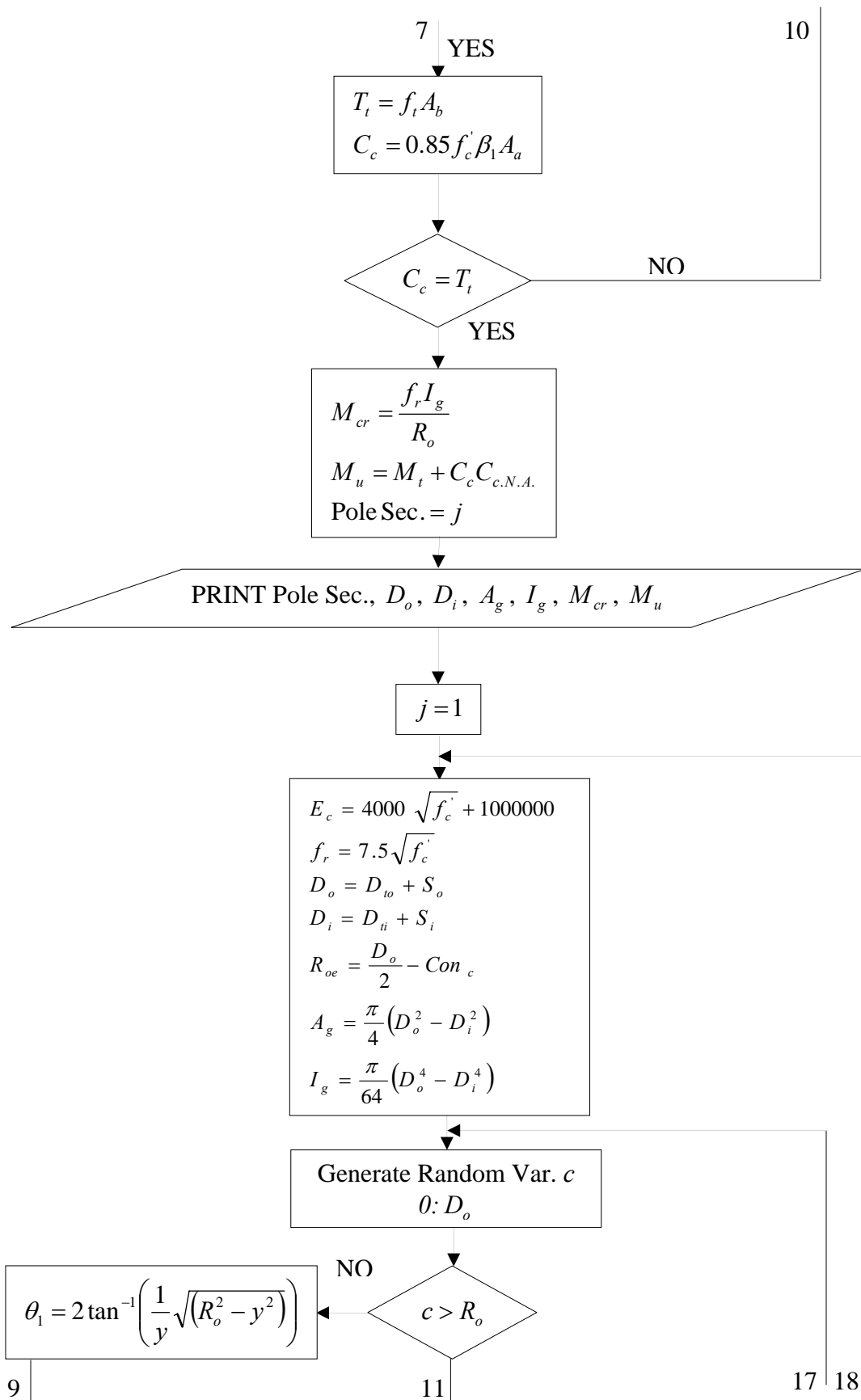
FLOW CHART FOR THE SPREADSHEET DEVELOPED TO DESIGN SPUN CON-
CRETE POLES REINFORCED WITH CFRP BARS

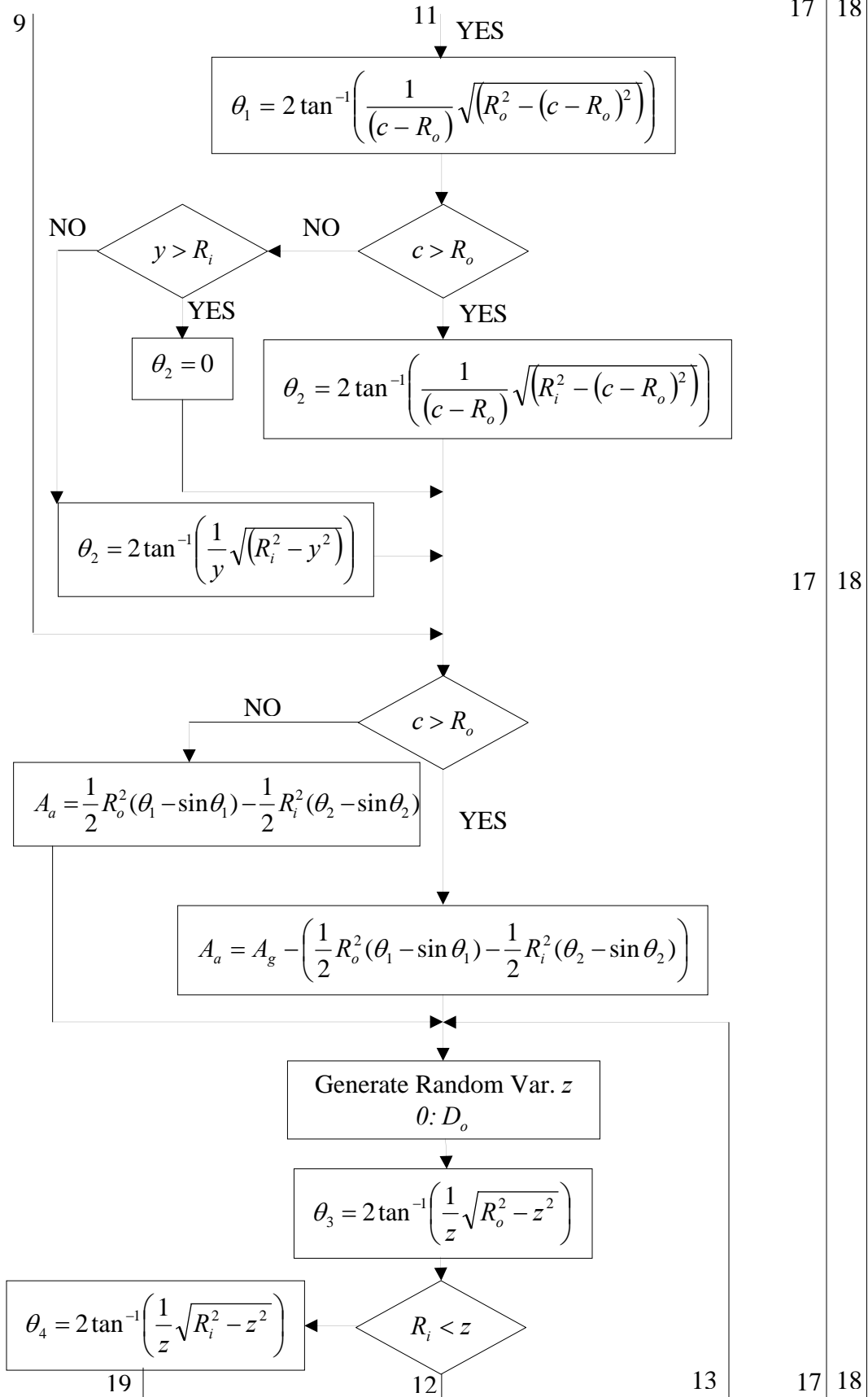


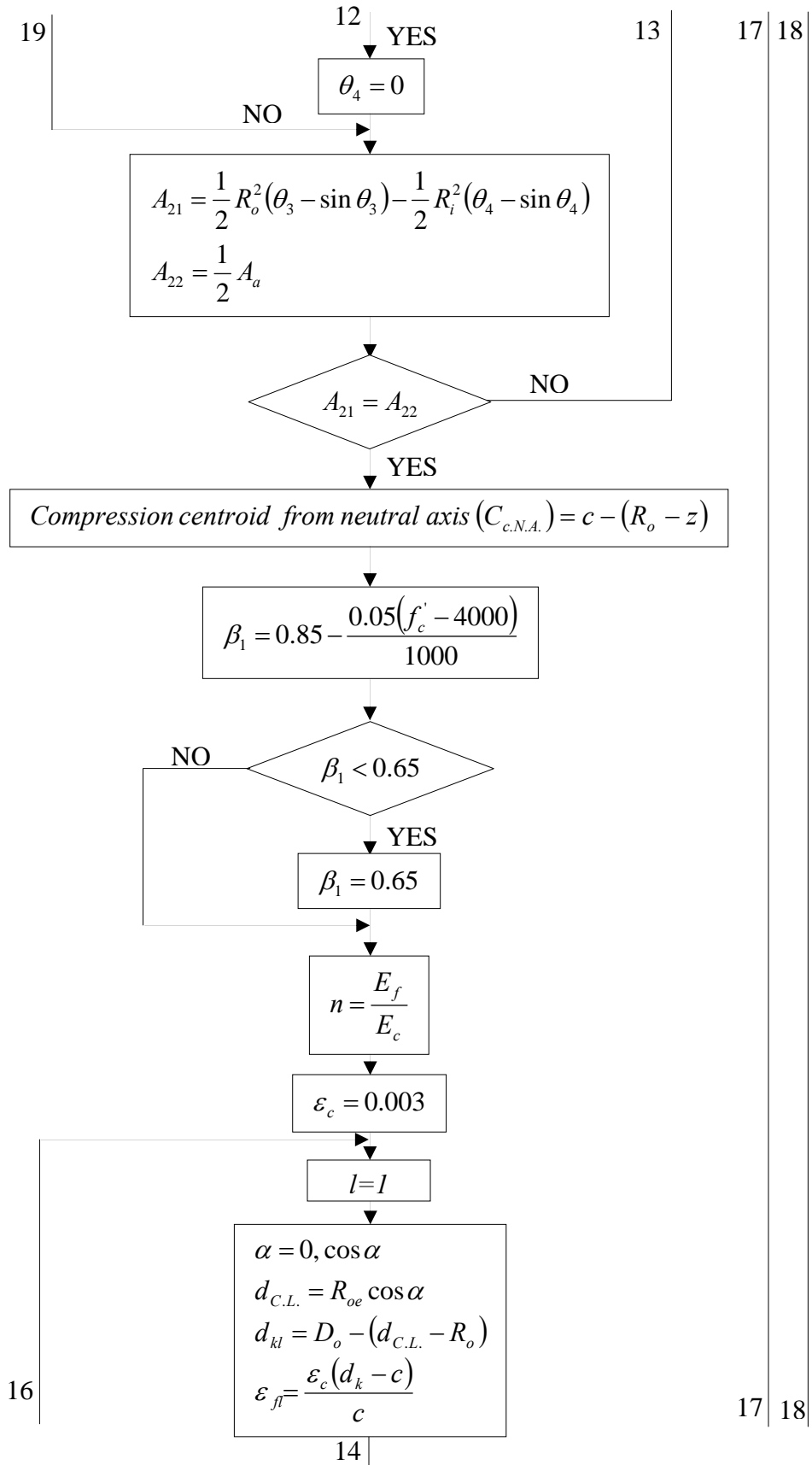


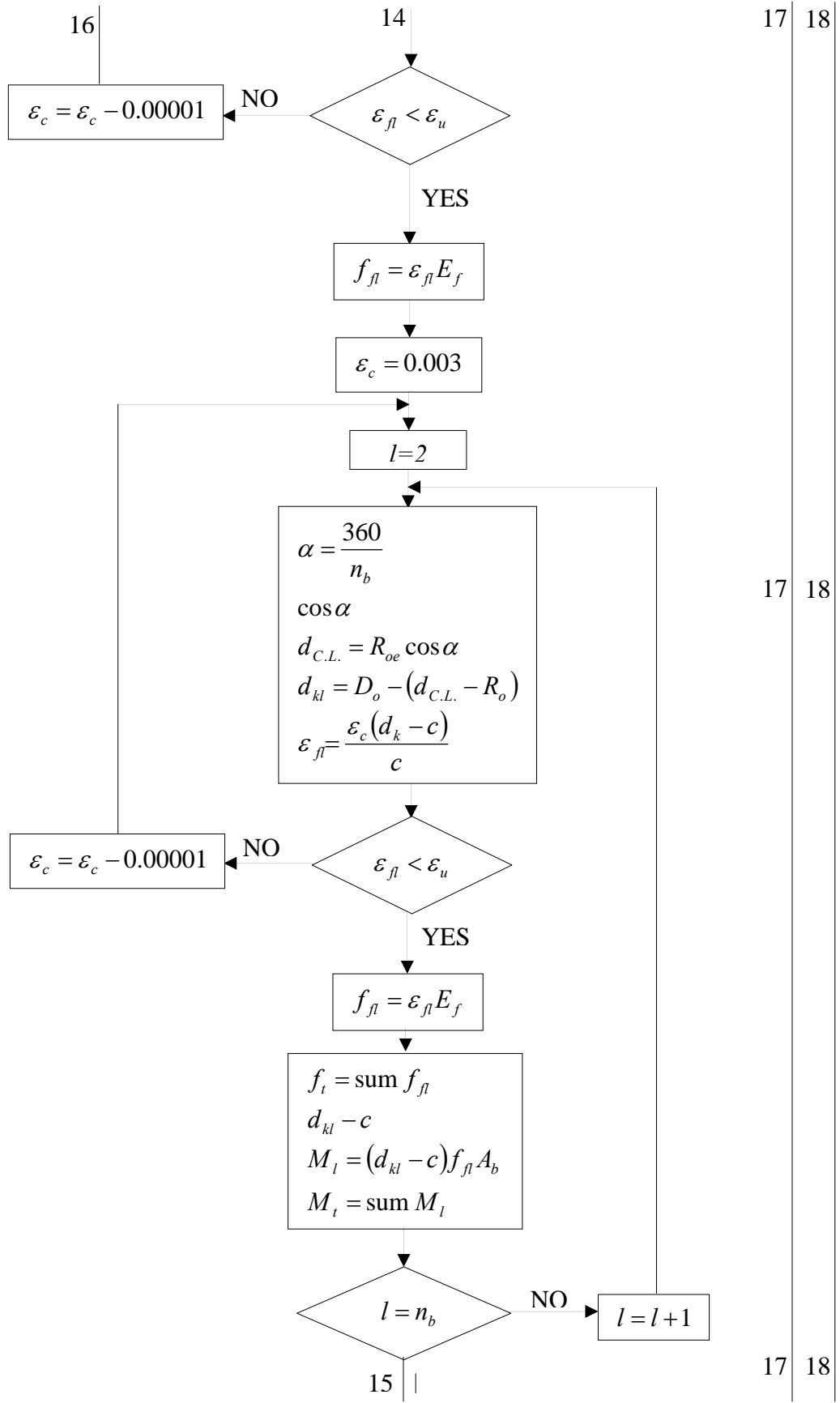


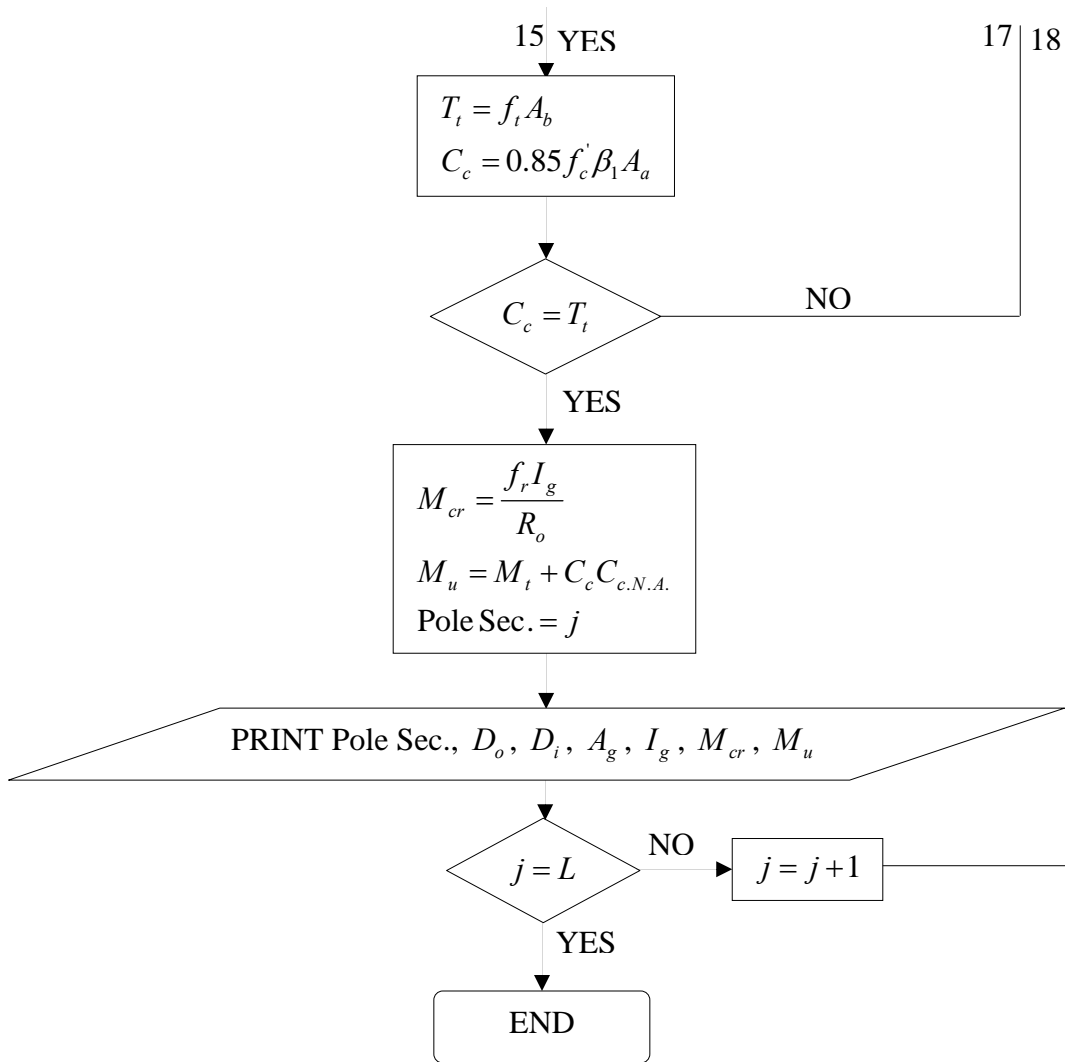








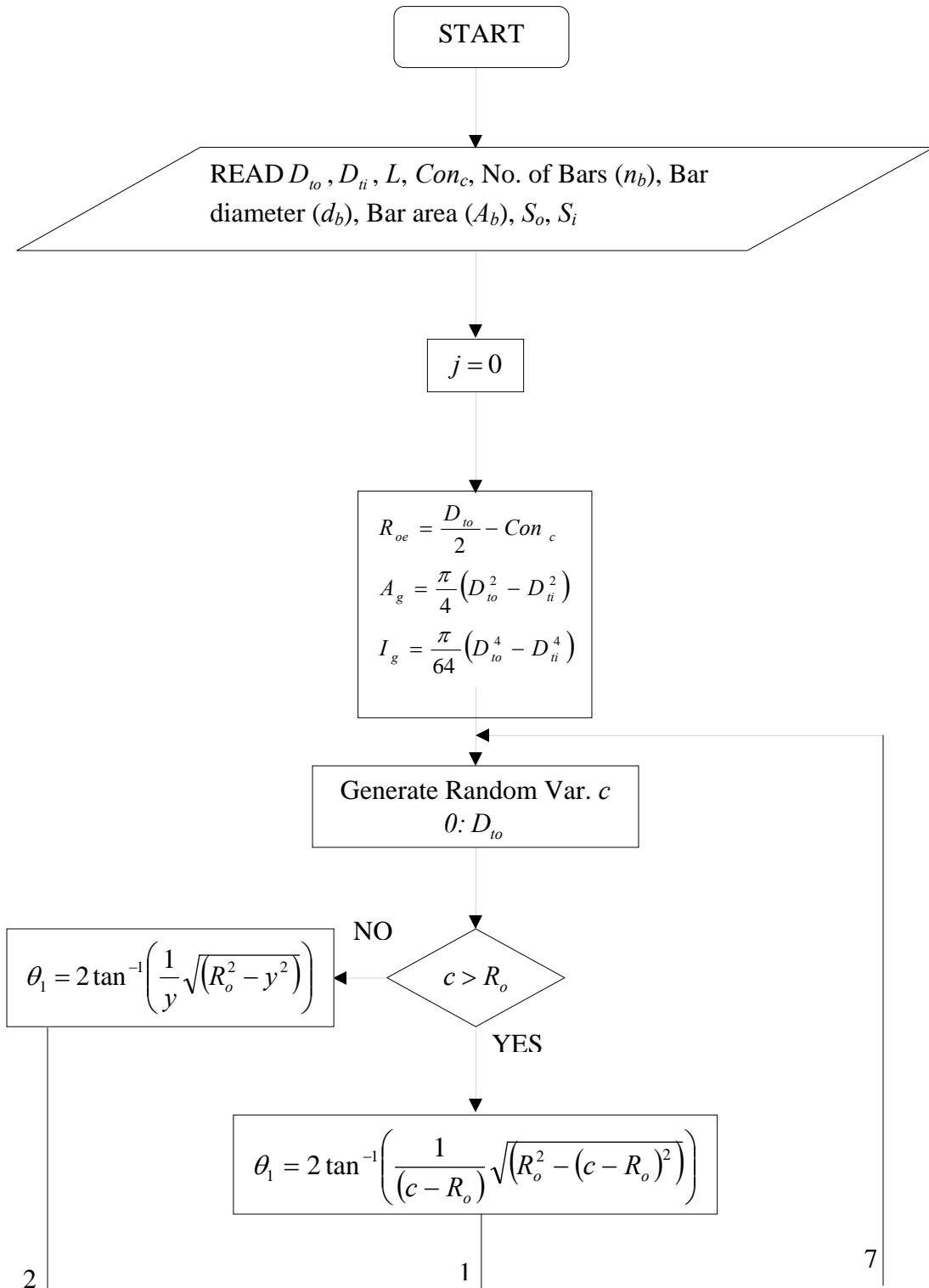


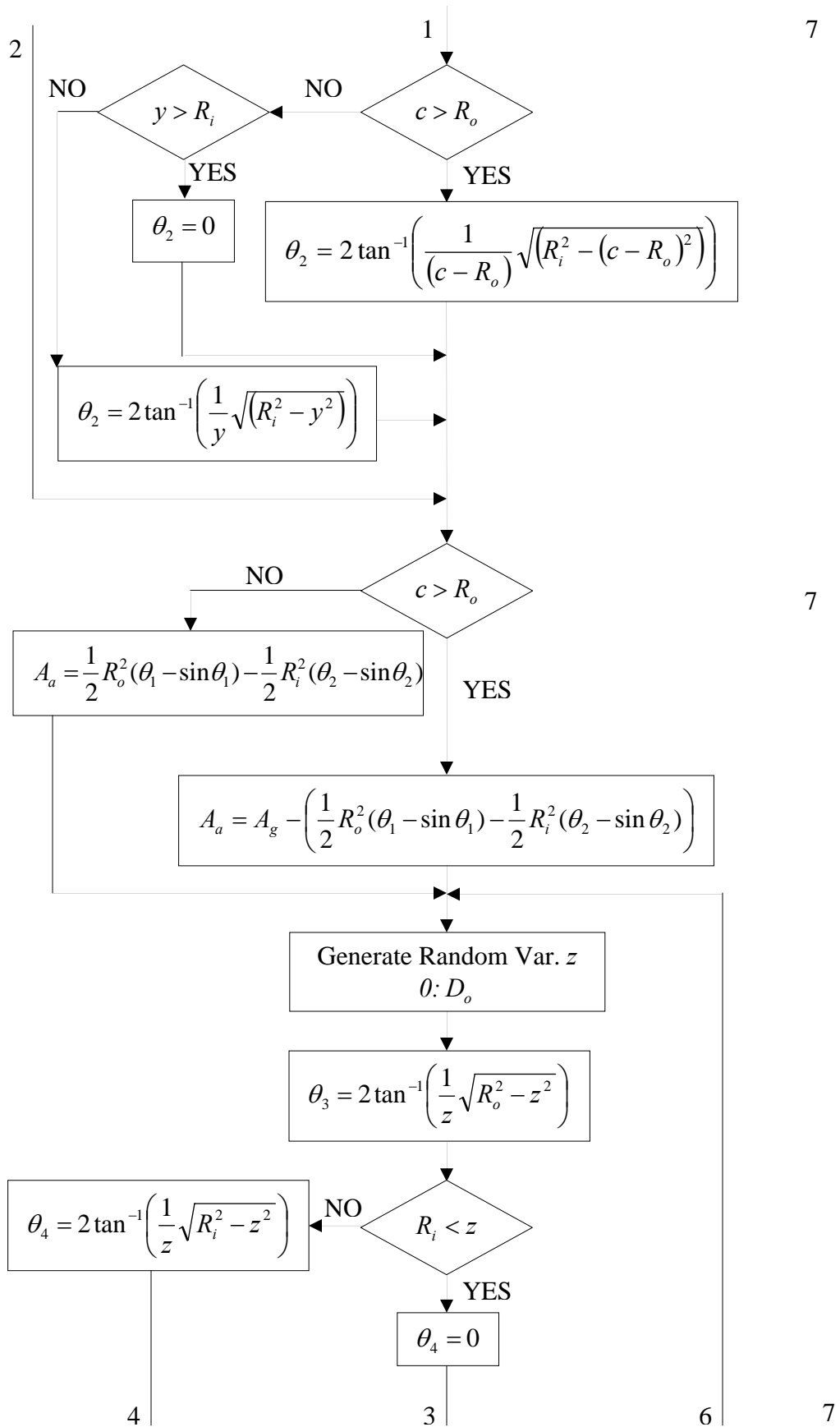


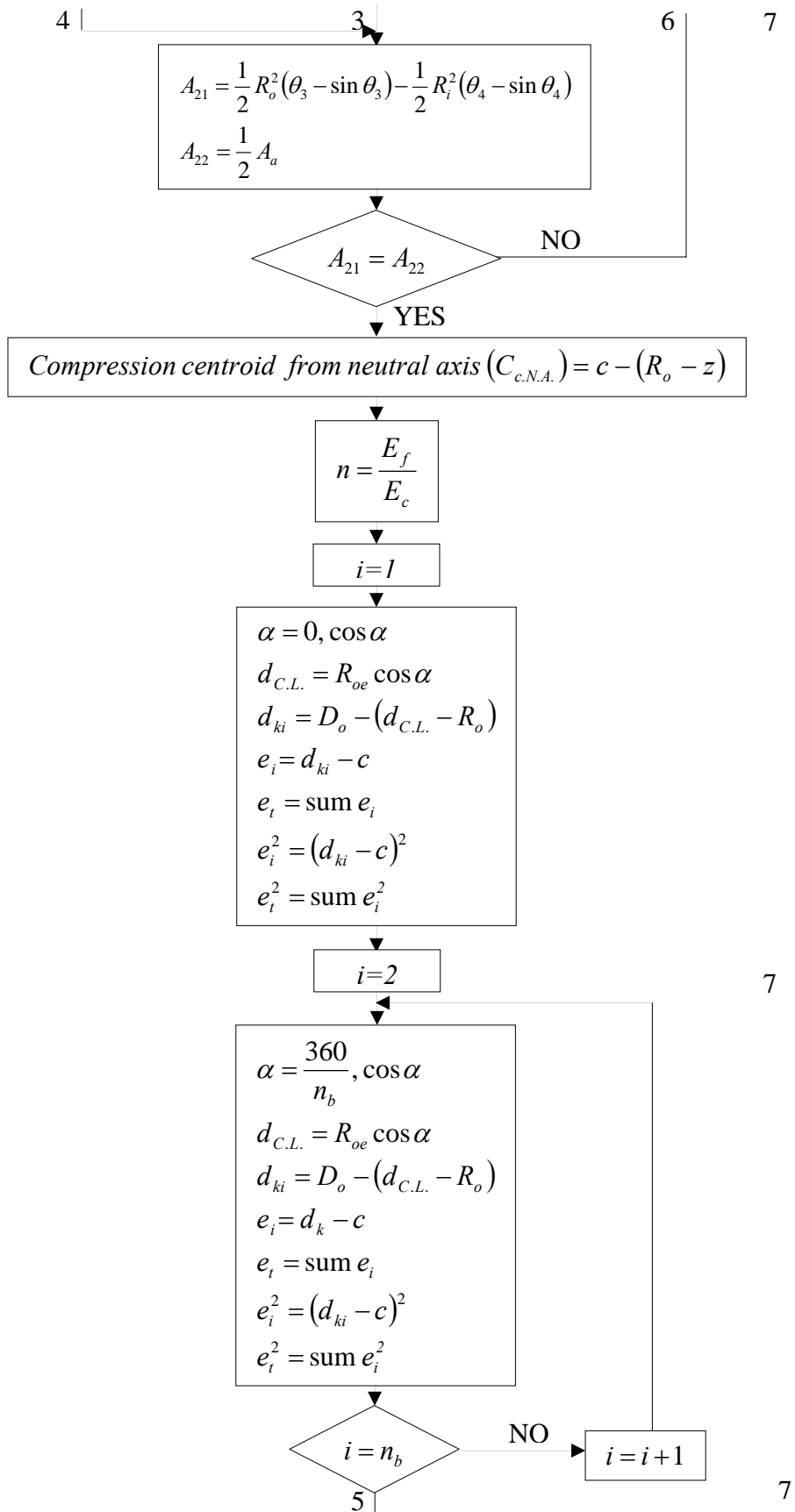
APPENDIX B

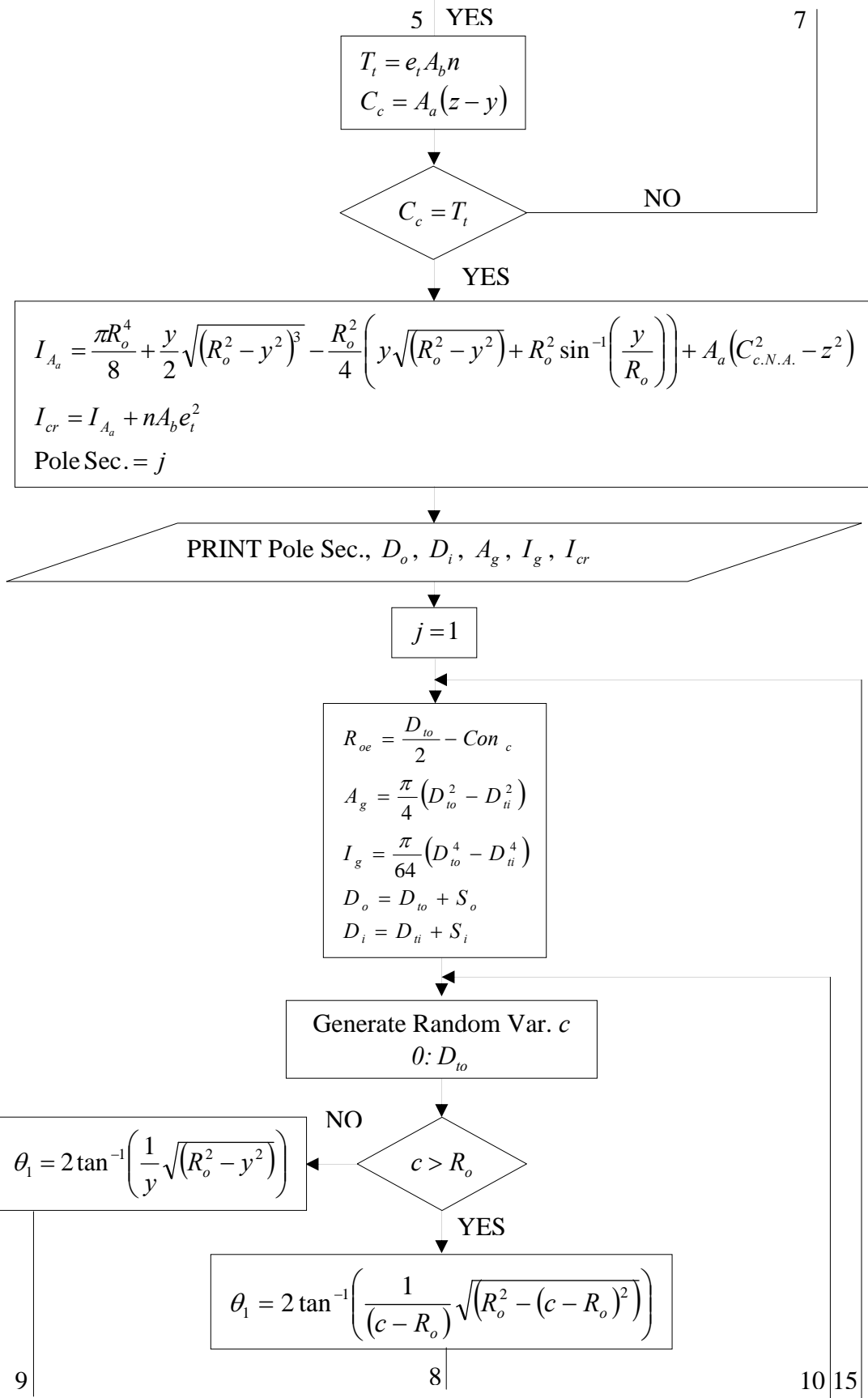
FLOW CHART FOR THE CALCULATION OF THE CRACKING MOMENT OF INERTIA FOR SPUN CONCRETE POLES REINFORCED WITH CFRP BARS

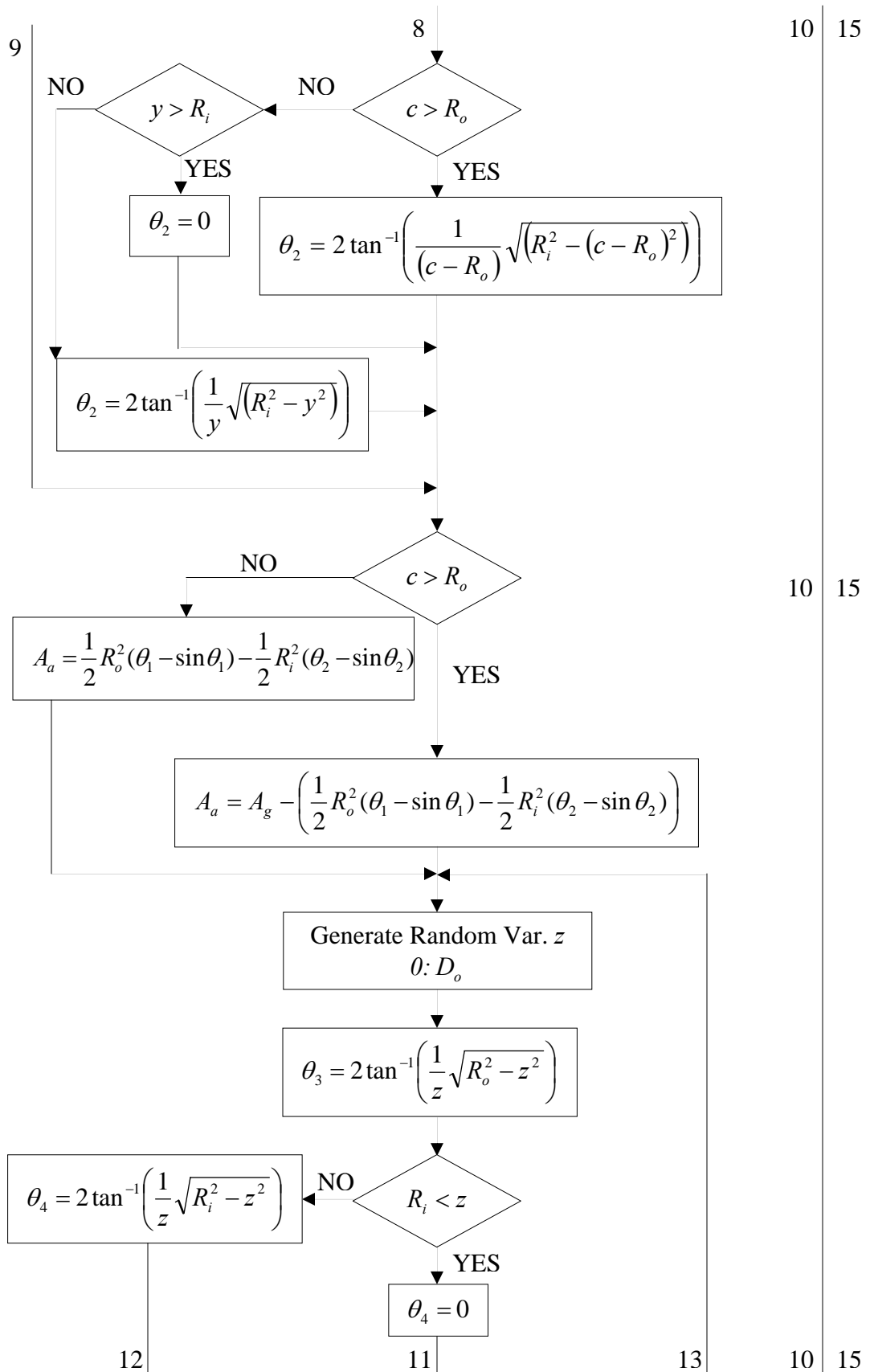
FLOW CHART FOR THE CALCULATION OF THE CRACKING MOMENT OF INERTIA FOR SPUN CONCRETE POLES REINFORCED WITH CFRP BARS

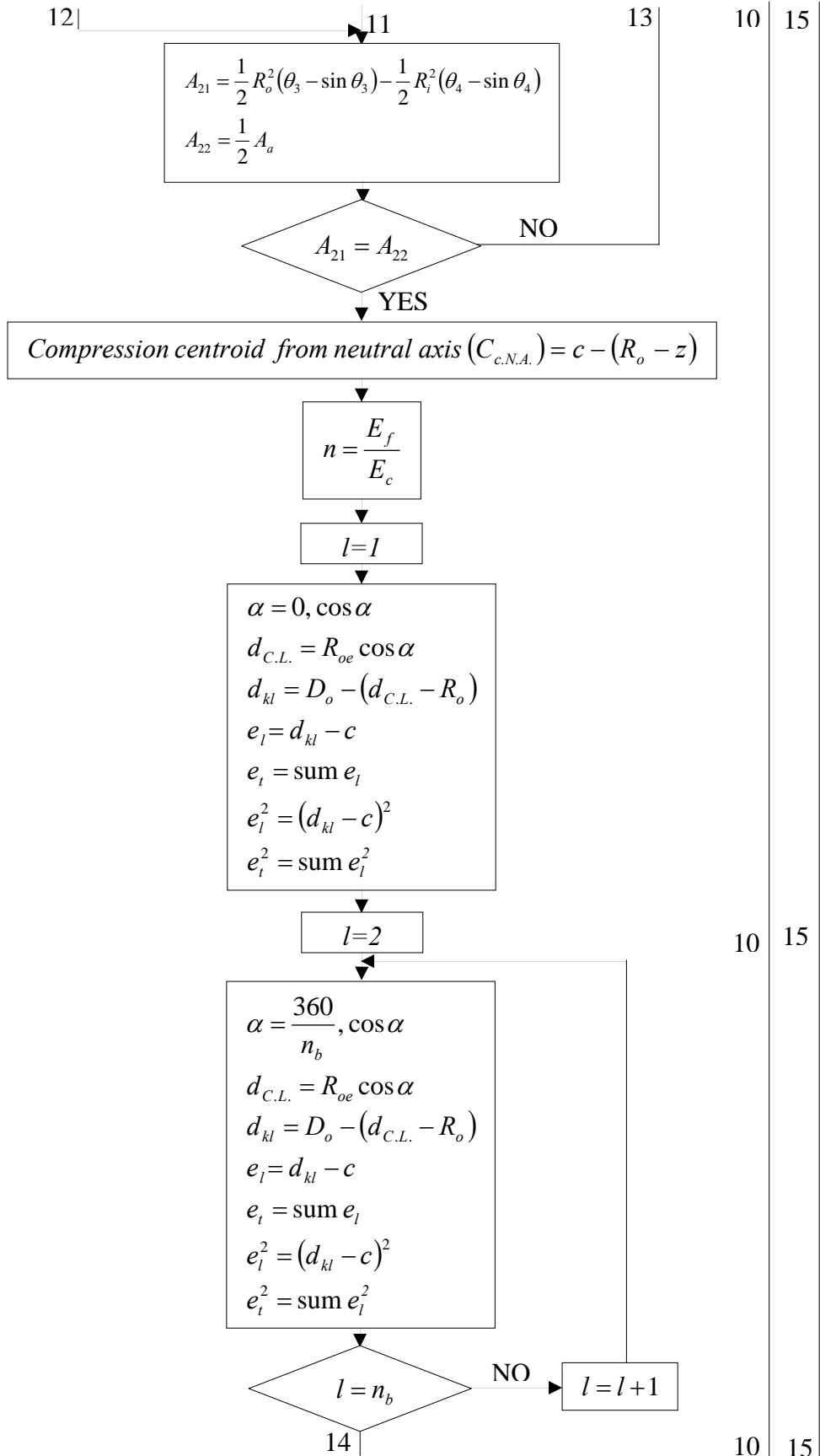


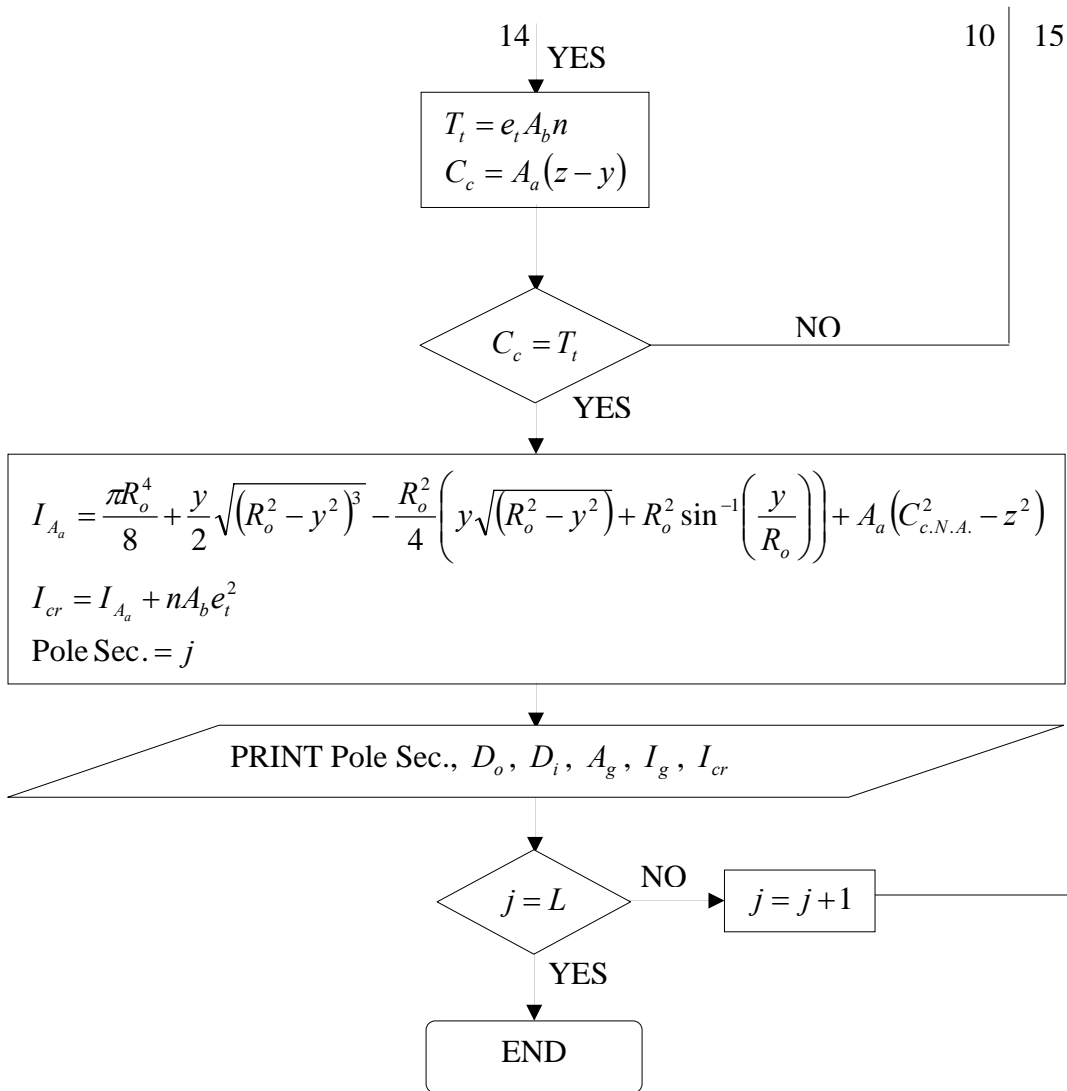








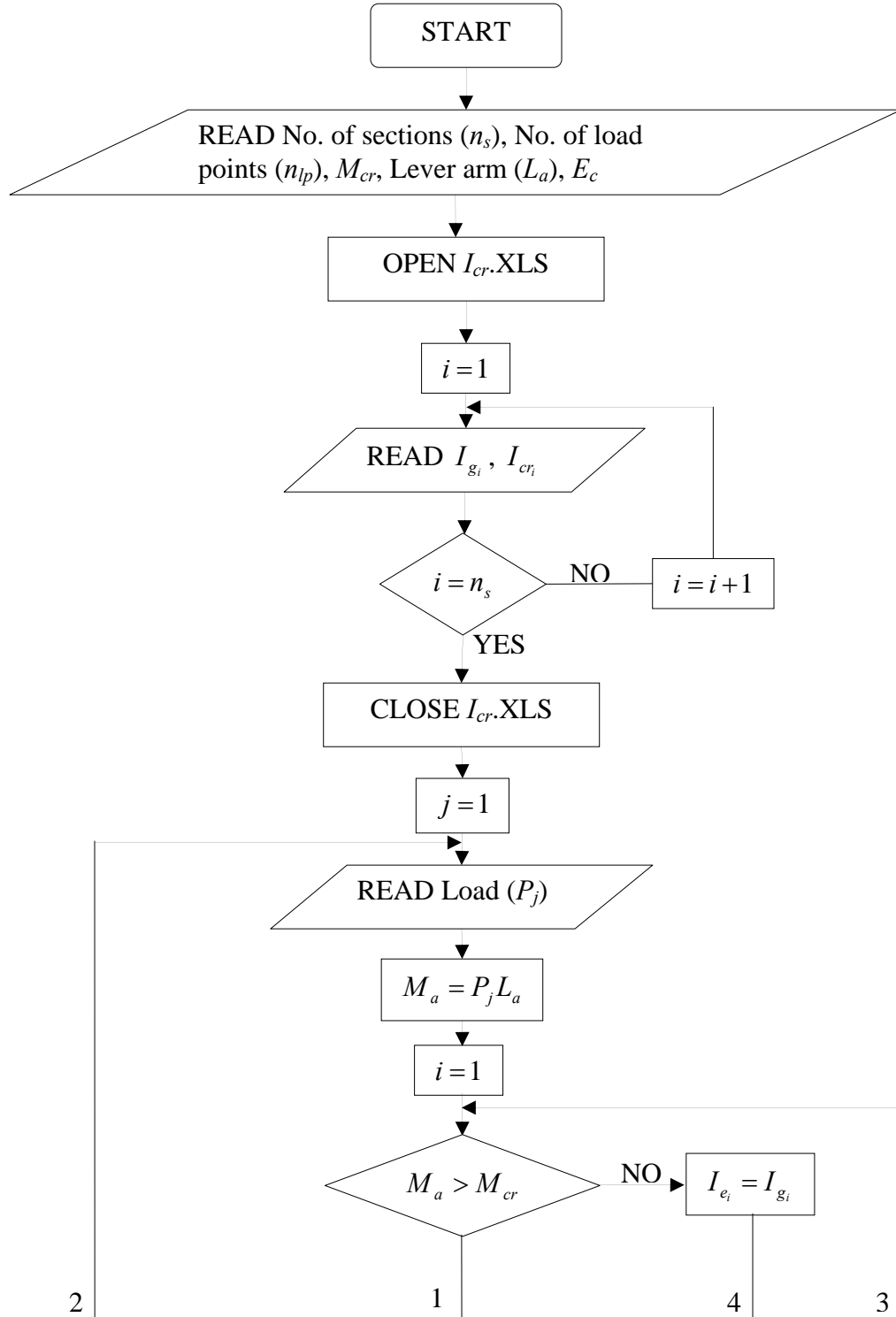




APPENDIX C

FLOW CHART FOR THE LOAD-DEFLECTION CALCULATIONS OF SPUN CON- CRETE POLES REINFORCED WITH CFRP BARS

FLOW CHART FOR THE LOAD-DEFLECTION CALCULATIONS OF SPUN CON-
CRETE POLES REINFORCED WITH CFRP BARS



2

4

3

